

FRACTURE ANALYSIS AND
CORROSION FATIGUE IN PIPELINES

by

F. Erdogan and R.P. Wei

Department of Mechanical Engineering and Mechanics

Lehigh University, Bethlehem, PA 18015

December 1984

ANNUAL REPORT

Prepared for

U.S. Department of Transportation

Research and Special Programs Administration

Office of University Research

Under the Contract DTRS 56 82-C-00014

TABLE OF CONTENTS

	<u>Page</u>
Scope of the Project	
General Information	
PART I. THE FLAW INTERACTION STUDIES	1
FURTHER DEVELOPMENT OF MODELS FOR WELD DEFECTS AND DEFECT INTERACTION STUDIES	1
1. Background	1
2. Planar Cracks - The Line Spring Model	7
2.1 Introduction	7
2.2 Description of the Model	11
2.3 Internal Cracks	18
2.4 Some Results	22
2.5 Conclusions	27
3. The Interaction Between Flat Inclusions of Finite Thickness and Cracks	33
3.1 Introduction	33
3.2 Integral Equations of the Problem	34
3.3 Stress Intensity Factors	42
3.4 Results	43
4. References for Part I	55
APPENDIX A - Surface Cracks in a Plate of Finite Width Under Tension or Bending	58
1. Introduction	58
2. The General Formulation of the Problem	59
3. The Integral Equations	64
4. The Results	69
APPENDIX B - Further Results on Crack-Inclusion Interaction Problems	97
1. Introduction	97
2. The Formulation	97
3. The Stress Intensity Factors	103
4. The Results	105

FRACTURE ANALYSIS AND CORROSION FATIGUE IN PIPELINS

Scope of the Project

The primary objectives of this research program are

- (a) Classification and assessment of the relative importance of various types of weld defects
- (b) An in-depth study of the problem of interaction between two flaws and between flaws and pipe surfaces
- (c) Fracture analysis of pipes with crack arrestors
- (d) The effect of crack orientation on the strength of pipes
- (e) The development of quantitative understanding of the early stage of chemical reactions in relation to the corrosion fatigue crack initiation and propagation
- (f) Elucidating the mechanisms for corrosion fatigue crack initiation and propagation, including the influences of chemical, mechanical and metallurgical variables in pipeline steels
- (g) The formulation and evaluation of models for predicting cracking response and service performance by using a combined fracture mechanics, surface chemistry and materials science approach.

In this second annual report the completed part of the research program during September 1983 to October 1984 is described and the results are presented.

General Information

The research presented in this report is supported by the U.S. Department of Transportation, Office of University Research, and by the U.S. Department of Interior, Minerals Management Service. Mr. Douglas B. Chisholm of DOT Research and Special Programs Administration, Office of Pipeline Safety Regulation is the Project Monitor. Dr. Charles

E. Smith, Research Program Manager, Technology Assessment and Research Branch, Minerals Management Service is the Department of Interior technical representative.

Part I of the report describes the theoretical research carried out by Professor F. Erdogan, the Principal Investigator, Mr. B. Aksel, Dr. H. Boduroglu and Dr. X-H Liu. Part II presents the experimental work which was carried out by Professor R.P. Wei, the Co-Principal Investigator and Mr. S. Chiou.

FRACTURE ANALYSIS AND CORROSION FATIGUE IN PIPELINES

PART I

FURTHER DEVELOPMENT OF MODELS FOR WELD DEFECTS AND DEFECT INTERACTION STUDIES

In the previous report [1] various kinds of flaws which may be found in pipelines, particularly in girth welds were considered, a broad classification was made, and the results of some defect-defect and defect-free surface interaction studies were presented. In this report further inclusion and planar crack models are developed and some inclusion-crack, crack-crack and crack-free surface interaction problems are studied. These problems have a bearing in and application to the fitness for purpose type studies in pipelines which may contain known or conjectured flaws. As in the previous report, the emphasis in this report too is on the fracture mechanics approach to the evaluation of flaws.

1. BACKGROUND

The standards of acceptability of welds in pipelines are generally based on certain empirical criteria in which primary importance is placed on flaw length. Specifically for girth welds such standards are described in API STANDARD 1104 prepared by the "American Petroleum Institute - American Gas Association Joint Committee on Oil and Gas Pipeline Field Welding Practices". However, the API Standard also recognizes fitness for purpose criteria based on fracture mechanics methodology as an alternative technique for flaw evaluation. The advantage of the fracture mechanics approach is that since it takes into account all factors which may be relevant to the failure of the pipe such as the type and the relative size, shape, orientation and location of the flaw, the effect of multiple flaws, the nature of the applied stresses, and the environmental conditions, it could be somewhat more precise than the empirical rules which are largely based on the flaw length.

In fracture mechanics approach to flaw evaluation it is implicitly assumed that the material contains some macroscopic flaws which may form the nucleus of fracture initiation. Generally, these flaws may be mapped by using an appropriate nondestructive flaw detection technique. Aside from the weld defects the pipe may also have flaws which may be external in origin. Generally the initial phase of the failure in a pipe is the rupture of the net ligament adjacent to the critical flaw in the pipe wall. In most cases the resulting through crack is arrested and the pipe is repaired before further damage. However, in some cases the resulting through crack, after some stable growth, may become unstable leading to circumferential pipe break or dynamic propagation of an axial crack. The initial rupture of the net ligament in the pipe wall is usually preceded by some subcritical crack growth due to fatigue, corrosion fatigue, or stress corrosion cracking and the actual net ligament rupture is generally a ductile fracture process.

Therefore, it is seen that in order to apply fracture mechanics analysis to welded pipes, first one needs to characterize the material itself (the base metal, the weld material and the material in the heat affected zone) with regard to fatigue and corrosion fatigue crack propagation, stress corrosion cracking, fracture toughness and ductile fracture. Next, for a given flaw geometry and loading conditions one has to solve the related mechanics problem to calculate the appropriate fracture mechanics parameter such as the stress intensity factor, the crack tip opening displacement, or the J-integral. The third step in the process would be the selection or development of a proper failure theory and the application of the related quantitative failure criterion. The type of analysis and the experimental work to be performed and the particular criterion to be used are clearly dependent on the expected or the most likely mode of failure.

Even though the primary applied load in the pipelines is the internal pressure which is largely time-independent, there may be some small variations in pressure and some vibrations particularly near the pumping stations which may add a fluctuating component to the static stresses just high enough to cause concern. There are also secondary stresses which are mainly time-varying in nature and therefore would enhance the subcritical crack propagation. Some of the sources of these secondary stresses are misalignment and fit-up, daily, seasonal and other thermal fluctuations, ground settlement and possible

earthquakes, axial constraint, and gross bending in offshore piping due to buoyancy and other hydroelastic effects. It should be added that the "stress transients" may also play a major role in the subcritical crack propagation and particularly in the final phase of the fracture process, if one takes place. These stresses are generally caused by the pressure waves resulting from changes in flow rate due to partially or fully closing of the valves. In the case of pipes carrying liquids such as petroleum pipelines this is known as the "water hammer" effect due to which the peak pressure may be as high as multiples of the then operating pressure in the pipe. In the natural gas pipelines, this increase in the peak pressure may be somewhat more moderate. Nevertheless, in either case, such sudden surges of pressure are probably responsible in most cases for the final stage of the net ligament failure in the pipe wall resulting in leaks or in a catastrophic failure.

A detailed description and classification of weld discontinuities (including "flaws" which are considered to be undesirable) and a critical review of the literature as well as very extensive references on the subject up to 1976 may be found in [2]. The problem of interaction between two (planar) cracks and some empirical rules to define a single equivalent crack are discussed in [3]. The procedures dealing with the subcritical crack propagation by using the tools of linear elastic fracture mechanics (LEFM) is highly standardized and may be found, for example, in [4] or [5]. Similarly, the process of brittle or quasi-brittle fracture is relatively well-understood and is easily dealt with techniques based on LEFM and the concept of fracture toughness. The process which is not well-understood and not standardized, however, is the ductile fracture. The Appendix in the API Standard 1104 concerning the fracture mechanics applications is based on the critical crack tip opening displacement concept, whereas the J-integral seems to be more widely used in pressure vessel technology. The description, some applications of and extensive references on the crack opening displacement approach to fracture may be found in [6]-[8]. Application of a general fracture instability concept based on the crack opening displacement to shells and plates with a part-through crack is described in [9].

Generally a "flaw" may be defined as a discontinuity in material constants or geometry. Variety of inclusions come under first and notches, pores and cracks come under the second group of flaws. A common feature of all flaws is

that they disturb or perturb the stress field around them. Very often this perturbation gives rise to a stress concentration around the flaw. However, for certain types of flaws there may also be a reduction in key components of the stresses. From a viewpoint of fracture mechanics applications following are some of the typical and important flaw geometries.

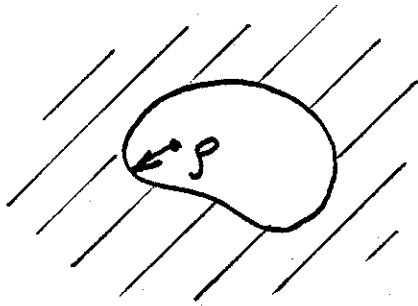
(a) Pores and Solid Inclusions

Pores are the holes or voids in the material having entirely smooth surfaces (Fig. 1.a1). If σ_0 refers to the magnitude of the uniform stress field outside the perturbation region of the pore, then the pore leads to a stress concentration which is of the form

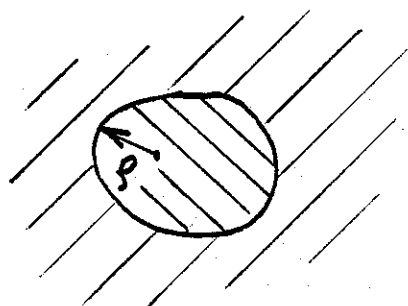
$$\sigma_{\max} = K\sigma_0, \quad K = \frac{A}{\sqrt{\rho}}, \quad (1)$$

where K is the "stress concentration factor", A is a (finite) constant which depends on the geometry of the medium and ρ is radius of curvature of the pore. Generally K is greater than one. We note that surface notches with finite radius of curvature ρ would also come under this category.

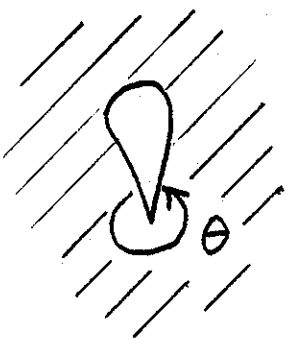
Solid inclusions are the second phase materials in the medium also having entirely smooth surfaces. The modulus E_i of the inclusion may be greater or less than the modulus E of the matrix or the base material, the two limiting cases being the rigid inclusion ($E_i = \infty$) and the hole ($E_i = 0$). If $E_i < E$, qualitatively the perturbed stress field of the inclusion is similar to that of a pore, meaning that there would be a stress concentration around the inclusion. On the other hand, if $E_i > E$ there would be a reduction in the net section stress. However, in this case there would also be a stress concentration in other planes perpendicular to the applied stress. For example, Fig. 2 of [1] shows the stress distribution in a medium containing a circular inclusion under plane strain or plane stress conditions. Note that for $c > R$ around the inclusion there is indeed some stress concentration. In this figure, μ is the shear modulus, $\kappa = 3 - 4\nu$ for plane strain, and $\kappa = (3 - \nu)/(1 + \nu)$ for plane stress, ν being the Poisson's ratio.



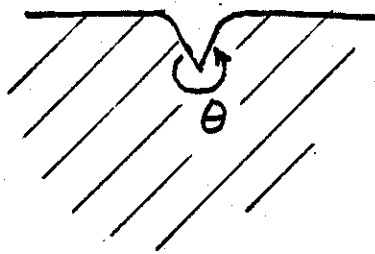
(a1)



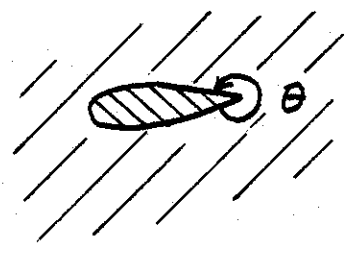
(a2)



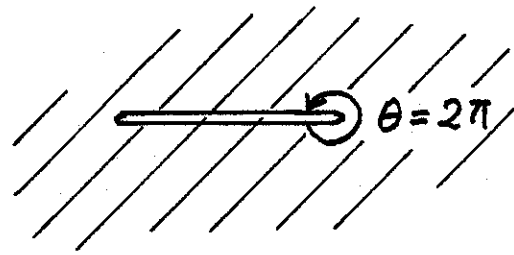
(b1)



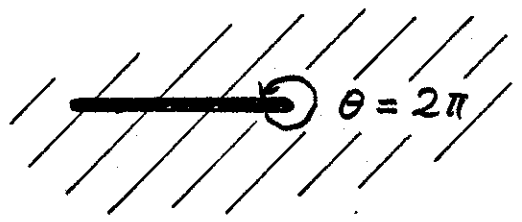
(b2)



(b3)



(c1)



(c2)

Fig. 1 Types of Flaws

(b) Pores, Notches and Solid Inclusions with Sharp Corners

From Eq. (1) it may be seen that from a viewpoint of failure analysis a distinguishing feature of the pores, notches and solid inclusions with smooth surfaces is that the stress state around such flaws is always bounded. Eq. (1) also indicates that as the root radius ρ of the notch tends to zero, the stress state around notch tip would tend to infinity. Particularly in problems concerning brittle fracture and fatigue crack initiation such flaws may have to be treated differently. In these nonplanar flaw problems it is said that the inclusion or the notch tip is a point of stress singularity around which the stress state would have the following behavior:

$$\sigma_{ij} = \frac{k}{r^\lambda} , \quad 0 < \text{Re}(\lambda) \leq 1/2 , \quad (2)$$

where k and λ are constants representing the strength and the power of the stress singularity and r is a (small) distance from the notch tip. Generally, Eq. (2) is valid for values of the material angle $\theta > \pi$ (Fig. 1 b1, b2, b3). Even though the term "stress intensity factor" is commonly used in relation with crack problems for which $\lambda = 0.5$, in the more general problem leading to an expression such as (2) k is also called the "stress intensity factor".

In the case of notches with a material angle $\pi < \theta < 2\pi$ the power of singularity λ is dependent on θ only and may be obtained from (see, for example, [10] where the general problem of bimaterial wedge under variety of boundary conditions are discussed)

$$\cos[2(\lambda-1)\theta] - 1 + (\lambda-1)^2(1-\cos 2\theta) = 0 . \quad (3)$$

(c) Cracks and Flat Inclusions

These are simply the planar flaws in which the material angle θ (theoretically) is 2π (Fig. 1 c1, c2). Again, the inclusion may be elastic or rigid, the crack being a limiting case with zero modulus. In all planar inclusion as well as crack problems eq. (2) is valid with $\lambda = 0.5$.

In the previous report [1] the interaction problems between a crack and an elastic inclusion or a pore, between cracks of various configurations near and at the boundary and between flat inclusions and planar cracks were considered and limited results for planar cracks of finite size were presented. In this report the details of the interaction problem for the multiple planar

cracks of finite size are presented and some of the results are discussed. Also, a new model for a flat elastic inclusion of finite thickness interacting with a plane crack is developed and numerical results are given.

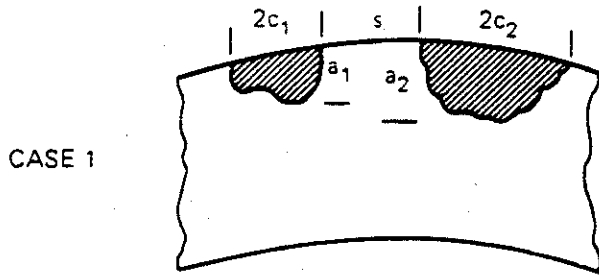
2. PLANAR CRACKS - THE LINE SPRING MODEL

In this section the general description of the line spring model for internal as well as surface cracks is presented and results for various crack geometries are given. Referring to Fig. 2 which is reproduced from API Standard 1104 and which describes a set of empirical rules regarding the interaction between planar cracks it may be seen that somewhat more quantitative results are needed. The general method to provide such results is described below.

2.1 Introduction

From the viewpoint of practical applications the analysis of a part-through crack in a structural component which may locally be represented by a "plate" or a "shell" is certainly one of the most important problems in fracture mechanics. In its general form the problem is a three-dimensional crack problem in a bounded geometry where the stress field perturbed by the crack interacts very strongly with the surfaces of the solid. At present even for the linearly elastic solids a neat analytical treatment of the problem appears to be intractable. Consequently, as indicated in references [1] and [9], the available solutions of the problem very heavily rely on some kind of numerical technique, most notably on the finite element method. The renewed interest in recent years in the so-called "line-spring model" first described in [11] has been due partly to the desire of providing simpler and less expensive solutions to the part-through crack problem and partly to the fact that for certain important crack geometries the model seems to give results that have an acceptable degree of accuracy.

In a plate or a shell containing a part-through crack and subjected to membrane and bending loads, the net ligament(s) around the crack would generally have a constraining effect on the crack surface displacements. The basic idea underlying the "line-spring model" consists of approximating the three-dimensional crack problem by a two-dimensional coupled bending-membrane problem through the reduction of the net ligament stresses to the neutral surface of the plate or shell as a membrane load N and a bending moment M . In the resulting two-dimensional



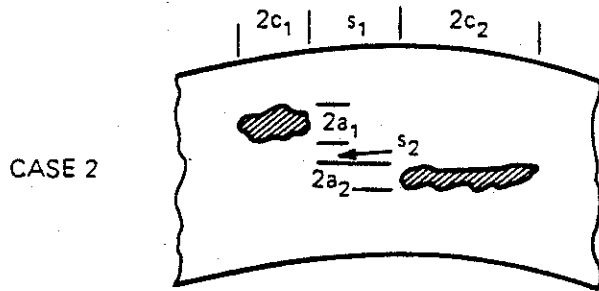
INTERACTION
EXISTS IF:

IF INTERACTION EXISTS
EFFECTIVE FLAW SIZE IS:

$$s < c_1 + c_2$$

$$a_e = a_2$$

$$2c_e = 2c_1 + s + 2c_2$$



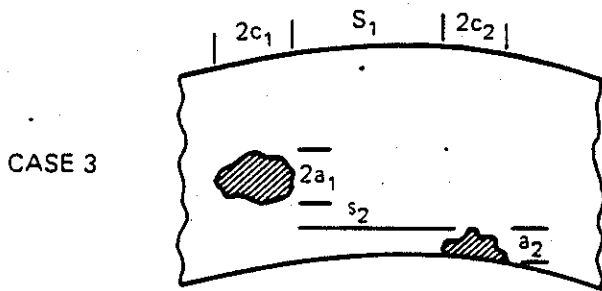
$$s_1 < c_1 + c_2$$

$$2a_e = 2a_1 + s_2 + 2a_2$$

and

$$s_2 < a_1 + a_2$$

$$2c_e = 2c_1 + s_1 + 2c_2$$



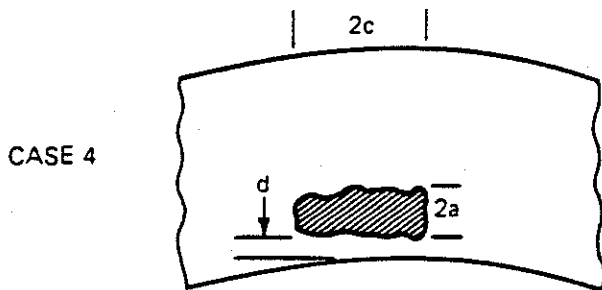
$$s_1 < c_1 + c_2$$

$$a_e = 2a_1 + s_2 + a_2$$

and

$$s_2 < a_1 + \frac{a_2}{2}$$

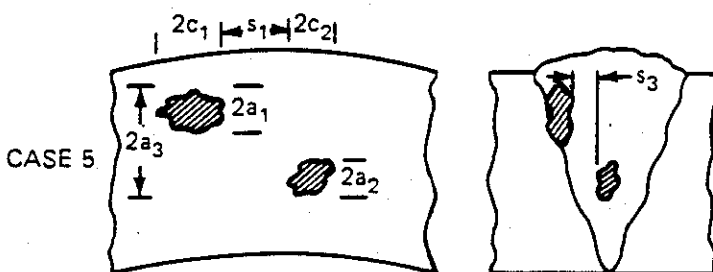
$$2c_e = 2c_1 + s_1 + 2c_2$$



$$d < a$$

$$a_e = d + 2a$$

$$2c_e = 2c$$



$$s_1 < c_2 + c_2$$

$$2a_e = 2a_3$$

and

$$s_3 < a_1 + a_2$$

$$2c_e = 2c_1 + s_1 + 2c_2$$

Fig. 2. RULES FOR EVALUATION OF FLAW INTERACTION

problem the crack surface displacements are represented by a crack opening displacement δ and a crack surface rotation θ , referred to, again, the neutral surface. The quantities N , M , δ and θ are assumed to be functions of a single variable, namely the coordinate x_1 along the crack in the neutral surface (Fig. 3). The pair of functions (δ, θ) or (N, M) are determined from the corresponding mixed boundary value problem for the "plate" or the "shell" having a through crack in which N and M are treated as unknown crack surface loads. Once N and M are determined the stress intensity factors are evaluated from the two-dimensional elasticity solution of a strip under the membrane force N and the bending moment M (Fig. 3b).

The model introduced in [11] is based on the classical plate bending theory. There is no need here to go into a detailed discussion on the necessity of using a higher order plate (or shell) theory in studying the crack problems (see, for example, [12]-[14]). It is, however, sufficient to point out that the asymptotic stress field around the crack tip given by the classical plate bending theory is not consistent with the elasticity solutions, whereas a transverse shear theory (such as that of Reissner's [15], [16]) which can accommodate all stress and moment resultants on the crack surface separately (i.e., three boundary conditions in plates, five in shells) give results which are identical to the asymptotic solutions obtained from the plane strain and anti-plane shear crack problems [17], [18]. The line spring model was later used in [19] and [20] to treat the longitudinal part-through crack problem in a cylinder by using, again, the classical shell theory. The solution obtained by using a transverse shear theory in plates and shells may be found in [21] and [22] (see also [23] for more extensive results in line pipes). Rather extensive results for corner cracks and for collinear surface cracks in a plate having a finite width are given in [24].

The concept of "line spring" may be used to treat also the problem of plastic deformations in the net ligament [25], [19], [20]. For materials without any strain hardening a simpler fully-plastic version of the model was used in [26] and [27] to calculate the crack opening displacement (see also [23] for the application to pipes containing a circumferential part-through crack).

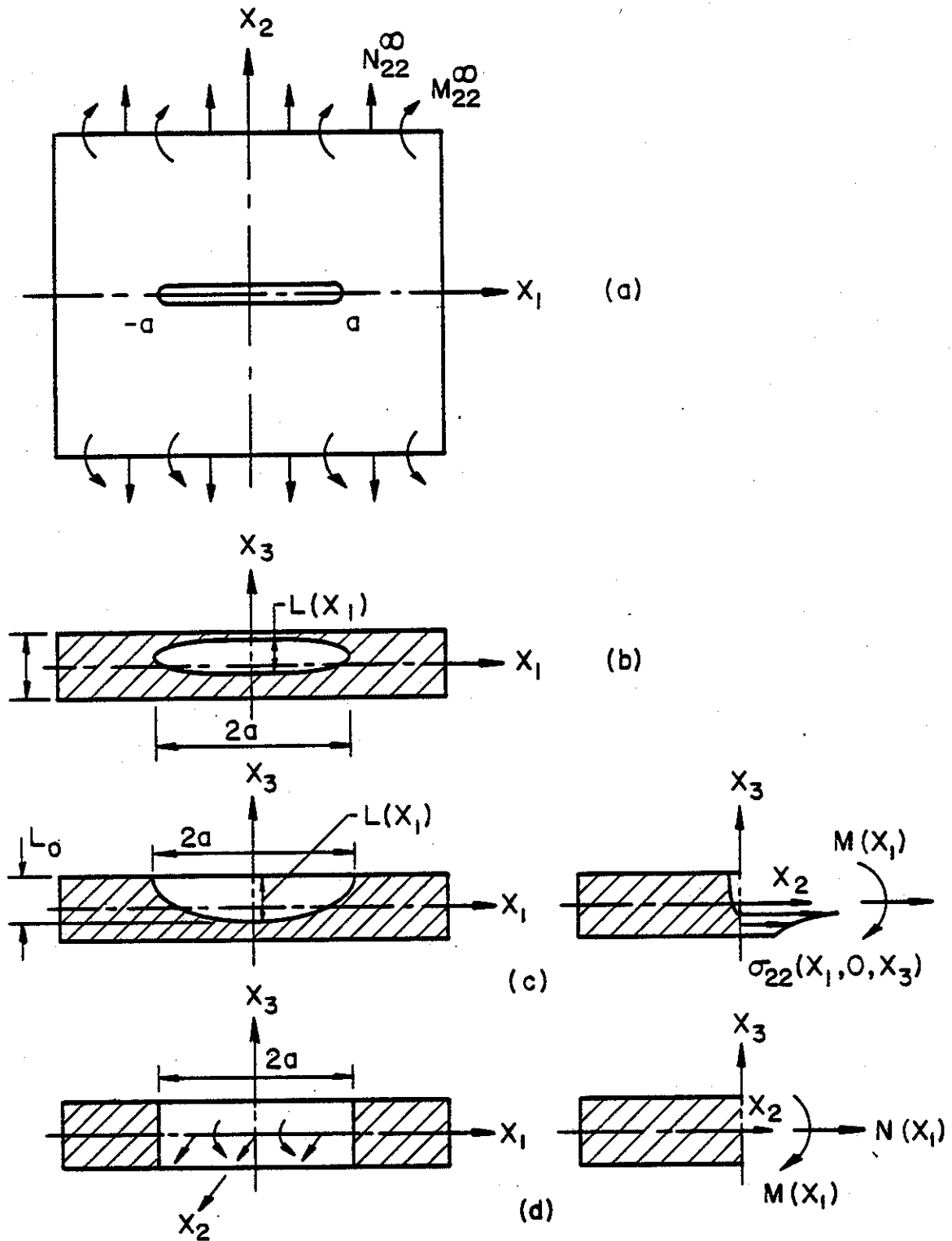


Fig. 3 Notation for the part-through crack problem.

2.2 Description of the Model

The problem under consideration is a surface or an internal crack problem for a relatively thin-walled structural component which is solved basically as a plate or shell problem. In the usual notation it will therefore be assumed that referred to the local coordinate system shown in Fig. 3, u_1, u_2, u_3 are the components of the displacement vector, β_1 and β_2 are the angles of rotation of the normal to the neutral surface in x_1x_3 and x_2x_3 planes, respectively, and N_{ij}, M_{ij} and V_i , ($i, j=1, 2$) are respectively the membrane, moment and transverse shear resultants. It will further be assumed that the through crack problem for the plate or the shell has already been formulated and has been reduced to a system of integral equations. In the solutions given in [21]-[24] the derivatives of the crack surface displacement and the crack surface rotation on the neutral surface are assumed to be the unknown functions in the integral equations. This comes quite naturally out of the formulation of the related mixed boundary value problem for the plate or the shell. For a symmetric problem of a through crack (located in one of the principal planes of curvature) along $-a < x_1 < a$ in a plate or shell under Mode I loading conditions, invariably the integral equations are of the following form:

$$\begin{aligned} \frac{a(1-\nu^2)}{2\pi h\lambda^4} \int_{-1}^1 \left[\frac{3+\nu}{1+\nu} \frac{1}{t-x} + k_{11}(x,t) \right] g_1(t) dt + \int_{-1}^1 k_{12}(x,t) g_2(t) dt \\ = -\frac{m_\infty}{6E} + \frac{m(x)}{6E}, \quad -1 < x < 1, \end{aligned} \quad (4)$$

$$\begin{aligned} \frac{1}{2\pi} \int_{-1}^1 \frac{g_2(t)}{t-x} dt + \int_{-1}^1 [k_{21}(x,t) g_1(t) + k_{22}(x,t) g_2(t)] dt \\ = -\frac{\sigma_\infty}{E} + \frac{\sigma(x)}{E}, \quad -1 < x < 1, \end{aligned} \quad (5)$$

where the unknown functions are defined by

$$g_1(x) = \frac{\partial}{\partial x} \beta_y(x, +0), \quad g_2(x) = \frac{\partial}{\partial x} v(x, +0), \quad \beta_y = \beta_2, \quad \nu = \frac{u_2}{a}. \quad (6)$$

The external loads

$$\sigma_{\infty} = N_{22}^{\infty}/h, \quad m_{\infty} = 6M_{22}^{\infty}/h^2 \quad (7)$$

represent uniform membrane and bending resultant applied to the plate or the shell away from the crack region (Fig. 3a) and σ and m which are defined by

$$\sigma(x) = N(x_1, 0)/h, \quad m(x) = 6M(x_1, 0)/h^2, \quad (-1 < x < 1, x = x_1/a) \quad (8)$$

are the membrane and bending loads applied to the crack surfaces (Fig. 3d). $2a$ is the length and $L(x_1)$ the depth of the part-through crack^(*). The thickness h and the principal radii of curvature R_1 and R_2 are the other length parameters of the structure. The formulation is given in terms of the dimensionless quantities defined in Table 1. E and ν are the elastic constants of the material. The integral equations are obtained from the following mixed boundary conditions in $x_2 = 0$ plane (Fig. 3d):

$$N_{22}(x_1, 0) = -N_{22}^{\infty} + N(x_1), \quad -a < x_1 < a, \quad (9a)$$

$$u_2(x_1, 0) = 0, \quad |x_1| > a, \quad (9b)$$

$$M_{22}(x_1, 0) = -M_{22}^{\infty} + M(x_1), \quad -a < x_1 < a, \quad (10a)$$

$$\beta_2(x_1, 0) = 0, \quad |x_1| > a, \quad (10b)$$

where the general principle of superposition is used to account for the loading N_{22}^{∞} and M_{22}^{∞} applied to the structure away from the crack region. From $v = u_2/a$, $\beta_y = \beta_2$ and the definitions (6) it follows that the unknown functions g_1 and g_2 must satisfy the single-valuedness conditions given by

$$\int_{-1}^1 g_1(t) dt = 0, \quad \int_{-1}^1 g_2(t) dt = 0. \quad (11)$$

(*) Clearly any additional known external loads may be accommodated by using the notion of superposition and thereby adding appropriate functions to the right hand sides of (4) and (5).

In all Mode I plate and shell problems the dominant part of the kernels in (4) and (5) namely, the terms having the Cauchy singularity $1/(t-x)$ are the same. The Fredholm kernels k_{ij} , ($i,j=1,2$) represent the details of the plate or shell geometry. For the through crack problem in plates the integral equations (4) and (5) are uncoupled, i.e., $k_{12}=0$, $k_{21}=0$. Thus, the through crack problem for the plate under membrane and bending loads can be solved separately. As will be shown below, in the case of a part-through crack the equations are coupled through the loading terms $\sigma(x)$ and $m(x)$ (which are also unknown). For example, for an infinite plate (4) (5) may be expressed as [12-14], [21]

$$\frac{a(1-\nu^2)}{2\pi h\lambda^4} \int_{-1}^1 \left[\frac{3+\nu}{1+\nu} \frac{1}{t-x} - \frac{4\kappa(1-\nu)}{1+\nu} \frac{1}{(t-x)^3} + \frac{4}{1+\nu} \frac{1}{t-x} K_2(\alpha|t-x|) \right] g_1(t) dt = -\frac{m_\infty}{6E} + \frac{m(x)}{6E}, \quad -1 < x < 1, \quad (12)$$

$$\frac{1}{2\pi} \int_{-1}^1 \frac{1}{t-x} g_2(t) dt = -\frac{\sigma_\infty}{E} + \frac{\sigma(x)}{E}, \quad -1 < x < 1, \quad (13)$$

$$\alpha = [2/\kappa(1-\nu)]^{1/2}, \quad (14)$$

where K_2 is the modified Bessel function of the second kind and the constants λ and κ are defined in Table 1. In shells the kernels k_{ij} , ($i,j=1,2$) are always nonzero.

Let us now assume that the local plate or shell geometry is represented by Fig. 3 and for simplicity we also assume that the structure contains only a single surface crack as shown in Fig. 3c. Let $N(x_1)$ and $M(x_1)$ be the membrane and bending resultants acting on the neutral surface which are statically equivalent to the net ligament stress $\sigma_{22}(x_1, 0, x_3)$, ($-a < x_1 < a, -h/2 < x_3 < h/2 - L(x_1)$) (Fig. 3c). The first approximating assumption made in introducing the line spring model is that the crack may now be assumed as being a through crack of length $2a$ (Fig. 3d) and the constraint caused by the net ligament stress $\sigma_{22}(x_1, 0, x_3)$ (tending to prevent the crack faces from opening and rotating) may be accounted for by applying the membrane and bending resultants $N(x_1)$ and $M(x_1)$ on the crack surfaces. Note that N and M tend to close the crack surfaces whereas the external loads N_{22}^∞ and M_{22}^∞ tend to open them.

The second major assumption made in developing the model is that the stress intensity factor at a location x_1 along the crack front may be approximated by the corresponding plane strain value obtained from a plate which contains an edge crack of (uniform) depth $L(x_1)$ and which is subjected to uniform bending moment $M(x_1)$ and uniform tension $N(x_1)$ away from the crack region (Fig. 3c). This assumption makes it possible to express $N(x_1)$ and $M(x_1)$ in terms of the unknown functions g_1 and g_2 in (4) and (5), which may then be solved in a straightforward manner. It should again be emphasized that it is because of these two rather gross approximating assumptions that a basically intractable three-dimensional problem is reduced to a relatively straightforward plate or shell problem.

In order to obtain N and M in terms of g_1 and g_2 the energy available for fracture along the crack front is expressed in two different ways, namely as the crack closure energy and as the product of load-load point displacement. In a plate with an edge crack subjected to a uniform tension N and uniform bending moment M (Fig. 4a), if K_1 is the stress intensity factor given by the plane strain solution, from the crack closure energy the energy (per unit width) available for fracture may be obtained as

$$G = \frac{\partial}{\partial L} (U-V) = \frac{1-\nu^2}{E} K_1^2 \quad (15)$$

where U is the work done by the external loads and V is the strain energy.

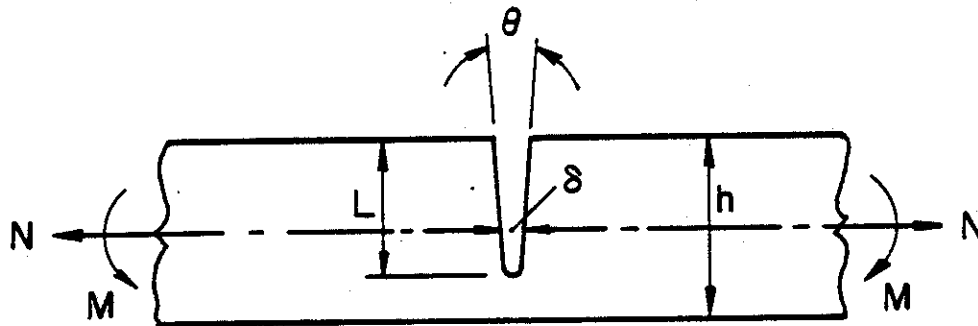
Now, let δ and θ be the load line "displacements" corresponding to N and M as shown in Fig. 4a. Let $d\delta$ and $d\theta$ be the changes in δ and θ as the crack length goes from L to $L+dL$ under "fixed load" conditions. Then referring to Fig. 4b the changes in U and V may be expressed as

$$dU = Nd\delta + Md\theta \quad , \quad (16)$$

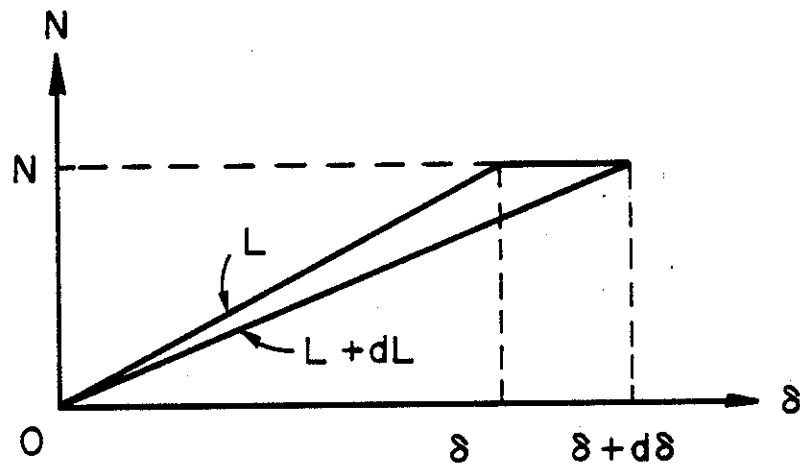
$$dV = \frac{1}{2} [N(\delta+d\delta) + M(\theta+d\theta)] - \frac{1}{2} (N\delta + M\theta) = \frac{1}{2} (Nd\delta + Md\theta) \quad . \quad (17)$$

Equations (13) and (14) give the energy available for a crack growth dL as follows:

$$d(U-V) = \frac{1}{2} (Nd\delta + Md\theta) \quad . \quad (18)$$



(a)



(b)

Fig. 4 Notation for the related plane strain problem.

On the other hand for constant N and M and for a change of dL in the crack length we have

$$d\delta = \frac{\partial\delta}{\partial L} dL, \quad d\theta = \frac{\partial\theta}{\partial L} dL. \quad (19)$$

Thus, from (15) and (16) it follows that

$$\frac{\partial}{\partial L} (U-V) = G = \frac{1}{2} \left(N \frac{\partial\delta}{\partial L} + M \frac{\partial\theta}{\partial L} \right), \quad (20)$$

and, by using (12) we find

$$\frac{1}{2} \left(N \frac{\partial\delta}{\partial L} + M \frac{\partial\theta}{\partial L} \right) = \frac{1-\nu^2}{E} K_1^2. \quad (21)$$

Let us now define the membrane and bending stresses by

$$\sigma = N/h, \quad m = 6M/h^2 \quad (22)$$

and assume that the solution of the plane strain problem shown in Fig. 4a give the stress intensity factor as follows:

$$K_1 = \sqrt{h} [\sigma g_t(s) + m g_b(s)], \quad s = L/h, \quad (23)$$

where g_t and g_b are known functions. If we also define the following matrices

$$\tau = (\tau_i) = \begin{bmatrix} m \\ \sigma \end{bmatrix}, \quad \omega = (\omega_i) = \begin{bmatrix} h \\ \delta \end{bmatrix}, \quad G(s) = (g_{ij}) = \begin{bmatrix} g_b^2 & g_t g_b \\ g_t g_b & g_t^2 \end{bmatrix}, \quad (24)$$

from (15) and (23) we obtain

$$G = \frac{1-\nu^2}{E} K_1^2 = \left(\frac{1-\nu^2}{E} h \right) \tau^T G \tau. \quad (25)$$

Similarly, from (20), (22) and (24) we find

$$G = \frac{1}{2} (h\tau_2 \frac{\partial \omega_2}{\partial L} + \frac{h^2}{6} \tau_1 \frac{6}{h} \frac{\partial \omega_1}{\partial L}) = \frac{h}{2} \tau^T \frac{\partial \omega}{\partial L} \quad (26)$$

From (25) and (26) it is seen that

$$\frac{\partial \omega}{\partial L} = \frac{2}{E} (1-v^2) G \tau \quad (27)$$

By observing that G is a function of L , τ is independent of L and $\omega=0$ for $L=0$, from (27) we find

$$\omega = \frac{2}{E} (1-v^2) \left(\int_0^L G dL \right) \tau = \frac{2}{E} (1-v^2) A \tau, \quad A = \int_0^L G dL \quad (28)$$

If we also define

$$B = \begin{bmatrix} h/6 & 0 \\ 0 & a \end{bmatrix}, \quad n = \begin{bmatrix} \beta_y(x,+0) \\ v(x,+0) \end{bmatrix} \quad (29)$$

from $\delta = 2u_2(x_1,0) = 2av(x,0)$, $\theta = 2\beta_2(x_1,0) = 2\beta_y(x,0)$ and (28), (29), and (6) it may be seen that

$$\tau = \frac{E}{1-v^2} A^{-1} B n, \quad C(x) = \frac{1}{1-v^2} A^{-1} B, \quad \tau = EC \begin{bmatrix} \int_{-1}^x g_1(t) dt \\ \int_{-1}^x g_2(t) dt \end{bmatrix} \quad (30)$$

Note that since $L = L(x_1) = L(ax)$ is a known function of x the matrix A and consequently $C = (1-v^2)^{-1} A^{-1} B$ consist of also known functions of x .

Substituting now from (30) into (4) and (5) we obtain

$$\begin{aligned} \frac{a(1-v^2)}{2\pi h \lambda^4} \int_{-1}^1 \left[\frac{3+v}{1+v} \frac{1}{t-x} + k_{11}(x,t) \right] g_1(t) dt + \int_{-1}^1 k_{12}(x,t) g_2(t) dt \\ - \frac{c_{11}(x)}{6} \int_{-1}^x g_1(t) dt - \frac{c_{12}(x)}{6} \int_{-1}^x g_2(t) dt = -\frac{m_\infty}{6E}, \quad -1 < x < 1, \end{aligned} \quad (31)$$

$$\begin{aligned} \frac{1}{2\pi} \int_{-1}^1 \frac{1}{t-x} g_2(t) dt + \int_{-1}^1 [k_{21}(x,t) g_1(t) + k_{22}(x,t) g_2(t)] dt \\ - c_{21}(x) \int_{-1}^x g_1(t) dt - c_{22}(x) \int_{-1}^x g_2(t) dt = -\frac{\sigma_\infty}{E}, \quad -1 < x < 1, \end{aligned} \quad (32)$$

where the functions c_{ij} are the elements of C which is defined by (30).

The functions g_t and g_b giving the stress intensity factor in an edge-notched strip as defined by (23) (see Fig. 4a), and the elements of the matrix A defined by (28) are given in [21]. The functions g_t and g_b valid for $0 < L/h \leq 0.8$ were obtained as follows [21]:

$$g_t(s) = \sqrt{\pi s} (1.1215 + 6.5200s^2 - 12.3877s^4 + 89.0554s^6 - 188.6080s^8 + 207.3870s^{10} - 32.0524s^{12}), \quad s = L/h, \quad (33)$$

$$g_b(s) = \sqrt{\pi s} (1.1202 - 1.8872s + 18.0143s^2 - 87.3851s^3 + 241.9124s^4 - 319.9402s^5 + 168.0105s^6), \quad s = L/h. \quad (34)$$

The dominant part of the system of integral equations (31) and (32) has only a Cauchy kernel and, therefore, the solution is of the following form:

$$g_i(t) = \frac{f_i(t)}{\sqrt{1-t^2}}, \quad i = 1, 2 \quad (35)$$

where the functions f_1 and f_2 are bounded in the closed interval $-1 \leq t \leq 1$. Even in the simplest case (of the infinite plate considered in [21]) the system has no closed form solution. However, the unknown functions f_1 and f_2 may be determined numerically within any desired degree of accuracy by using the quadrature formulas given, for example, in [28]. After determining f_1 and f_2 the net ligament resultants m and σ are obtained from (27) and the stress intensity factor from (23).

2.3 Internal Cracks

The line spring model described in the previous section may easily be extended to internal cracks such as that, for example, shown in Fig. 3b. In this case the basic integral equations for a through crack in a plate or shell under membrane or bending loads remain the same and are again given by (4) and (5). The major difference is in expressing the resultants $\sigma(x)$ and $m(x)$ of the net ligament stress $\sigma_{22}(x_1, 0, x_3)$ in terms of δ and θ or

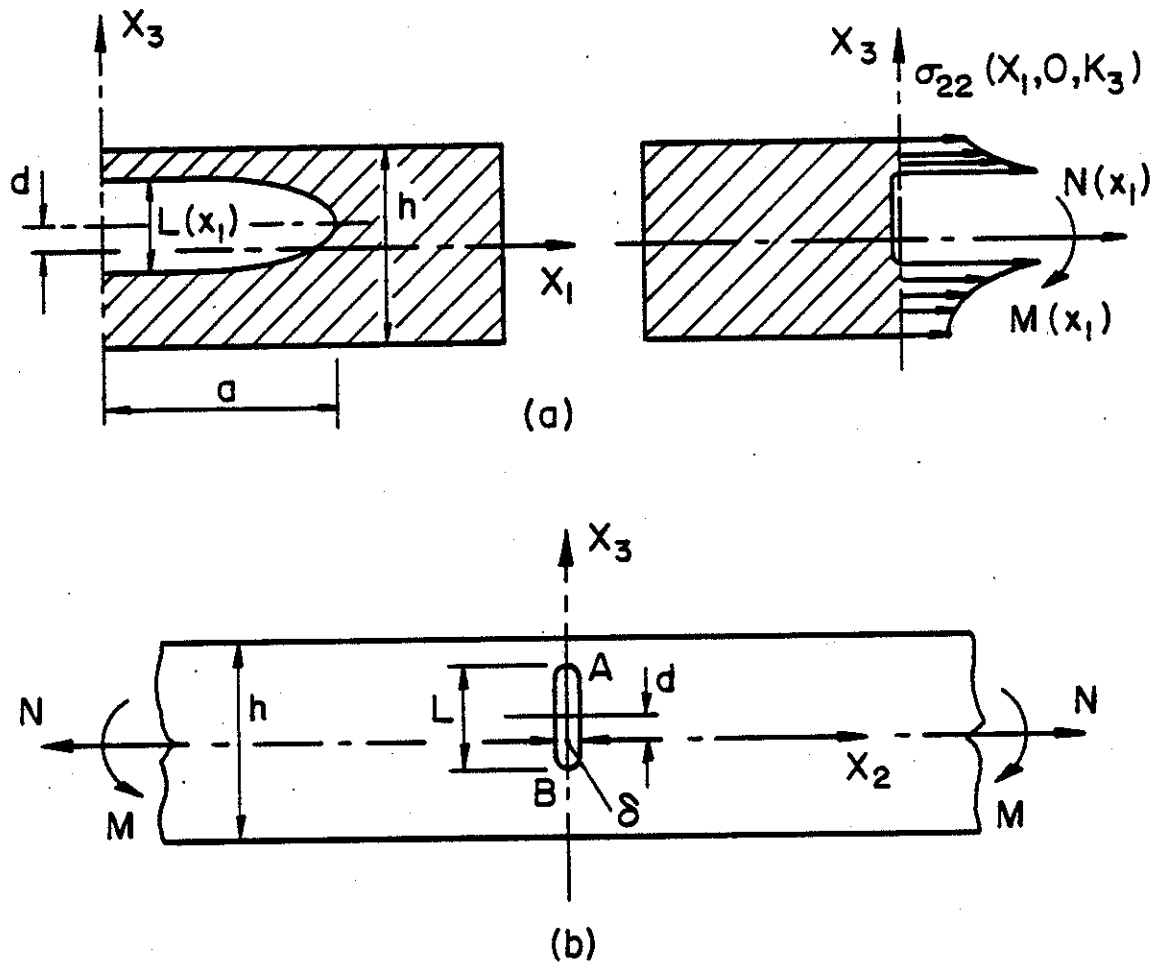


Fig. 5 Geometry and notation for an internal crack.

$v(x)$ and $\beta_y(x)$ which represent the crack opening displacement and rotation on the load line (Fig. 5). Let the plane internal crack be defined by

$$-a < x_1 < a, \quad x_2 = 0, \quad d - \frac{L(x_1)}{2} < x_3 < d + \frac{L(x_1)}{2} \quad (36)$$

where, for simplicity, d is assumed to be constant. Thus, if K_A and K_B are the stress intensity factors at the crack tips A and B in the corresponding plane strain problem shown in Fig. 5b, as L increases by dL the energy increment available for fracture may be expressed as

$$d(U-V) = \frac{1-\nu^2}{E} [K_A^2 d(L/2) + K_B^2 d(L/2)] \quad (37)$$

giving

$$G = \frac{\partial}{\partial L} (U-V) = \frac{1-\nu^2}{2E} (K_A^2 + K_B^2) \quad (38)$$

which replaces (15). The rate of energy available for fracture as expressed in terms of load line "displacements" and "forces" remains the same and is given by (20).

Let us now assume that the stress intensity factors for the plane strain problem shown in Fig. 5b are known as follows:

$$K_A = \sqrt{h} [\sigma g_{At}(s) + m g_{Ab}(s)], \quad s = L/h, \quad (39)$$

$$K_B = \sqrt{h} [\sigma g_{Bt}(s) + m g_{Bb}(s)], \quad s = L/h \quad (40)$$

where σ and m are again given by (22). The solution of the problem is given in [29] from which the functions g_{At} , g_{Ab} , g_{Bt} and g_{Bb} are obtained by a suitable curve-fitting. It is clear that the derivation given in the previous section, particularly the integral equations (31) and (32) will remain unchanged and the only change will be in the matrix $G(s)$ defined by (24). For the internal crack problem shown in Fig. 5 the matrix G now becomes

$$G(s) = \frac{1}{2} \begin{bmatrix} g_{Ab}^2 + g_{Bb}^2 & g_{Ab}g_{At} + g_{Bb}g_{Bt} \\ g_{Ab}g_{At} + g_{Bb}g_{Bt} & g_{At}^2 + g_{Bt}^2 \end{bmatrix} \quad (41)$$

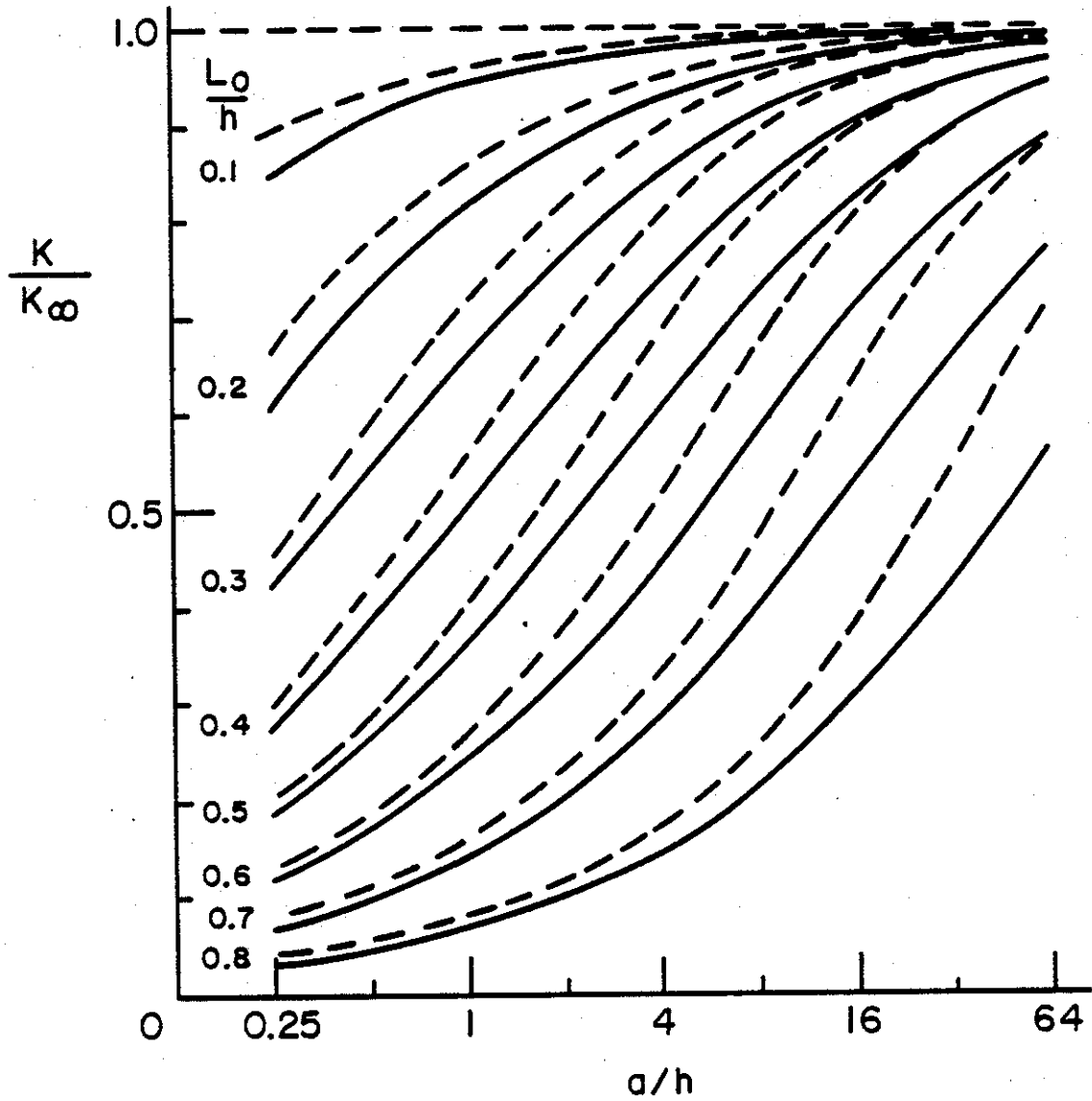
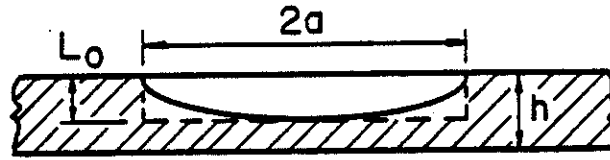


Fig. 6 Stress intensity factors for a semi-elliptic (full lines) and a rectangular (dashed lines) surface crack in a plate under uniform tension ($\nu=0.3$).

and the matrices τ , A and C are again defined by (27)-(30). After solving the integral equations (31) and (32) for g_1 and g_2 , σ and m are obtained from (24) and (30) and the stress intensity factors from (39) and (40).

From the derivation of the model given in this report it is clear that the technique can be used to estimate the stress intensity factors in any plate or shell containing part-through cracks provided the integral equations for the corresponding through crack problem is available and the related plane strain crack problem has a reliable solution which can be properly parametrized. Thus, extending the method to such problems as the corner cracks [14], collinear surface or internal cracks [24], part-through cracks in reinforced plates and shells, and other crack-crack and crack-boundary interaction problems becomes quite straightforward.

2.4 Some Results

As noted before for the application of the line spring model the contour of the part-through crack can be any reasonable curve provided the crack is relatively long (i.e., $a > h$). Figure 6 shows the stress intensity factor in an infinite plate containing a surface crack and subjected to uniform membrane loading N_{22}^{∞} away from the crack region: The normalizing stress intensity factor K_{∞} which is defined by

$$K_{\infty} = \left(\frac{N_{22}^{\infty}}{h}\right) \sqrt{h} g_t(s_0), \quad s_0 = L_0/h \quad (42)$$

is the corresponding plane strain value for an edge-cracked strip (see eq. 33). The figure shows the stress intensity factor at the midsection (i.e., at $x_1=0$) of a semi-elliptic and a rectangular crack respectively defined by

$$L(x_1) = L_0 \sqrt{1-(x_1/a)^2} = L_0 \sqrt{1-x^2}, \quad L(x_1) = L_0, \quad -a < x_1 < a \quad (43)$$

Note that the limiting values of the stress intensity factor are

$$K \rightarrow 0 \quad \text{for} \quad a/h \rightarrow 0; \quad K \rightarrow K_{\infty} \quad \text{for} \quad a/h \rightarrow \infty \quad (44)$$

As one may expect, the stress intensity factor for the rectangular crack is somewhat greater than that for the semi-elliptic crack and converges faster to the asymptotic value K_{∞} as $a/h \rightarrow \infty$.

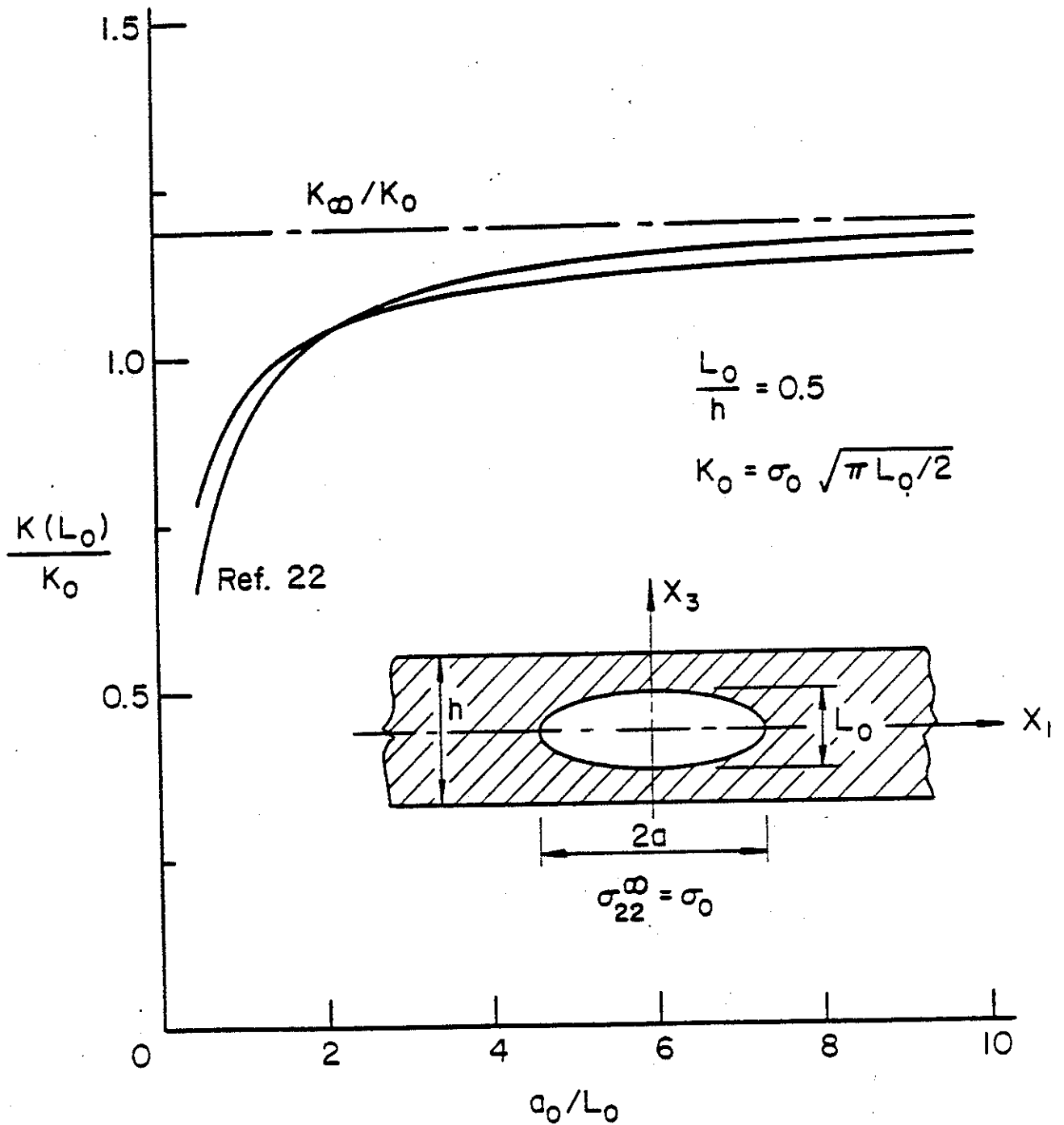


Fig. 7 Stress intensity factor at the mid section of a symmetrically located elliptic crack in a plate under uniform tension; $\sigma_{22}^\infty = \sigma_0$, $L_0/h = 0.5$, $K_0 = \sigma_0 \sqrt{\pi L_0/2}$; K_∞ is the corresponding plane strain value in a strip (i.e., for $a_0 = \infty$).

From a viewpoint of applying the line spring model perhaps the simplest part-through crack problem is that of a symmetrically located internal crack in an infinite plate under uniform tension (see the insert in Fig. 7). In this case since there is no bending the problem is reduced to a simple integral equation given by (32) in which k_{21} , k_{22} and c_{21} are zero. In (41) $g_{At} = g_{Bt}$ and $G(s)$ reduces to g_{At}^2 and the function c_{22} becomes

$$c_{22}(x) = a[(1-\nu^2)] \int_0^{L(x)} g_{At}^2(L/h)dL]^{-1}. \quad (45)$$

Figure 7 shows the result of a simple example which is compared with that given in [30] for a plate containing a symmetrically located elliptic crack and subjected to uniform tension $\sigma_0 = N_{22}^\infty/h$.

If the plate is also subjected to uniform bending moment M_{22}^∞ , then in (41) $g_{Ab} = -g_{Bb}$ and $g_{At} = g_{Bt}$ and the integral equations (31) and (32) would be uncoupled. It should, however, be noted that because of crack closure on the compression side, in this case taken separately the bending results are meaningless. They may be used together with tension results which are sufficiently large so that the stress intensity factors on both sides of the crack are positive. The functions g_{At} and g_{Ab} are obtained from the results given in [29] as follows:

$$g_{At}(s) = \sqrt{\pi s} \sum_1^n b_j s^{2(j-1)}, \quad s = L/h, \quad (46)$$

$$g_{Ab}(s) = \sqrt{\pi s} \sum_1^n c_j s^{j-1}, \quad s = L/h \quad (47)$$

where the constants b_j and c_j are given in Table 2 which is based on the stress intensity ratios shown in Table 3 (see [29]). Extensive results for multiple part-through cracks of various configurations will be provided in a subsequent report.

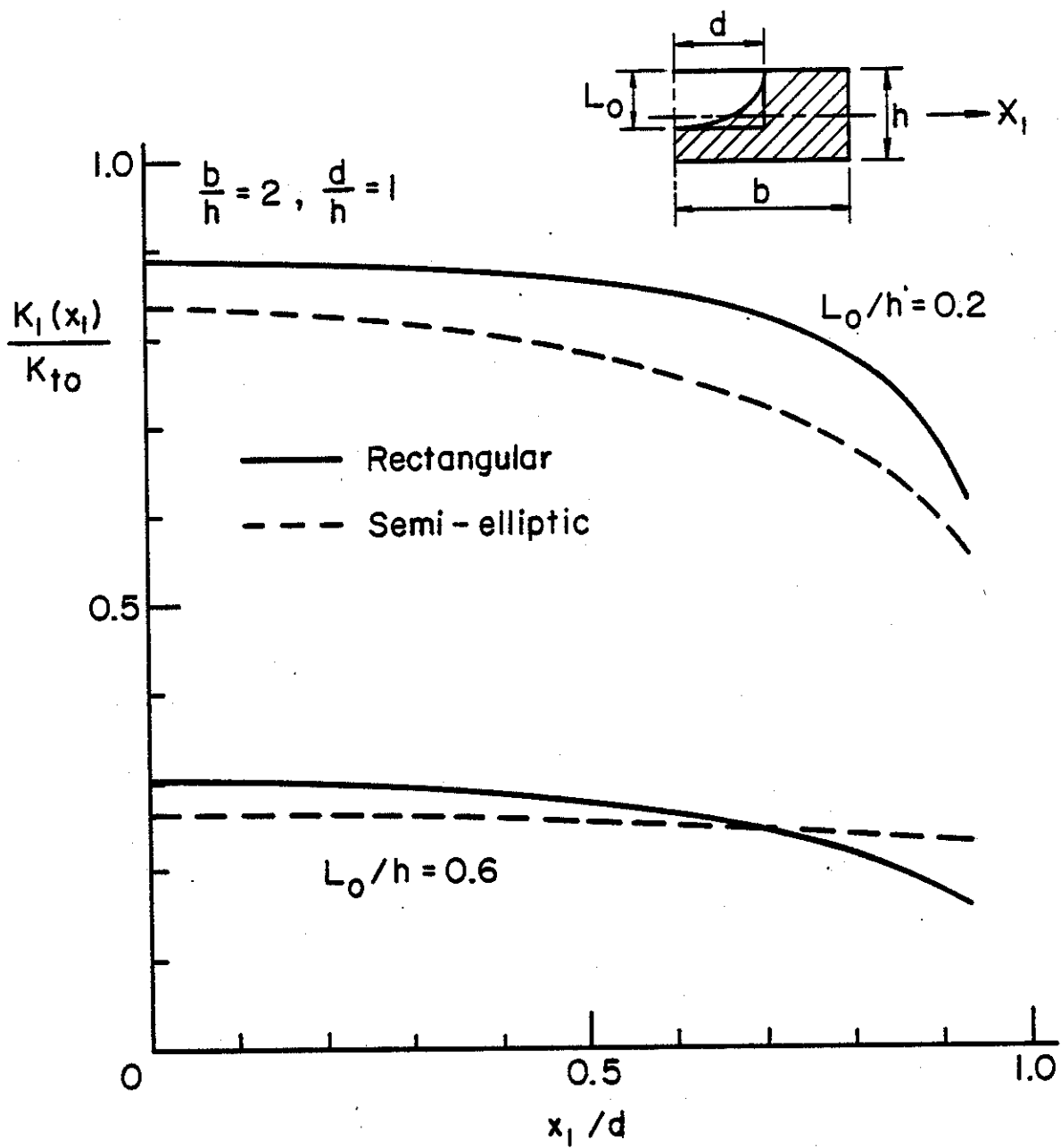


Fig. 8 Stress intensity factors for a semi-elliptic (dashed lines) and a rectangular (full lines) surface crack in a plate of finite width under uniform tension N_{22}^{∞} .

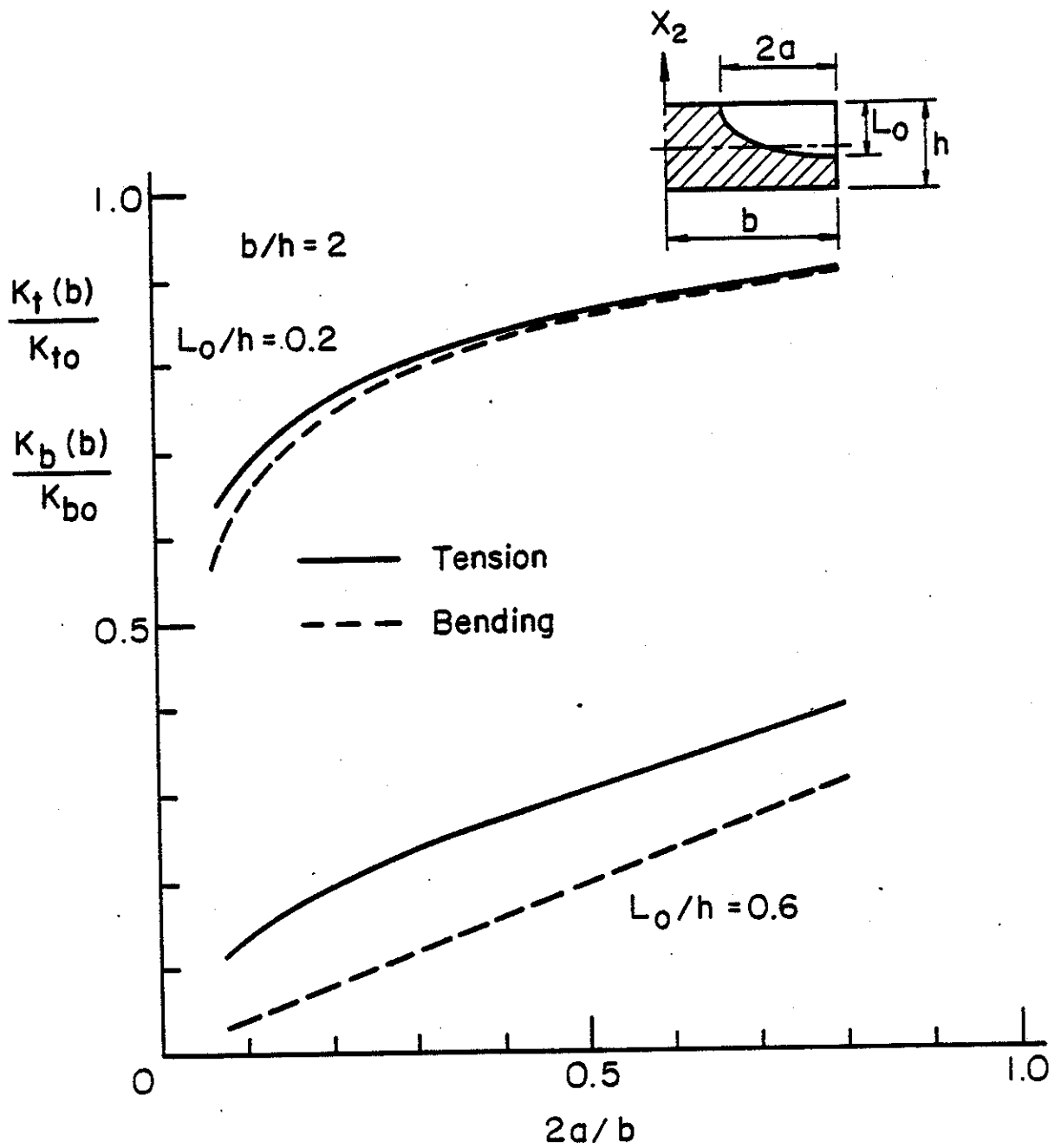


Fig. 9 Stress intensity factors in a plate of finite width containing two symmetrically located quarter elliptic corner cracks and subjected to uniform tension N_{22}^{∞} or bending M_{22}^{∞} .

The problem of a plate having a finite width with the emphasis on collinear part-through cracks and corner cracks was considered in [24]. Figures 8 and 9 show some sample results for central and corner cracks. Figure 8 shows the comparison of the stress intensity factors along the crack front for a symmetrically located, semi-elliptic and a rectangular surface crack in a plate under uniform tension. The normalizing stress intensity factors K_{t0} and K_{b0} shown in Figures 8 and 9 are defined by

$$K_{t0} = \left(\frac{N_{22}^{\infty}}{h}\right) \sqrt{h} g_t(s_0), \quad K_{b0} = \left(\frac{6M_{22}^{\infty}}{h^2}\right) \sqrt{h} g_b(s_0), \quad s_0 = \frac{L_0}{h} \quad (48)$$

and are the corresponding plane strain values for an edge-cracked strip under tension or bending. Figure 9 shows the stress intensity factor at the free surfaces of the plate $x_1 = \pm b$ in a plate containing two symmetric corner cracks under uniform tension or bending with crack length being the variable.

The form of the integral equations such as that given by (31) and (32) is quite general and is applicable to a great variety of part-through crack problems in plates and shells. The details of the problem influence only the kernels k_{ij} . The analysis and extensive results for collinear surface cracks and for corner cracks in a plate of finite width are given in Appendix A of this report.

Extensive results for an infinite cylindrical shell containing an external or internal, axial or circumferential part-through crack under local membrane loading or bending moment may be found in [9] (see, also [23] for some of the results). Tables 4 and 5 show some sample results for a 24 in. diameter pipe. The crack profile is again semi-elliptic which is defined by (43). The normalizing stress intensity factor K_0 used in these tables is the corresponding edge crack plane strain value and is defined by (48a) for $N_{22}^{\infty} = N_{\infty} \neq 0$, $M_{22}^{\infty} = M_{\infty} = 0$ and by (48b) $N_{22}^{\infty} = N_{\infty} = 0$, $M_{22}^{\infty} = M_{\infty} \neq 0$.

2.5 Conclusions

Despite its simplicity, if carefully applied the line spring model may give very useful results for certain group of three-dimensional surface and internal cracks which are otherwise analytically intractable. The application of the model to the plasticity problems in plates and shells appears to be

also highly promising [19], [20], [25]. If the material has no strain hardening, then the plastic line spring reduces to some version of the Dugdale model which can be analyzed in a relatively straightforward manner [9], [23], [26]. The extension of the model to mixed mode part-through crack problems in plates and shells is being studied and appears to be quite feasible.

Table 1

Table 1. The dimensionless quantities used in plate and shell problems.

$$x = x_1/a, y = x_2/a, z = x_3/a,$$

$$u = u_1/a, v = u_2/a, w = u_3/a,$$

$$\beta_x = \beta_1, \beta_y = \beta_2,$$

$$\lambda_1^4 = 12(1-\nu^2) \frac{a^4}{h^2 R_1^2}, \lambda_2^4 = 12(1-\nu^2) \frac{a^4}{h^2 R_2^2},$$

$$\lambda^4 = 12(1-\nu^2) \frac{a^2}{h^2}, \kappa = \frac{h^2}{5(1-\nu)a^2}$$

R_1, R_2 : principal radii of curvature

Table 2. The coefficients b_j and c_j for the shape functions g_{At} and g_{Ab} (eqs. 46 and 47).

j	b_j	c_j
1	0.7071	0.1013
2	0.4325	-2.7775
3	-0.1091	90.3734
4	7.3711	-862.4307
5	-57.7894	4843.4692
6	271.1551	-17069.1142
7	-744.4204	38813.4897
8	1183.9529	-56865.3055
9	-1001.4920	51832.6941
10	347.9786	-26731.2995
11		5959.4888

Table 3. Stress intensity factors for a centrally cracked plate subjected to tension (N) or bending (M) under plane strain conditions, ($\sigma=N/h$, $m=6M/h^2$; Fig. 5b).

L/h	$\frac{K_N}{\sigma\sqrt{\pi L/2}}$	$\frac{K_M}{m\sqrt{\pi L/2}}$
0.05		0.1500
0.1	1.0060	0.3000
0.2	1.0246	0.6004
0.3	1.0577	0.9031
0.4	1.1094	1.2135
0.5	1.1867	1.5435
0.6	1.3033	1.9179
0.7	1.4884	2.3918
0.8	1.8169	3.1113
0.9	2.585	4.6653
0.95	4.252	6.8526

Table 4. K/K_0 in a line pipe with OD = 24 in., $h = 0.344$ in.

L_0/h	0.1	0.2	0.3	0.4	0.5	0.6	0.7	0.8	0.9
Outer circumferential crack, $N_\infty \neq 0, M_\infty = 0$									
1.0	0.945	0.817	0.664	0.508	0.366	0.247	0.147	0.073	0.033
2.0	0.967	0.882	0.766	0.628	0.481	0.340	0.210	0.106	0.048
3.0	0.976	0.911	0.817	0.695	0.553	0.405	0.257	0.132	0.060
4.0	0.980	0.928	0.847	0.739	0.604	0.455	0.297	0.155	0.070
5.0	0.983	0.938	0.868	0.769	0.642	0.493	0.329	0.175	0.080
6.0	0.985	0.945	0.882	0.791	0.670	0.524	0.357	0.193	0.088
7.0	0.987	0.950	0.892	0.807	0.692	0.549	0.380	0.209	0.097
8.0	0.987	0.953	0.899	0.819	0.709	0.570	0.400	0.223	0.104
Outer circumferential crack, $N_\infty = 0, M_\infty \neq 0$									
1.0	0.944	0.805	0.627	0.443	0.273	0.133	0.040	-0.011	-0.034
2.0	0.966	0.874	0.741	0.581	0.407	0.242	0.109	0.020	-0.028
3.0	0.975	0.905	0.798	0.657	0.492	0.318	0.164	0.048	-0.021
4.0	0.980	0.923	0.832	0.707	0.551	0.376	0.209	0.072	-0.012
5.0	0.983	0.934	0.854	0.741	0.594	0.421	0.246	0.094	-0.004
6.0	0.985	0.941	0.869	0.765	0.626	0.457	0.277	0.114	0.005
7.0	0.986	0.946	0.880	0.783	0.651	0.485	0.303	0.131	0.013
8.0	0.987	0.950	0.888	0.797	0.670	0.508	0.325	0.146	0.020
Inner circumferential crack, $N_\infty \neq 0, M_\infty = 0$									
1.0	0.944	0.814	0.659	0.503	0.361	0.243	0.145	0.073	0.033
2.0	0.965	0.877	0.756	0.615	0.467	0.327	0.201	0.102	0.048
3.0	0.974	0.904	0.803	0.675	0.530	0.383	0.241	0.124	0.058
4.0	0.978	0.919	0.831	0.714	0.573	0.423	0.271	0.141	0.066
5.0	0.981	0.929	0.849	0.740	0.604	0.453	0.296	0.156	0.074
6.0	0.983	0.935	0.862	0.759	0.628	0.477	0.316	0.168	0.080
7.0	0.984	0.940	0.871	0.773	0.646	0.497	0.332	0.179	0.086
8.0	0.985	0.943	0.878	0.784	0.660	0.513	0.347	0.189	0.091
Inner circumferential crack, $N_\infty = 0, M_\infty \neq 0$									
1.0	0.943	0.801	0.621	0.436	0.267	0.129	0.037	-0.012	-0.034
2.0	0.964	0.868	0.729	0.565	0.390	0.226	0.099	0.015	-0.030
3.0	0.973	0.897	0.782	0.634	0.463	0.291	0.143	0.037	-0.024
4.0	0.977	0.914	0.813	0.677	0.513	0.337	0.177	0.055	-0.018
5.0	0.980	0.924	0.833	0.706	0.548	0.372	0.204	0.070	-0.012
6.0	0.982	0.931	0.846	0.728	0.575	0.399	0.227	0.084	-0.007
7.0	0.983	0.936	0.856	0.743	0.595	0.421	0.246	0.095	-0.002
8.0	0.984	0.939	0.864	0.755	0.611	0.439	0.261	0.105	0.003

Table 5. K/K_0 in a line pipe with OD = 24 in., $h = 0.344$ in.

L/h	0.1	0.2	0.3	0.4	0.5	0.6	0.7	0.8	0.9
Outer axial crack, $N_\infty \neq 0, M_\infty = 0$									
1.0	0.946	0.820	0.668	0.512	0.370	0.250	0.149	0.074	0.033
2.0	0.968	0.887	0.774	0.639	0.492	0.350	0.217	0.110	0.050
3.0	0.977	0.917	0.829	0.712	0.574	0.425	0.273	0.142	0.063
4.0	0.983	0.935	0.863	0.762	0.634	0.485	0.323	0.171	0.077
5.0	0.986	0.947	0.886	0.797	0.679	0.535	0.367	0.200	0.090
6.0	0.988	0.955	0.902	0.824	0.715	0.577	0.406	0.227	0.103
7.0	0.990	0.961	0.914	0.844	0.744	0.611	0.441	0.253	0.117
8.0	0.991	0.965	0.924	0.860	0.767	0.640	0.472	0.277	0.130
Outer axial crack; $N_\infty = 0, M_\infty \neq 0$									
1.0	0.944	0.807	0.631	0.448	0.278	0.137	0.042	-0.010	-0.034
2.0	0.967	0.879	0.750	0.593	0.421	0.255	0.118	0.025	-0.027
3.0	0.977	0.912	0.811	0.678	0.517	0.343	0.183	0.059	-0.016
4.0	0.982	0.931	0.849	0.734	0.586	0.415	0.241	0.092	-0.005
5.0	0.985	0.944	0.875	0.775	0.639	0.473	0.292	0.124	0.008
6.0	0.988	0.952	0.893	0.805	0.681	0.521	0.338	0.155	0.022
7.0	0.989	0.959	0.907	0.828	0.713	0.562	0.378	0.183	0.036
8.0	0.991	0.963	0.917	0.845	0.740	0.595	0.413	0.210	0.050
Inner axial crack, $N_\infty \neq 0, M_\infty = 0$									
1.0	0.944	0.815	0.660	0.504	0.362	0.244	0.145	0.073	0.034
2.0	0.966	0.879	0.760	0.620	0.472	0.332	0.205	0.104	0.049
3.0	0.975	0.908	0.810	0.685	0.542	0.394	0.250	0.130	0.060
4.0	0.980	0.925	0.842	0.730	0.593	0.443	0.288	0.151	0.071
5.0	0.983	0.937	0.864	0.762	0.632	0.483	0.321	0.172	0.081
6.0	0.985	0.945	0.880	0.787	0.664	0.517	0.351	0.191	0.090
7.0	0.987	0.951	0.892	0.807	0.690	0.546	0.378	0.209	0.099
8.0	0.988	0.956	0.902	0.823	0.713	0.572	0.402	0.226	0.108
Inner axial crack, $N_\infty = 0, M_\infty \neq 0$									
1.0	0.943	0.802	0.622	0.437	0.268	0.129	0.038	-0.012	-0.034
2.0	0.965	0.871	0.734	0.570	0.396	0.232	0.103	0.017	-0.029
3.0	0.974	0.902	0.790	0.646	0.478	0.305	0.154	0.043	-0.022
4.0	0.979	0.920	0.825	0.696	0.537	0.362	0.198	0.066	-0.014
5.0	0.983	0.932	0.850	0.733	0.583	0.409	0.236	0.090	-0.005
6.0	0.985	0.941	0.868	0.762	0.620	0.449	0.270	0.110	0.004
7.0	0.987	0.948	0.882	0.784	0.650	0.484	0.301	0.131	0.013
8.0	0.988	0.953	0.893	0.803	0.676	0.514	0.330	0.150	0.022

3. THE INTERACTION BETWEEN FLAT INCLUSIONS OF FINITE THICKNESS AND CRACKS

3.1 Introduction

In studying the strength and fracture of welded components it is often necessary to take into account, among other factors, the effect of the imperfections in the material. Generally such imperfections are in the form of either geometric discontinuities or material inhomogeneities. For example, in welded joints, various shapes of voids, cracks, notches and regions of lack of fusion may be mentioned as examples for the former and variety of inclusions for the latter. From a viewpoint of fracture mechanics two important classes of imperfections are the planar flaws which may be idealized as cracks and relatively thin inhomogeneities which may be represented by flat inclusions.

Few unusual results aside, the problem of interaction between two cracks is relatively well-understood in the sense that the resulting stress field or the stress intensity factors would either be amplified or reduced as the distance between the cracks decreases. Almost in all cases the qualitative nature of the result could be predicted intuitively. For example, if the cracks are parallel then they would be in each other's shadow and there would be a reduction in the stress intensity factors. On the other hand if the cracks are co-planar then one would expect an amplification in the stress intensity factors. The exception or the unusual result in this case is the reduction in the stress intensity factors at the inner crack tips for certain relative crack locations in plates with relatively smaller thicknesses. Some specific problems relating to interaction between cracks were discussed in the previous report [1].

Intuitively what is not as well understood is the problem of interaction between cracks and flat inclusions. Separately both flaws have singular stresses and consequently are locations for potential fracture initiation. However, the inclusions are also "stiffeners" and therefore, properly oriented, they should tend to arrest crack propagation. For this reason in this study it is found to be worthwhile to undertake a detailed investigation of the problem on which the technical literature seems to be extremely weak. Particularly interesting in this problem is the behavior of the stress state around the ends

of the inclusions and at the points of intersection between inclusions and cracks. The details of the analysis of this crack-inclusion interaction problem and very detailed results are given in Appendix A of the previous report [1]. Additional results on the special case of the inclusion intersecting the crack are given in Appendix B of this report. The interesting problem in this case is the peculiar stress singularities at the end of the inclusion which terminates at the crack surface rather than the crack tip which was discussed in [1].

The correct way of modeling an inclusion would perhaps be to consider it as an elastic continuum fully bonded to the surrounding matrix. In this case, however, the crack-inclusion problems are generally difficult and only simple geometries and orientations can be treated analytically (see, for example, [31], [32]). A simple feature of such crack-inclusion interaction problems is that generally the stress intensity factors are magnified if the stiffness of the inclusion is less than that of the matrix and are diminished if the inclusion is stiffer than the matrix. For certain types of "flat" inclusions a simpler way of modeling may be to represent them as either a membrane with no bending stiffness or a perfectly rigid plane stiffener with negligible thickness. In these problems one may use the basic body force solution as the Green's function to derive the related integral equations. On the other hand, since the flat inclusion with an elastic modulus smaller than that of the matrix would itself have a behavior similar to a crack, it needs to be modeled basically as a "cavity" rather than a "stiffener".

Even though the technical literature on cracks, voids and inclusions which exist in the material separately is quite extensive, the problems of interaction between cracks and inclusions do not seem to be as widely studied. Such problems may be important in studying, for example, the micromechanics of fatigue and the fracture in welded joints. In this section a simple model for flat elastic inclusions is presented and the crack-inclusion interaction problem is considered for various relative orientations.

3.2 Integral Equations of the Problem

The plane strain or the generalized plane stress interaction problem under consideration is described in Fig. 10. It is assumed that the boundaries of the medium are sufficiently far away from the crack-inclusion region so that

their effect on the stress state perturbed by the crack and the inclusion may be neglected and the plane may be considered as being infinite.

Referring to Fig. 10 we define the following unknown functions

$$g_1(x_1) = \frac{\partial}{\partial x_1} [v_1(x_1, +0) - v_1(x_1, -0)] , \quad (a < x_1 < b) , \quad (49)$$

$$h_1(x_1) = \frac{\partial}{\partial x_1} [u_1(x_1, +0) - u_1(x_1, -0)] , \quad (a < x_1 < b) , \quad (50)$$

$$g_2(x_2) = \frac{\partial}{\partial x_2} [v_2(x_2, +0) - v_2(x_2, -0)] , \quad (c < x_2 < d) , \quad (51)$$

$$h_2(x_2) = \frac{\partial}{\partial x_2} [u_2(x_2, +0) - u_2(x_2, -0)] , \quad (c < x_2 < d) \quad (52)$$

where u and v are, respectively, x and y components of the displacement vector in the coordinate systems shown in the figure. It is assumed that the inclusion fills a flat cavity the initial thickness of which is $h_0(x)$ which is "small" compared to its length $2a_1$. It is also assumed that the thickness variation of the stresses and the strain ϵ_{xx}^i in the inclusion are negligible. Thus, for the plane strain case, from the Hooke's Law we obtain the following stress-strain relations in the inclusion

$$\epsilon_{yy}^i(x_1) = \frac{1 - \nu_0 - 2\nu_0^2}{E_0(1 - \nu_0)} \sigma_{yy}^i(x_1) , \quad \epsilon_{xy}^i(x_1) = \frac{1}{2\mu_0} \sigma_{xy}^i(x_1) , \quad (53)$$

where E_0 , ν_0 , μ_0 are the elastic constants of the inclusion. Now, by observing that

$$\epsilon_{yy}^i(x_1) \equiv [v_1(x_1, +0) - v_1(x_1, -0)] / h_0(x_1) , \quad (54)$$

$$2\epsilon_{xy}^i(x_1) \equiv [u_1(x_1, +0) - u_1(x_1, -0)] / h_0(x) , \quad (55)$$

and

$$E_0 = 2\mu_0(1 + \nu_0) , \quad \kappa_0 = 3 - 4\nu_0 , \quad (56)$$

from (1), (2) and (5)-(8) we find

$$\sigma_{yy}^i(x_1) = \frac{\kappa_0 + 1}{\kappa_0 - 1} \frac{\mu_0}{h_0(x_1)} \int_a^{x_1} g_1(t) dt , \quad (57)$$

$$\sigma_{xy}^i(x_1) = \frac{\mu_0}{h_0(x_1)} \int_a^{x_1} h_1(t) dt . \quad (58)$$

If we let the medium to be uniformly loaded away from the crack-inclusion region as shown in Fig.10, for the stress components along the x_1 and x_2 axes we obtain

$$\sigma_{yy}^{1\infty}(x_1,0) = \sigma_{yy}^{\infty} , \quad \sigma_{xy}^{1\infty}(x_1,0) = \sigma_{xy}^{\infty} , \quad (59)$$

$$\sigma_{yy}^{2\infty}(x_2,0) = \sigma_{yy}^{\infty} \cos^2\theta + \sigma_{xx}^{\infty} \sin^2\theta - 2\sigma_{xy}^{\infty} \sin\theta \cos\theta , \quad (60)$$

$$\sigma_{xy}^{2\infty}(x_2,0) = (\sigma_{yy}^{\infty} - \sigma_{xx}^{\infty}) \sin\theta \cos\theta + \sigma_{xy}^{\infty} (\cos^2\theta - \sin^2\theta) . \quad (61)$$

From the basic dislocation solution given in, for example, [33], referred to the coordinate system x_1, y_1 the stress state at a point (x_1, y_1) in the plane due to the displacement derivatives g_1, h_1 defined by (49) and (50) may be expressed as

$$\sigma_{xx}^{11}(x_1, y_1) = \int_a^b [G_{xx}(x_1, y_1, t) g_1(t) + H_{xx}(x_1, y_1, t) h_1(t)] dt , \quad (62)$$

$$\sigma_{yy}^{11}(x_1, y_1) = \int_a^b [G_{yy}(x_1, y_1, t) g_1(t) + H_{yy}(x_1, y_1, t) h_1(t)] dt , \quad (63)$$

$$\sigma_{xy}^{11}(x_1, y_1) = \int_a^b [G_{xy}(x_1, y_1, t) g_1(t) + H_{xy}(x_1, y_1, t) h_1(t)] dt , \quad (64)$$

where

$$\begin{aligned}
G_{xx}(x,y,t) &= A(t-x)[(t-x)^2-y^2] , \\
G_{yy}(x,y,t) &= A(t-x)[3y^2+(t-x)^2] , \\
G_{xy}(x,y,t) &= Ay[y^2-(t-x)^2] , \\
H_{xx}(x,y,t) &= Ay[y^2+3(t-x)^2] , \\
H_{yy}(x,y,t) &= Ay[y^2-(t-x)^2] , \\
H_{xy}(x,y,t) &= A(t-x)[(t-x)^2-y^2] , \\
A(x,y,t) &= \frac{2\mu}{(1+\kappa)} \frac{1}{[(t-x)^2+y^2]^2} ,
\end{aligned} \tag{65}$$

and μ and κ are the elastic constants of the medium ($\mu=E/2(1+\nu)$, $\kappa=3-4\nu$ for plane strain and $\kappa=(3-\nu)/(1+\nu)$ for generalized plane stress). Similarly, referred to the axes x_2, y_2 the stress state σ_{ij}^{22} , ($i, j=x, y$) in the plane due to g_2, h_2 may be obtained from (14)-(17) by substituting (c, d) for (a, b) and (x_2, y_2) for (x_1, y_1) and (g_2, h_2) for (g_1, h_1) .

The integral equations to determine the unknown functions g_1, h_1, g_2 , and h_2 may be obtained from the following traction boundary conditions along $(y_1=0, a < x_1 < b)$ and $(y_2=0, c < x_2 < d)$:

$$\sigma_{yy}^{11}(x_1, 0) + \sigma_{yy}^{12}(x_1, 0) + \sigma_{yy}^{1\infty}(x_1, 0) = \sigma_{yy}^i(x_1) , \quad (a < x_1 < b) , \tag{66}$$

$$\sigma_{xy}^{11}(x_1, 0) + \sigma_{xy}^{12}(x_1, 0) + \sigma_{xy}^{1\infty}(x_1, 0) = \sigma_{xy}^i(x_1) , \quad (a < x_1 < b) , \tag{67}$$

$$\sigma_{yy}^{22}(x_2, 0) + \sigma_{yy}^{21}(x_2, 0) + \sigma_{yy}^{2\infty}(x_2, 0) = 0 , \quad (c < x_2 < d) , \tag{68}$$

$$\sigma_{xy}^{22}(x_2, 0) + \sigma_{xy}^{21}(x_2, 0) + \sigma_{xy}^{2\infty}(x_2, 0) = 0 , \quad (c < x_2 < d) , \tag{69}$$

where all except the coupling stresses in the second column are given by (57)-(65). The coupling stresses have the following meaning: $\sigma_{yy}^{12}(x_1, 0)$ is

the normal stress on $y_1=0$ plane due to the displacement derivatives $g_2(x_2)$ and $h_2(x_2)$ and $\sigma_{yy}^{21}(x_2,0)$ is the normal stress on $y_2=0$ plane due to g_1, h_1 , etc. Thus, after making the necessary stress transformations similar to (60) and (61), we obtain

$$\sigma_{yy}^{12}(x_1,0) = \int_c^d [G_{yy}^{12}(x_1,t)g_2(t) + H_{yy}^{12}(x_1,t)h_2(t)]dt, \quad (70)$$

$$\sigma_{xy}^{12}(x_1,0) = \int_c^d [G_{xy}^{12}(x_1,t)g_2(t) + H_{xy}^{12}(x_1,t)h_2(t)]dt, \quad (71)$$

$$\sigma_{yy}^{21}(x_2,0) = \int_a^b [G_{yy}^{21}(x_2,t)g_1(t) + H_{yy}^{21}(x_2,t)h_1(t)]dt, \quad (72)$$

$$\sigma_{xy}^{21}(x_2,0) = \int_a^b [G_{xy}^{21}(x_2,t)g_1(t) + H_{xy}^{21}(x_2,t)h_1(t)]dt, \quad (73)$$

where from

$$\sigma_{yy}^{12}(x_1,0) = \sigma_{yy}^{22}(x_2,y_2)\cos^2\theta + \sigma_{xx}^{22}\sin^2\theta + \sigma_{xy}^{22}\sin 2\theta \quad (74)$$

calculated at $x_2=x_1\cos\theta, y_2=-x_1\sin\theta$ we have

$$\begin{aligned} G_{yy}^{12}(x_1,t) &= G_{yy}(x_1\cos\theta, -x_1\sin\theta, t)\cos^2\theta + G_{xx}(x_1\cos\theta, -x_1\sin\theta, t) \\ &+ G_{xy}(x_1\cos\theta, x_1\sin\theta, t)\sin 2\theta, \end{aligned} \quad (75)$$

$$\begin{aligned} H_{yy}^{12}(x_1,t) &= H_{yy}(x_1\cos\theta, -x_1\sin\theta, t)\cos^2\theta + H_{xx}(x_1\cos\theta, -x_1\sin\theta, t) \\ &+ H_{xy}(x_1\cos\theta, -x_1\sin\theta, t)\sin 2\theta. \end{aligned} \quad (76)$$

Similar expressions for the remaining kernels in (71)-(73) are obtained by using the stress transformations

$$\begin{aligned}\sigma_{xy}^{12}(x_1, 0) &= [\sigma_{xx}^{22}(x_2, y_2) - \sigma_{yy}^{22}(x_2, y_2)] \sin\theta \cos\theta \\ &+ \sigma_{xy}^{22}(x_2, y_2) (\cos^2\theta - \sin^2\theta), \quad (x_2 = x_1 \cos\theta, y_2 = -x_1 \sin\theta),\end{aligned}\quad (77)$$

$$\begin{aligned}\sigma_{yy}^{21}(x_2, 0) &= \sigma_{yy}^{11}(x_1, y_1) \cos^2\theta + \sigma_{xx}^{11}(x_1, y_1) \sin^2\theta \\ &- \sigma_{xy}^{11}(x_1, y_1) \sin 2\theta, \quad (x_1 = x_2 \cos\theta, y_1 = x_2 \sin\theta),\end{aligned}\quad (78)$$

$$\begin{aligned}\sigma_{xy}^{21}(x_2, 0) &= [\sigma_{yy}^{11}(x_1, y_1) - \sigma_{xx}^{11}(x_1, y_1)] \sin\theta \cos\theta \\ &+ \sigma_{xy}^{11}(x_1, y_1) (\cos^2\theta - \sin^2\theta), \quad (x_1 = x_2 \cos\theta, y_1 = x_2 \sin\theta).\end{aligned}\quad (79)$$

Thus, from (62)-(73) and (77)-(79) it follows that

$$\begin{aligned}G_{xy}^{12}(x_1, t) &= [G_{xx}(x, y, t) - G_{yy}(x, y, t)] \sin\theta \cos\theta \\ &+ G_{xy}(x, y, t) \cos 2\theta, \quad (x = x_1 \cos\theta, y = -x_1 \sin\theta),\end{aligned}\quad (80)$$

$$\begin{aligned}H_{xy}^{12}(x_1, t) &= [H_{xx}(x, y, t) - H_{yy}(x, y, t)] \sin\theta \cos\theta \\ &+ H_{xy}(x, y, t) \cos 2\theta, \quad (x = x_1 \cos\theta, y = -x_1 \sin\theta),\end{aligned}\quad (81)$$

$$\begin{aligned}G_{yy}^{21}(x_2, t) &= G_{yy}(x, y, t) \cos^2\theta + G_{xx}(x, y, t) \sin^2\theta \\ &- G_{xy}(x, y, t) \sin 2\theta, \quad (x = x_2 \cos\theta, y = x_2 \sin\theta),\end{aligned}\quad (82)$$

$$\begin{aligned}H_{yy}^{21}(x_2, t) &= H_{yy}(x, y, t) \cos^2\theta + H_{xx}(x, y, t) \sin^2\theta \\ &- H_{xy}(x, y, t) \sin 2\theta, \quad (x = x_2 \cos\theta, y = x_2 \sin\theta),\end{aligned}\quad (83)$$

$$G_{xy}^{21}(x_2, t) = [G_{yy}(x, y, t) - G_{xx}(x, y, t)] \sin \theta \cos \theta + G_{xy}(x, y, t) \cos 2\theta, \quad (x = x_2 \cos \theta, y = x_2 \sin \theta), \quad (84)$$

$$H_{xy}^{21}(x_2, t) = [H_{yy}(x, y, t) - H_{xx}(x, y, t)] \sin \theta \cos \theta + H_{xy}(x, y, t) \cos 2\theta, \quad (x = x_2 \cos \theta, y = x_2 \sin \theta). \quad (85)$$

From (66)-(69) the integral equations of the problem may then be obtained as

$$\frac{1}{\pi} \int_a^b \frac{1}{t-x_1} g_1(t) dt + \int_a^{x_1} G(x_1) g_1(t) dt + c_0 \int_c^d G_{yy}^{12}(x_1, t) g_2(t) dt + c_0 \int_c^d H_{yy}^{12}(x_1, t) h_2(t) dt = -c_0 \sigma_{yy}^{\infty}, \quad (a < x_1 < b), \quad (86)$$

$$\frac{1}{\pi} \int_a^b \frac{1}{t-x_1} h_1(t) dt + \int_a^{x_1} H(x_1) h_1(t) dt + c_0 \int_c^d G_{xy}^{12}(x_1, t) g_2(t) dt + c_0 \int_c^d H_{xy}^{12}(x_1, t) h_2(t) dt = -c_0 \sigma_{xy}^{\infty}, \quad (a < x_1 < b), \quad (87)$$

$$c_0 \int_a^b G_{yy}^{21}(x_2, t) g_1(t) dt + c_0 \int_a^b H_{yy}^{21}(x_2, t) h_1(t) dt + \frac{1}{\pi} \int_c^d \frac{1}{t-x_2} g_2(t) dt = -c_0 (\sigma_{yy}^{\infty} \cos^2 \theta + \sigma_{xx}^{\infty} \sin^2 \theta - \sigma_{xy}^{\infty} \sin 2\theta), \quad (c < x_2 < d), \quad (88)$$

$$\begin{aligned}
& c_0 \int_a^b G_{xy}^{21}(x_2, t) g_1(t) dt + c_0 \int_a^b H_{xy}^{21}(x_2, t) h_1(t) dt + \frac{1}{\pi} \int_c^d \frac{1}{t-x_2} h_2(t) dt \\
& = -c_0 [(\sigma_{yy}^\infty - \sigma_{xx}^\infty) \sin\theta \cos\theta + \sigma_{xy}^\infty \cos 2\theta], \quad (c < x_2 < d), \quad (89)
\end{aligned}$$

where

$$\begin{aligned}
c_0 &= \frac{1+\kappa}{2\mu}, \quad G(x_1) = -\frac{\mu_0(\kappa+1)(\kappa_0+1)}{2\mu(\kappa_0-1)} \frac{1}{h_0(x_1)}, \\
H(x_1) &= -\frac{\mu_0(\kappa+1)}{2\mu} \frac{1}{h_0(x_1)}. \quad (90)
\end{aligned}$$

If there is no crack in the medium, $g_2=0=h_2$, the integral equations uncouple and (86) and (87) give the unknown functions g_1 and h_1 . For example, if the inclusion has an elliptic cross-section given by

$$h_0(x) = b_0 \sqrt{1-x^2}, \quad (91)$$

(86) becomes

$$\frac{1}{\pi} \int_{-1}^1 \frac{g_1(t)}{t-x} dt - \int_{-1}^x \frac{c_1}{\sqrt{1-x^2}} g_1(t) dt = -c_0 \sigma_{yy}^\infty \quad (92)$$

where

$$c_1 = \frac{\mu_0(1+\kappa)(1+\kappa_0)}{2\mu b_0(\kappa_0-1)}, \quad (93)$$

and without any loss in generality it is assumed that $a=-1, b=1, x_1=x$. The solution of (92) is found to be

$$g_1(t) = -\frac{c_0 \sigma_{yy}^\infty}{1+c_1} \frac{t}{\sqrt{1-t^2}}, \quad (-1 < t < 1) \quad (94)$$

which, for $\mu_0=0$ reduces to the well-known crack solution. By using the following definition of the stress intensity factor

$$k_1(t) = -\lim_{x \rightarrow 1} \frac{2\mu}{1+\kappa} \sqrt{2(1-x)} g_1(x), \quad (95)$$

from (94) it follows that

$$k_1(1) = \frac{\sigma_{yy}^{\infty}}{1+c_1} . \quad (96)$$

Similarly, in the absence of a crack from (87), (90) and (91) it may be shown that

$$h_1(t) = - \frac{c_0 \sigma_{xy}^{\infty}}{1+c_2} \frac{t}{\sqrt{1-t^2}} , \quad (-1 < t < 1) \quad (97)$$

$$k_2(1) = \frac{\sigma_{xy}^{\infty}}{1+c_2} , \quad c_2 = \frac{\mu_0(1+\kappa)}{2\mu b_0} . \quad (98)$$

As another special case if we assume that the stiffness of the inclusion $\mu_0=0$, then the functions G and H defined by (90) vanish and the integral equations (86)-(89) reduce to that of two arbitrarily oriented cracks shown in Fig. 10.

3.3 Stress Intensity Factors

In the linearly elastic medium under consideration the intensity of the stress state around the end points of the crack and the inclusion is governed by the singular behavior of the displacement derivatives g_1 , g_2 , h_1 and h_2 which are defined by (49)-(52). If we assume the following standard definition of Modes I and II stress intensity factors

$$k_1(a) = \lim_{x_1 \rightarrow a} \sqrt{2(a-x_1)} \sigma_{yy}^1(x_1, 0) , \quad (99)$$

$$k_2(a) = \lim_{x_1 \rightarrow a} \sqrt{2(a-x_1)} \sigma_{yy}^1(x_1, 0) , \quad (100)$$

$$k_1(c) = \lim_{x_2 \rightarrow c} \sqrt{2(c-x_2)} \sigma_{yy}^2(x_2, 0) , \text{ etc. } , \quad (101)$$

and observe that the system of integral equations (86)-(89) which has simple Cauchy type kernels has a solution of the form

$$g_i(t) = \frac{G_i(t)}{\sqrt{(b-t)(t-a)}}, \quad h_i(t) = \frac{H_i(t)}{\sqrt{(d-t)(t-c)}}, \quad (i=1,2), \quad (102)$$

from (86)-(89) and (99)-(102) it can be shown that

$$k_1(a) = \frac{2\mu}{1+\kappa} \lim_{x_1 \rightarrow a} \sqrt{2(x_1-a)} g_1(x_1), \quad (103)$$

$$k_1(b) = -\frac{2\mu}{1+\kappa} \lim_{x_1 \rightarrow b} \sqrt{2(b-x_1)} g_1(x_1), \quad (104)$$

$$k_2(a) = \frac{2\mu}{1+\kappa} \lim_{x_1 \rightarrow a} \sqrt{2(x_1-a)} h_1(x_1), \quad (105)$$

$$k_2(b) = -\frac{2\mu}{1+\kappa} \lim_{x_1 \rightarrow b} \sqrt{2(b-x_1)} h_1(x_1). \quad (106)$$

The stress intensity factors $k_i(c)$ and $k_i(d)$, ($i=1,2$) may be expressed in terms of g_2 and h_2 by means of equations similar to (103)-(106).

3.4 Results

The integral equations (86)-(89) are solved by using the technique described in [28] and the stress intensity factors are calculated from (103)-(106) and from similar expressions written for the crack. For various crack-inclusion geometries and stiffness ratios μ_0/μ (μ_0 being the shear modulus of the inclusion) the calculated results are given in Tables 6-11. The main interest in this paper is in relatively "thin" and flat inclusions. Hence in the numerical analysis it is assumed that the thickness h_0 is constant. Table 6 shows the normalized stress intensity factors in a plane which contains a crack equal in size and coplanar with an inclusion and subjected to uniform tension and shear away from the crack-inclusion region (Fig.11a). The inclusion model used in this analysis is basically a crack the surfaces of which are held together by an elastic medium of shear modulus μ_0 . Thus, for $\mu_0=0$ one recovers the two crack solution. It may be observed that for $\mu_0>0$ there is a significant reduction in the stress intensity factors around the end points $x_1=a$ and $x_1=b$ (Fig.11a). In Table 6 the variables are the

stiffness ratio μ_0/μ and the thickness of the inclusion h_0/a_1 with the spacing $a/a_1 = 0.01$ being constant, where $2a_1$ is the length of the inclusion (Fig.11a). Similar results calculated by assuming that $h_0/a_1 = 1/20$ and a/a_1 is variable are shown in Table 7.

For various values of the stiffness ratio μ_0/μ and fixed values of the inclusion thickness ($h_0/a_1=1/20$) and the distance a ($a/a_1=0.1$), the effect of the angle θ on the crack tip stress intensity factors are given in Table 8. The geometry and the loading condition away from the crack-inclusion region are shown in Fig.11b. In this example, too, it is assumed that the inclusion and the crack are of equal length ($a_2=a_1$). For the special case of $\mu_0=0$, that is, for the case of two cracks of equal lengths oriented at an angle θ the stress intensity factors are given in Table 9.

The stress intensity factors for the symmetric crack-inclusion geometries shown in Figures 12a and 12b are given in Table 10, where the length ratio a_2/a_1 is assumed to be the variable. In both examples the inclusion (half) length a_1 is used as the normalizing length parameter and the relative distance c/a_1 (Fig.12a) or a/a_1 (Fig.12b) is assumed to be constant.

Table 11 gives the stress intensity factors for a crack perpendicular to the inclusion where, referring to Fig.10, $\theta=\pi/2$, $a=0$, $\mu_0=\mu/20$ and $c/a_1=0.05$ are fixed and a_2 is variable.

It should be noted that since the superposition is valid, the tables give the stress intensity factors for the most general homogeneous loading conditions away from the crack-inclusion region. Also, the tables give the stress intensity factors which are normalized with respect to $\sigma_{ij}^\infty \sqrt{a_1}$ where $2a_1$ is the length of the inclusion and $(i,j)=(x,y)$, (Fig.10). The notation used in the tables is

$$k_{1a} = \frac{k_1(a)}{\sigma_{ij}^\infty \sqrt{a_1}}, \quad k_{2a} = \frac{k_2(a)}{\sigma_{ij}^\infty \sqrt{a_1}}, \quad k_{1c} = \frac{k_1(c)}{\sigma_{ij}^\infty \sqrt{a_1}}, \quad \text{etc.} \quad (107)$$

where k_1 and k_2 are, respectively, Modes I and II stress intensity factors defined by equations such as (99)-(101) and calculated from the expressions such as (103)-(106).

Table 6. Modes I and II stress intensity factors for the case of a crack located in the plane of the inclusion in a medium subjected to σ_{yy}^{∞} or σ_{xy}^{∞} away from the crack-inclusion region (Fig. 11); $c=-a$, $d=-b$, $a/a_1=0.01$, $k_{1c}=k_1(c)/\sigma_{yy}^{\infty}\sqrt{a_1}$, $k_{1d}=k_1(d)/\sigma_{yy}^{\infty}\sqrt{a_1}$, $k_{2c}=k_2(c)/\sigma_{xy}^{\infty}\sqrt{a_1}$, $k_{2d}=k_2(d)/\sigma_{xy}^{\infty}\sqrt{a_1}$, $k_{1a}=k_1(a)/\sigma_{yy}^{\infty}\sqrt{a_1}$, $k_{2a}=k_2(a)/\sigma_{xy}^{\infty}\sqrt{a_1}$, $k_{1b}=k_1(b)/\sigma_{yy}^{\infty}\sqrt{a_1}$, $k_{2b}=k_2(b)/\sigma_{xy}^{\infty}\sqrt{a_1}$, $a_1=(b-a)/2$.

	$\frac{2h_0}{b-a}$	μ_0/μ							
		0	0.05	0.1	0.25	0.5	1.0	2.0	5.0
k_{1b}	0.01	1.2063	.1578	.1031	.0535	.0303	.0163	.0085	.0035
	0.02	1.2063	.2320	.1578	.0888	.0535	.0303	.0163	.0068
	0.1	1.2063	.5146	.3713	.2320	.1578	.1031	.0634	.0303
	0.2	1.2063	.6836	.5146	.3323	.2320	.1578	.1031	.0535
k_{1a}	0.01	2.9642	.5725	.3908	.2104	.1207	.0654	.0342	.0140
	0.02	2.9642	.7941	.5725	.3404	.2104	.1207	.0654	.0276
	0.1	2.9642	1.5036	1.1620	.7941	.5725	.3908	.2478	.1207
	0.2	2.9642	1.8803	1.5036	1.0636	.7941	.5725	.3908	.2104
k_{1c}	0.01	2.9642	1.1795	1.1045	1.0479	1.0255	1.0132	1.0067	1.0027
	0.02	2.9642	1.2952	1.1795	1.0870	1.0480	1.0255	1.0132	1.0054
	0.1	2.9642	1.7825	1.5321	1.2952	1.1795	1.1045	1.0583	1.0255
	0.2	2.9642	2.0764	1.7825	1.4645	1.2952	1.1795	1.1045	1.0479
k_{1d}	0.01	1.2063	1.0116	1.0063	1.0027	1.0014	1.0007	1.0004	1.0001
	0.02	1.2063	1.0211	1.0116	1.0051	1.0027	1.0014	1.0007	1.0003
	0.1	1.2063	1.0693	1.0432	1.0211	1.0116	1.0063	1.0033	1.0014
	0.2	1.2063	1.1019	1.0693	1.0366	1.0211	1.0116	1.0063	1.0027
k_{2b}	0.01	1.2063	.3106	.2159	.1275	.0810	.0482	.0269	.0117
	0.02	1.2063	.4368	.3106	.1910	.1275	.0810	.0482	.0221
	0.1	1.2063	.8214	.6500	.4368	.3106	.2159	.1459	.0810
	0.2	1.2063	.9673	.8214	.5946	.4368	.3106	.2159	.1275
k_{2a}	0.01	2.9642	1.0075	.7480	.4743	.3122	.1900	.1076	.0470
	0.02	2.9642	1.3214	1.0075	.6747	.4743	.3122	.1900	.0885
	0.1	2.9642	2.1749	1.8071	1.3214	1.0075	.7480	.5345	.3122
	0.2	2.9642	2.4785	2.1749	1.6847	1.3214	1.0075	.7480	.4743
k_{2c}	0.01	2.9642	1.4272	1.2691	1.1366	1.0778	1.0425	1.0225	1.0093
	0.02	2.9642	1.6463	1.4272	1.2298	1.1366	1.0778	1.0425	1.0182
	0.1	2.9642	2.3136	2.0183	1.6463	1.4272	1.2691	1.1622	1.0778
	0.2	2.9642	2.5619	2.3136	1.9221	1.6463	1.4272	1.2691	1.1366
k_{2d}	0.01	1.2063	1.0330	1.0188	1.0085	1.0045	1.0023	1.0012	1.0005
	0.02	1.2063	1.0549	1.0330	1.0156	1.0085	1.0045	1.0023	1.0010
	0.1	1.2063	1.1292	1.0954	1.0549	1.0330	1.0188	1.0103	1.0045
	0.2	1.2063	1.1583	1.1292	1.0846	1.0549	1.0330	1.0188	1.0085

Table 7. Modes I and II stress intensity factors for the case of a crack located in the plane of the inclusion in a medium subjected to σ_{yy}^{∞} or σ_{xy}^{∞} away from the crack-inclusion region (Fig. 11); $c=-a$, $d=-b$, $h_0/a_1=1/20$.

	$\frac{2a}{b-a}$	μ_0/μ							
		0	0.05	0.1	0.25	0.5	1.0	2.0	5.0
k_{1b}	0.01	1.2063	.3713	.2611	.1578	.1031	.0635	.0366	.0163
	0.5	1.0517	.3544	.2513	.1527	.0998	.0615	.0354	.0158
	1	1.0280	.3493	.2479	.1508	.0986	.0607	.0350	.0156
	2	1.0125	.3453	.2452	.1492	.0976	.0601	.0347	.0154
k_{1a}	0.01	2.9642	1.1620	.8751	.5725	.3908	.2478	.1454	.0654
	0.5	1.1125	.3877	.2768	.1693	.1110	.0685	.0395	.0176
	1	1.0480	.3604	.2564	.1563	.1023	.0630	.0364	.0162
	2	1.0176	.3481	.2474	.1506	.0985	.0607	.0350	.0156
k_{1c}	0.01	2.9642	1.5321	1.3433	1.1795	1.1045	1.0583	1.0313	1.0132
	0.5	1.1125	1.0229	1.0130	1.0057	1.0030	1.0015	1.0008	1.0003
	1	1.0480	1.0096	1.0054	1.0024	1.0012	1.0006	1.0003	1.0001
	2	1.0176	1.0035	1.0020	1.0009	1.0004	1.0002	1.0001	1.0000
k_{1d}	0.01	1.2063	1.0432	1.0253	1.0116	1.0063	1.0033	1.0017	1.0007
	0.5	1.0517	1.0104	1.0058	1.0026	1.0013	1.0007	1.0003	1.0001
	1	1.0280	1.0056	1.0031	1.0014	1.0007	1.0004	1.0002	1.0001
	2	1.0125	1.0025	1.0014	1.0006	1.0003	1.0002	1.0001	1.0000
k_{2b}	0.01	1.2063	.6500	.4845	.3106	.2159	.1459	.0943	.0481
	0.5	1.0517	.6031	.4576	.2979	.2084	.1412	.0914	.0467
	1	1.0280	.5925	.4503	.2938	.2057	.1395	.0903	.0461
	2	1.0125	.5849	.4449	.2905	.2035	.1380	.0893	.0456
k_{2a}	0.01	2.9642	1.8071	1.4340	1.0075	.7480	.5345	.3601	.1900
	0.5	1.1125	.6498	.4971	.3272	.2302	.1567	.1017	.0520
	1	1.0480	.6081	.4636	.3035	.2129	.1446	.0937	.0479
	2	1.0176	.5889	.4483	.2930	.2053	.1393	.0902	.0461
k_{2c}	0.01	2.9642	2.0183	1.7299	1.4272	1.2691	1.1623	1.0937	1.0425
	0.5	1.1125	1.0523	1.0344	1.0172	1.0095	1.0050	1.0026	1.0011
	1	1.0480	1.0222	1.0145	1.0072	1.0040	1.0021	1.0011	1.0004
	2	1.0176	1.0081	1.0053	1.0026	1.0014	1.0008	1.0004	1.0002
k_{2d}	0.01	1.2063	1.0954	1.0637	1.0330	1.0188	1.0104	1.0055	1.0023
	0.5	1.0517	1.0239	1.0157	1.0078	1.0043	1.0023	1.0012	1.0005
	1	1.0280	1.0129	1.0084	1.0042	1.0023	1.0012	1.0006	1.0003
	2	1.0125	1.0057	1.0038	1.0019	1.0010	1.0005	1.0003	1.0001

Table 8. The effect of angular orientation θ and the modulus ratio μ_0/μ on the stress intensity factors in a medium under general in-plane loading (Fig.10); $c=a$, $d=b$, $2h_0/(b-a)=1/20$, $2a/(b-a)=0.1$.

σ^∞	k	θ°					
		30	60	90	120	150	180
$\mu_0/\mu = 0.05$							
σ_{xx}^∞	k_{1c}	0.2624	0.8047	1.0961	0.8097	0.2654	0
	k_{2c}	-0.4711	-0.4636	0.0163	0.4737	0.4585	0
	k_{1d}	0.2560	0.7618	1.0106	0.7562	0.2518	0
	k_{2d}	-0.4378	-0.4253	0.0122	0.4432	0.4383	0
σ_{yy}^∞	k_{1c}	0.6402	0.2232	-0.0311	0.2749	0.8366	1.1094
	k_{2c}	0.4596	0.4217	-0.0483	-0.5019	-0.4771	0
	k_{1d}	0.7052	0.2221	-0.0109	0.2568	0.7702	1.0250
	k_{2d}	0.4105	0.3981	-0.0386	-0.4636	-0.4493	0
σ_{xy}^∞	k_{1c}	-0.5020	-0.5895	0.2839	1.1440	1.0302	0
	k_{2c}	0.3394	-0.5681	-1.0010	-0.3793	0.7098	1.2367
	k_{1d}	-0.9072	-0.8566	0.0354	0.9049	0.8903	0
	k_{2d}	0.4353	-0.5284	-0.9911	-0.4631	0.5521	1.0567
$\mu_0/\mu = 0.1$							
σ_{xx}^∞	k_{1c}	0.2552	0.7786	1.0613	0.7908	0.2608	0
	k_{2c}	-0.4593	-0.4546	0.0095	0.4610	0.4512	0
	k_{1d}	0.2534	0.7570	1.0066	0.7540	0.2512	0
	k_{2d}	-0.4366	-0.4291	0.0072	0.4395	0.4366	0
σ_{yy}^∞	k_{2c}	0.6535	0.2334	-0.0181	0.2628	0.8003	1.0643
	k_{2c}	0.4533	0.4238	-0.0293	-0.4758	-0.4605	0
	k_{1d}	0.7248	0.2350	-0.0058	0.2540	0.7615	1.0143
	k_{2d}	0.4219	0.4145	-0.0215	-0.4506	-0.4425	0
σ_{xy}^∞	k_{1c}	-0.6023	-0.6717	0.1849	1.0482	0.9749	0
	k_{2c}	0.3956	-0.5401	-0.9996	-0.4197	0.6414	1.1599
	k_{1d}	-0.8892	-0.8588	0.0230	0.8910	0.8817	0
	k_{2d}	0.4617	-0.5172	-0.9943	-0.4762	0.5343	1.0374

Table 8 - cont.

		$\mu_0/\mu = 0.5$					
σ_{xx}^∞	k_{1c}	0.2478	0.7537	1.0157	0.7622	0.2535	0
	k_{2c}	-0.4414	-0.4405	0.0019	0.4418	0.4391	0
	k_{1d}	0.2509	0.7517	1.0017	0.7511	0.2503	0
	k_{2d}	-0.4341	-0.4322	0.0017	0.4347	0.4341	0
σ_{yy}^∞	k_{1c}	0.7013	0.2427	-0.0045	0.2523	0.7620	1.0158
	k_{2c}	0.4381	0.4288	-0.0078	-0.4448	-0.4407	0
	k_{1d}	0.7446	0.2469	-0.0012	0.2510	0.7527	1.0033
	k_{2d}	0.4312	0.4292	-0.0048	-0.4371	-0.4353	0
	k_{1c}	-0.7657	-0.8011	0.0517	0.9166	0.6971	0
	k_{2c}	0.4738	-0.5057	-0.9981	-0.4766	0.5420	1.0479
	k_{1d}	-0.8712	-0.8639	0.0061	0.8726	0.8702	0
	k_{2d}	0.4910	-0.5046	-0.9987	-0.4938	0.5094	1.0105
		$\mu_0/\mu = 2$					
σ_{xx}^∞	k_{1c}	0.2484	0.7504	1.0041	0.7535	0.2510	0
	k_{2c}	-0.4356	-0.4354	0.0003	0.4356	0.4349	0
	k_{1d}	0.2503	0.7505	1.0004	0.7503	0.2501	0
	k_{2d}	-0.4333	-0.4328	0.0004	0.4335	0.4333	0
σ_{yy}^∞	k_{1c}	0.7317	0.2473	-0.0012	0.2505	0.7531	1.0042
	k_{2c}	0.4330	0.4314	-0.0022	-0.4363	-0.4352	0
	k_{1d}	0.7487	0.2492	-0.0003	0.2503	0.7507	1.0009
	k_{2d}	0.4326	0.4321	-0.0012	-0.4341	-0.4336	0
σ_{xy}^∞	k_{1c}	-0.8318	-0.8460	0.0146	0.8801	0.8748	0
	k_{2c}	0.4947	-0.5001	-0.9989	-0.4932	0.5122	1.0139
	k_{1d}	-0.8674	-0.8655	0.0016	0.8678	0.8672	0
	k_{2d}	0.4976	-0.5013	-0.9997	-0.4983	0.5026	1.0029

Table 9. Interaction of two cracks (Fig. 11b); $\mu_0/\mu_1=0$, $c=a$, $d=b$,
 $2a/(b-a) = 0.1$.

		θ°					
		30	60	90	120	150	180
σ_{xx}^∞	k_{1a}	0.1834	-0.0122	-0.1604	-0.1271	-0.0361	0
	k_{2a}	0.1293	0.0928	0.2122	0.2877	0.1946	0
	k_{1b}	-0.1471	-0.1373	-0.0666	-0.0113	0.0024	0
	k_{2b}	0.1825	0.2323	0.2104	0.1371	0.0588	0
	k_{1c}	0.3637	1.0032	1.2370	0.8684	0.2790	0
	k_{2c}	-0.5576	-0.4950	0.0577	0.5191	0.4810	0
	k_{1d}	0.3073	0.8057	1.0308	0.7633	0.2536	0
	k_{2d}	-0.3956	-0.3708	0.0477	0.4591	0.4441	0
σ_{yy}^∞	k_{1a}	0.5843	0.9140	1.2370	1.3954	1.4643	1.4914
	k_{2a}	-0.1912	-0.0242	-0.0577	-0.1080	-0.0730	0
	k_{1b}	0.9210	1.0081	1.0308	1.0567	1.0994	1.1220
	k_{2b}	0.0215	-0.0427	-0.0477	-0.0168	0.0054	0
	k_{1c}	0.4051	-0.1004	-0.1604	0.3999	1.1491	1.4914
	k_{2c}	0.6195	0.4264	-0.2122	-0.6987	-0.6027	0
	k_{1d}	0.4666	0.0652	-0.0666	0.2821	0.8481	1.1220
	k_{2d}	0.1916	0.1811	-0.2104	-0.5795	-0.5082	0
σ_{xy}^∞	k_{1a}	0.1842	0.7402	0.6381	0.3381	0.1384	0
	k_{2a}	1.1741	1.1315	1.0152	1.1777	1.4058	1.4914
	k_{1b}	0.4327	0.1938	0.0748	0.0610	0.0532	0
	k_{2b}	0.5851	0.7960	0.9950	1.1104	1.1305	1.1220
	k_{1c}	-0.4402	-0.4311	0.6381	1.4876	1.2302	0
	k_{2c}	0.3095	-0.6671	-1.0152	-0.2462	0.9347	1.4914
	k_{1d}	-1.1414	-0.8951	0.0748	0.9554	0.9234	0
	k_{2d}	0.1531	-0.6362	-0.9950	-0.4219	0.6115	1.1220

Table 10. Stress intensity factors for the case of a crack perpendicular to the inclusion, $\mu_0/\mu=1/20$, $h_0/a_1=1/20$.

	σ^∞	k	a_2/a_1			
			0.1	0.5	1.0	5.0
Fig. 3a $a=-b=-a_1$ $c/a_1=0.1$	σ_{xx}^∞	$k_{1a}=k_{1b}$	-0.0088	-0.0479	-0.0938	-0.1449
		$k_{2a}=-k_{2b}$	-0.0058	-0.0820	-0.1428	-0.2729
		k_{1c}	+1.0636	1.1611	1.1572	1.1256
		k_{1d}	1.0320	1.0245	1.0109	1.0029
	σ_{yy}^∞	$k_{1a}=k_{1b}$	0.3424	0.3441	0.3441	0.3438
		$k_{2a}=-k_{2b}$	0.0006	0.0039	0.0039	0.0033
		k_{1c}	-0.1220	-0.0896	-0.0632	-0.0255
		k_{1d}	-0.0988	-0.0116	0.0067	0.0021
	σ_{xy}^∞	$k_{1a}=-k_{1b}$	-0.0004	-0.0162	-0.0850	-0.5164
$k_{2a}=k_{2b}$		0.5703	0.5162	0.4502	0.4199	
k_{2c}		-0.7288	-0.9533	-1.0730	-1.2431	
k_{2d}		-0.7856	-1.0338	-1.0638	-1.0200	
Fig. 3b $c=-d=-a_2$ $a/a_1=0.1$	σ_{xx}^∞	k_{1a}	0.0208	-0.1238	-0.2149	-0.2773
		k_{1b}	0.0006	0.0100	0.0234	-0.1170
		$k_{1c}=k_{1d}$	1.0037	1.0053	1.0101	1.0026
		$k_{2c}=-k_{2d}$	-0.0011	-0.0074	-0.0107	-0.0045
	σ_{yy}^∞	k_{1a}	0.3476	0.3543	0.3764	0.3057
		k_{1b}	0.3416	0.3418	0.3416	0.3469
		$k_{1c}=k_{1d}$	0.1584	-0.0186	-0.0324	-0.0048
		$k_{2c}=-k_{2d}$	-0.0353	0.0460	0.0406	0.0073
	σ_{xy}^∞	k_{2a}	0.6514	0.5903	0.4304	0.0544
		k_{2b}	0.5808	0.6066	0.6315	0.3702
		$k_{1c}=-k_{1d}$	-0.4813	-0.2431	-0.1012	-0.0010
		$k_{2c}=k_{2d}$	-1.3694	-0.9632	-0.9372	-0.9946

Table 11. Stress intensity factors for a crack perpendicular to the inclusion (Fig. 1); $\theta=\pi/2$, $a=0$, $2c/(b-a)=0.05$, $\mu_o/\mu=1/20$, $2h_o/(b-a)=0.05$.

σ^∞	k	a_2/a_1			
		0.1	0.5	1.0	5.0
σ_{xx}^∞	k_{1a}	.0399	.2055	.3675	1.1277
	k_{2a}	.0128	.0418	.0555	.1125
	k_{1b}	.0005	.0035	-.0081	-.0715
	k_{2b}	.0021	.0402	.1107	.3050
	k_{1c}	1.0762	1.1674	1.1729	1.1435
	k_{2c}	.0162	-.0056	-.0311	-.0740
	k_{1d}	1.0310	1.0274	1.0143	1.0018
	k_{2d}	.0207	.0212	.0115	-.0015
σ_{yy}^∞	k_{1a}	.3574	.3716	.3791	.3884
	k_{2a}	.0092	.0283	.0390	.0533
	k_{1b}	.3414	.3411	.3418	.3456
	k_{2b}	.0001	-.0010	-.0036	-.0062
	k_{1c}	-.0490	-.0607	-.0514	-.0250
	k_{2c}	-.3157	-.2298	-.1863	-.0933
	k_{1d}	-.0468	-.0250	-.0084	-.0009
	k_{2d}	-.1943	-.0830	-.0464	-.0048
σ_{xy}^∞	k_{1a}	.0887	.3231	.4952	1.1795
	k_{2a}	.6265	.7947	.9710	1.9112
	k_{1b}	.0002	.0001	.0079	.2709
	k_{2b}	.5805	.5910	.5713	.4743
	k_{1c}	1.1620	.6411	.4373	.1825
	k_{2c}	-1.0423	-1.1380	-1.1889	-1.2670
	k_{1d}	.6504	.1454	.0426	.0045
	k_{2d}	-.9292	-.9710	-1.0075	-1.0117

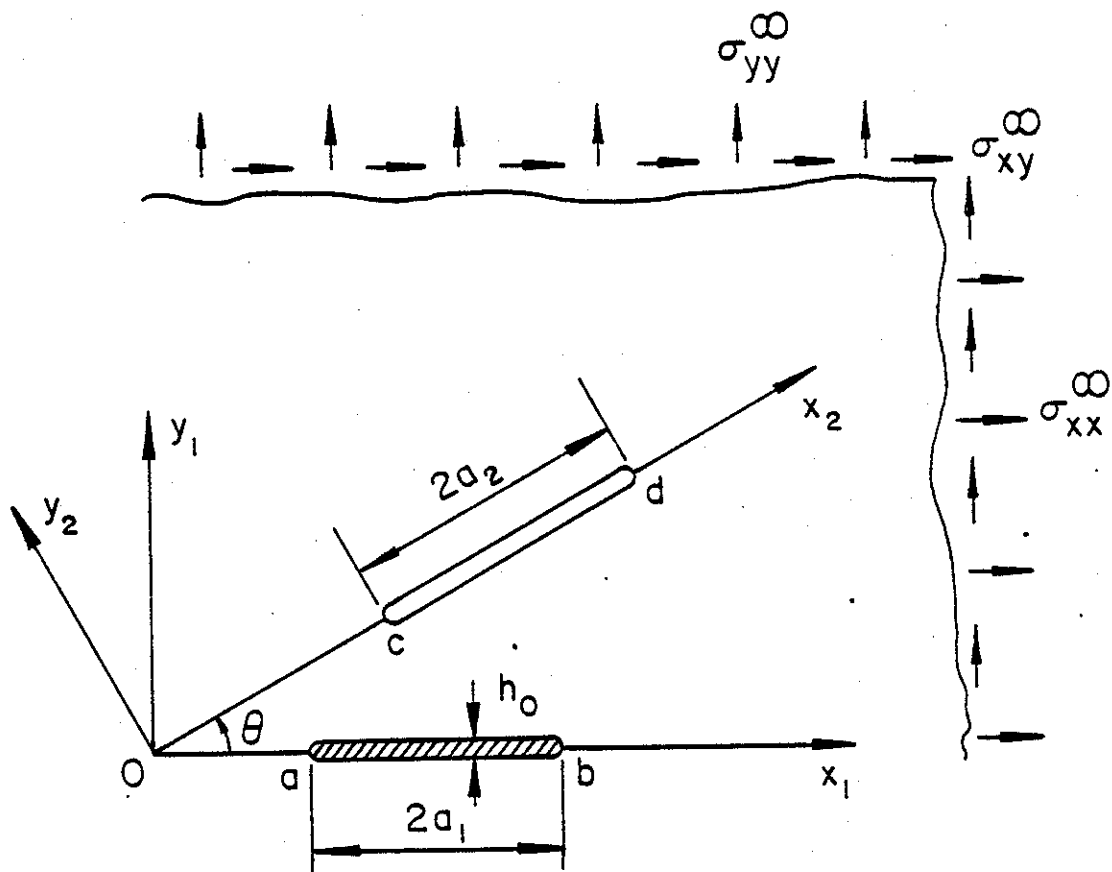


Fig. 10 The geometry of the crack-inclusion problem

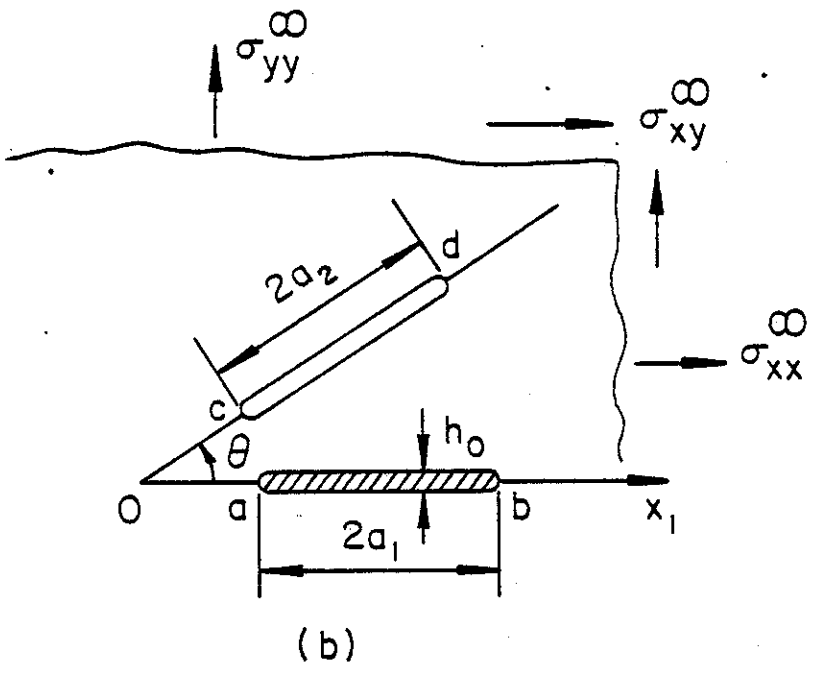
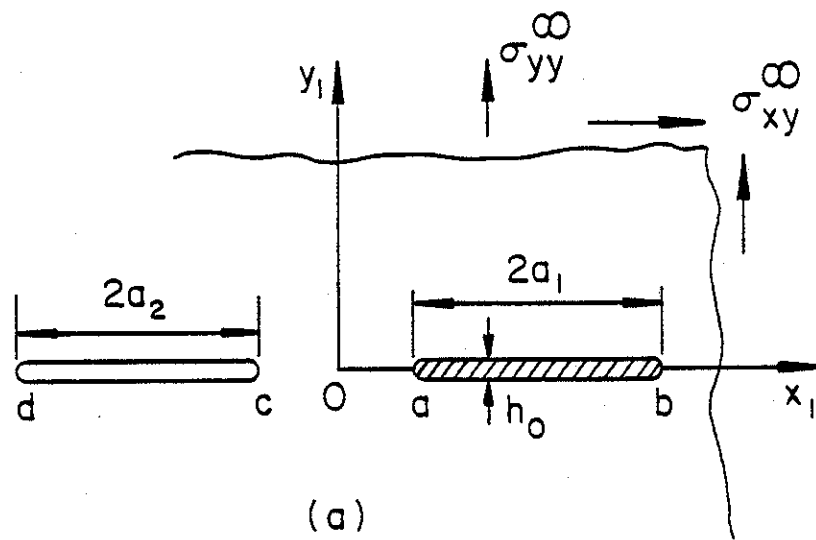
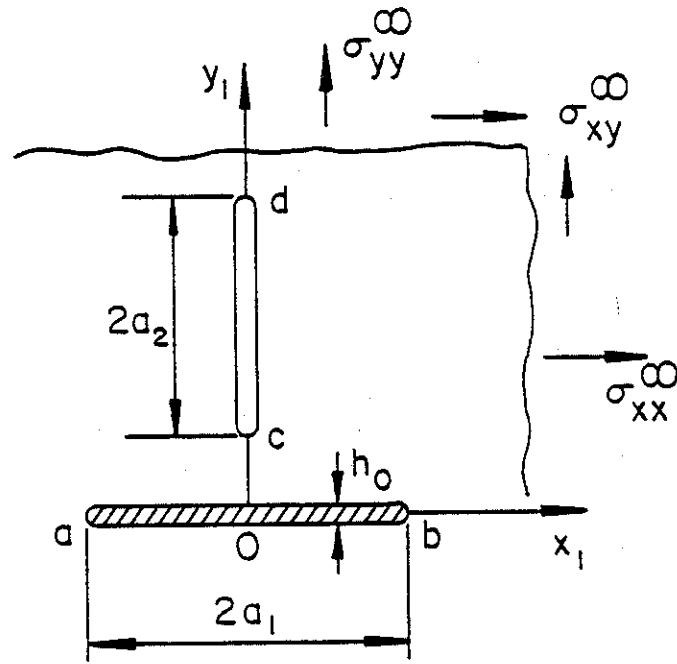
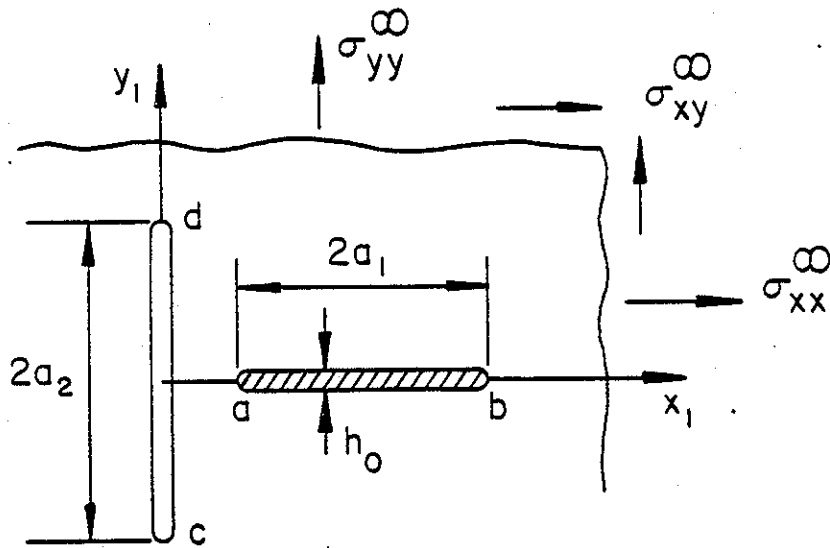


Fig. 11 Special crack-inclusion geometries used in numerical analysis



(a)



(b)

Fig. 12 Special crack-inclusion geometries used in numerical analysis

4. REFERENCES TO PART I

1. F. Erdogan and R.P. Wei, "Fracture Analysis and Corrosion Fatigue in Pipelines", Annual Report, DOT, RSPA Contract DTRS 56 82-C-00014, Sept. 1983.
2. C.D. Lundin, "The Significance of Weld Discontinuities - A Review of Current Literature", W.R.C. Bulletin, No. 222, Dec. 1976.
3. "Proposed Assessment Methods for Flaws with Respect to Failure by Brittle Fracture", Welding in the World, Vol. 13, No. 1/2, 1975.
4. S.T. Rolfe and J.M. Barsom, Fracture and Fatigue Control in Structures, Prentice Hall, 1977.
5. Fatigue Crack Propagation, ASTM-STP 415, 1967.
6. M.S. Kamath, "The COD Design Curve: An Assessment of Validity Using Wide Plate Tests", The Welding Institute Research Report 71/1978/E, Sept. 1978.
7. J.D. Harrison, "The 'State-of-the-Art' in Crack Tip Opening Displacement Testing and Analysis", the Welding Institute Research Report 108/1980, April 1980.
8. J.D. Harrison, M.G. Dawes, G.L. Archer, and M.S. Kamath, "The COD Approach and its Application to Welded Structures", ASTM-STP668, 1979.
9. F. Erdogan, "Theoretical and Experimental Study of Fracture in Pipelines Containing Circumferential Flaws", Final Report, DOT-RSPA-DMA-50/83/3, Sept. 1982.
10. V.L. Hein and F. Erdogan, "Stress Singularities in a Two-Material Wedge", Int. J. of Fracture Mechanics, Vol. 7, pp. 317-330, 1971.
11. J.R. Rice and N. Levy, "The Part-Through Surface Crack in an Elastic Plate", J. Appl. Mech., Vol. 39, Trans. ASME, pp. 185-194, 1972.
12. J.K. Knowles and N.M. Wang, "On the Bending of an Elastic Plate Containing a Crack", J. of Mathematics and Physics, Vol. 39, p. 223, 1960.
13. N.M. Wang, "Effects of Plate Thickness on the Bending of an Elastic Plate Containing a Crack", J. of Mathematics and Physics, Vol. 47, p. 371, 1968.
14. R.J. Hartranft and G.C. Sih, "Effect of Plate Thickness on the Bending Stress Distribution around Through Cracks", J. of Mathematics and Physics, Vol. 47, p. 276, 1968.
15. E. Reissner, "On Bending of Elastic Plates", Quarterly of Applied Mathematics, Vol. 5, p. 55, 1947.

(References - cont.)

16. E. Reissner and F.Y.M. Wan, "On the Equations of Linear Shallow Shell Theory", *Studies in Applied Mathematics*, Vol. 48, p. 132, 1969.
17. F. Delale and F. Erdogan, "Transverse Shear Effect in a Circumferentially Cracked Cylindrical Shell", *Quarterly of Applied Mathematics*, Vol. 37 p. 239, 1979.
18. F. Delale and F. Erdogan, "The Effect of Transverse Shear in a Cracked Plate under Skewsymmetric Loading", *J. Appl. Mech.*, Vol. 46, Trans. ASME, p.
19. D.M. Parks, "The Inelastic Line Spring: Estimates of Elastic-Plastic Fracture Parameters for Surface Cracked Plates and Shells", Paper 80-C2/PVP-109, ASME, 1980.
20. D.M. Parks, "Inelastic Analysis of Surface Flaws Using the Line Spring Model", *Proceedings of the 5th Int. Conf. on Fracture*, Cannes, France, 1981.
21. F. Delale and F. Erdogan, "Line Spring Model for Surface Cracks in a Reissner Plate", *Int. J. Engng. Sci.*, Vol. 19, p. 1331, 1981.
22. F. Delale and F. Erdogan, "Application of the Line Spring Model to a Cylindrical Shell Containing a Circumferential or an Axial Part-Through Crack", *J. Appl. Mech.*, Vol. 49, p. 97, Trans. ASME, 1982.
23. F. Erdogan and H. Ezzat, "Fracture of Pipelines Containing a Circumferential Crack", *Welding Research Council Bulletin* 288, WRC, 1983.
24. F. Erdogan and H. Boduroglu, "Surface Cracks in a Plate of Finite Width under Extension or Bending", *Theoretical and Applied Fracture Mechanics*, Vol. 1, 1985 (to appear).
25. J.R. Rice, "The Line Spring Model for Surface Flaws", The Surface Crack, Physical Problems and Computational Solutions, J.L. Swedlow, ed. p. 171, ASME, New York, 1972.
26. F. Erdogan, G.R. Irwin and M. Ratwani, "Ductile Fracture of Cylindrical Vessels Containing a Large Flaw", ASTM-STP601, p. 191, 1976.
27. F. Erdogan and F. Delale, "Ductile Fracture of Pipes and Cylindrical Containers with a Circumferential Flaw", *J. Pressure Vessel Technology*, Trans. ASME, Vol. 103, p. 160, 1981.
28. F. Erdogan, "Mixed Boundary Value Problems in Mechanics", Mechanics Today, S. Nemat-Nasser, ed. Vol. 4, p. 1, Pergamon Press, Oxford, 1978.
29. A.C. Kaya and F. Erdogan, "Stress Intensity Factors and COD in an Orthotropic Strip", *Int. Journal of Fracture*, Vol. 16, p. 171, 1980.

(References - cont.)

30. T.C. Newman and T.S. Raju, "Stress Intensity Factor Equations for Cracks in Three-Dimensional Finite Bodies", ASTM STP 791, 1983.
31. F. Erdogan and G.D. Gupta, "The Inclusion Problem with a Crack Crossing the Boundary", *Int. J. of Fracture*, Vol. 11, pp. 13-27, 1975.
32. F. Erdogan, G.D. Gupta and M. Ratwani, "Interaction Between a Circular Inclusion and an Arbitrarily Oriented Crack", *J. Appl. Mech.*, Vol. 41, *Trans. ASME*, pp. 1007-1013, 1974.
33. J. Dundurs, "Elastic Interaction of Dislocations with Inhomogeneities", Mathematical Theory of Dislocations, T. Mura, ed., pp. 70-115, ASME, New York, 1969.

APPENDIX A

SURFACE CRACKS IN A PLATE OF FINITE WIDTH UNDER EXTENSION OR BENDING

by

F. Erdogan and H. Boduroglu
Lehigh University, Bethlehem, PA

ABSTRACT

In this paper the problem of a finite plate containing collinear surface cracks is considered. The problem is solved by using the line spring model with plane elasticity and Reissner's plate theory. The main purpose of the study is to investigate the effect of interaction between two cracks or between cracks and stress-free plate boundaries on the stress intensity factors and to provide extensive numerical results which may be useful in applications. First, some sample results are obtained and are compared with the existing finite element results. Then the problem is solved for a single (internal) crack, two collinear cracks and two corner cracks for wide range of relative dimensions. Particularly in corner cracks the agreement with the finite element solution is surprisingly very good. The results are obtained for semi-elliptic and rectangular crack profiles which may, in practice, correspond to two limiting cases of the actual profile of a subcritically growing surface crack.

1. Introduction

Surface cracks are among the most common flaws in structural components, particularly in welded structures. Under cyclic loading or under static loading in the presence of corrosive environment any surface flaw has the potential of subcritically growing into a surface crack. Analysis of the structure containing such flaws is needed for modeling and prediction of the corresponding crack propagation rate. A review of the subject and a number of articles dealing with the analysis of the surface crack problem in plates may be found in [1]. At this

point the analytical treatment of the problem appears to be intractable. Therefore, the reliable solutions of the problem seem to be based on numerical techniques, most notably on the finite element method (see, for example, [2] for the solution of a wide plate containing a semi-elliptic surface crack). In recent years, however, there has been some renewed interest in the application of the line spring model which was first described in [3] to the analysis of surface crack problems. The method was used in [4] in conjunction with Reissner's plate theory and the stress intensity factors for a semi-elliptic and a rectangular surface crack were calculated for a wide plate under tension or bending. The semi-elliptic crack results described in [4] compare very favorably with the finite element solution given in [2].

In this paper the general problem is considered for a plate having a finite width. Analytically, it is known that if the stress fields of more than one crack or that of a crack and a stress-free boundary of the plate interact, there would be some magnification in the stress intensity factors. The problem may therefore be important in plate structures having more than one initial surface flaw or having a flaw near or at the boundary. Extensive finite element results for a single central or corner surface crack in a plate of finite width are given in [5] and [6]. Empirically developed expressions for stress intensity factors based on the results given in [5] are also described in [7]. The present study was undertaken partly to show that the line spring model may be used for cracks in finite plates, particularly for corner cracks just as effectively as the infinite plate and partly to supplement the results given in [5] and [6] by, for example, considering the cases of a rectangular crack profile and collinear surface cracks.

2. The General Formulation of the Problem

The problem under consideration is described in Fig. 1. It is assumed that x_1x_3 and x_2x_3 planes are planes of symmetry with respect to loading and geometry and the length of the plate in x_2 direction is relatively long compared to the width $2b$ so that in formulating the

perturbation problem one may assume the plate to be infinitely long. Even though the numerical results are given for uniform tension in x_2 direction and cylindrical bending in x_2x_3 plane applied to the plate away from the crack region, as will be seen from the formulation of the problem, there is no restriction on the external loads provided in the absence of any cracks the membrane and bending resultants in x_1x_3 plane can be obtained for the given plate geometry and the applied loads.

The problem is formulated for the collinear cracks shown in Fig. 1. The single central crack and the edge or the corner cracks are then considered as the special cases. One of the advantages of the line spring model is that the crack profile (as described by the function $L(x_1)$ giving the crack depth) can be arbitrary. However, the actual crack morphology studies indicate that for a given length $2a$ and a depth L_0 the crack profile may be bounded by a semi-ellipse and a rectangle. Hence, in this paper the calculated results will be given only for these two limiting crack shapes.

Ordinarily, the problems of in-plane loading (as expressed as a generalized plane stress problem) and bending of a plate are uncoupled. Consequently, the corresponding through crack problems can be solved independently. For the plate geometry shown in Fig. 1 the plane elasticity and plate bending solutions are given in [8] and [9], respectively. In the case of surface cracks, because of the absence of symmetry in thickness direction, the membrane and bending problems are clearly coupled. As in [9] in this paper, too, a transverse shear theory is used to formulate the bending component of the problem. The particular theory used is that of Reissner's [10] which is a sixth order theory and accounts for all three boundary conditions on the crack surfaces separately.

Referring to Appendix a for normalized quantities and, for example, to [11] for the general formulation, the basic equations of the plate problem may be expressed as follows:

$$\nabla^4 \phi = 0 , \quad (1)$$

$$\nabla^4 w = 0 , \quad (2)$$

$$\kappa \nabla^2 \psi - \psi - w = 0, \quad (3)$$

$$\kappa \frac{1-\nu}{2} \nabla^2 \Omega - \Omega = 0, \quad (4)$$

$$\sigma_{xx} = \frac{\partial^2}{\partial y^2} (h\phi), \quad \sigma_{yy} = \frac{\partial^2}{\partial x^2} (h\phi), \quad \sigma_{xy} = -\frac{\partial^2}{\partial x \partial y} (h\phi) \quad (5)$$

$$\beta_x = \frac{\partial \psi}{\partial x} + \frac{1-\nu}{2} \kappa \frac{\partial \Omega}{\partial y}, \quad \beta_y = \frac{\partial \psi}{\partial y} - \frac{1-\nu}{2} \kappa \frac{\partial \Omega}{\partial x}, \quad (6)$$

$$M_{xx} = \frac{a}{h\lambda^4} \left[\frac{\partial^2 \psi}{\partial x^2} + \nu \frac{\partial^2 \psi}{\partial y^2} + \frac{\kappa}{2} (1-\nu)^2 \frac{\partial^2 \Omega}{\partial x \partial y} \right], \quad (7)$$

$$M_{yy} = \frac{a}{h\lambda^4} \left[\frac{\partial^2 \psi}{\partial y^2} + \nu \frac{\partial^2 \psi}{\partial x^2} - \frac{\kappa}{2} (1-\nu)^2 \frac{\partial^2 \Omega}{\partial x \partial y} \right], \quad (8)$$

$$M_{xy} = \frac{a(1-\nu)}{2h\lambda^4} \left[2 \frac{\partial^2 \psi}{\partial x \partial y} + \frac{\kappa}{2} (1-\nu) \left(\frac{\partial^2 \Omega}{\partial y^2} - \frac{\partial^2 \Omega}{\partial x^2} \right) \right], \quad (9)$$

$$V_x = \frac{\partial w}{\partial x} + \frac{\kappa}{2} (1-\nu) \frac{\partial \Omega}{\partial y} + \frac{\partial \psi}{\partial x}, \quad (10)$$

$$V_y = \frac{\partial w}{\partial y} - \frac{\kappa}{2} (1-\nu) \frac{\partial \Omega}{\partial x} + \frac{\partial \psi}{\partial y} \quad (11)$$

where, in the usual notation, F (or ϕ) is the Airy stress function, N_{ij} , M_{ij} , and V_i , ($i, j=1, 2$) are the membrane, bending, and transverse shear resultants, β_1 and β_2 are the components of the rotation vector, u_1 , u_2 and u_3 are the components of the displacement vector, a^* is a length parameter representing the crack size ($a^*=a$ for $0 < c < d < b$ and $a^*=d$ for $c=0$, $d < b$, Fig. 1), E and ν are the elastic constants, the constants κ and λ are defined in Appendix a, ψ and Ω are auxiliary functions defined in [11], and the dimensions h , a , b , c , and d are shown in Fig. 1.

Because of symmetry, it is sufficient to consider the problem for $0 \leq x_1 < b$, $0 \leq x_2 < \infty$ only. Thus, the membrane and bending problems of the plate must be solved under the following boundary and symmetry conditions stated in terms of the normalized quantities (Fig. 1 and Appendix a):

$$u(0, y) = 0, \quad N_{xy}(0, y) = 0, \quad 0 \leq y < \infty, \quad (12)$$

$$N_{xx}(b', y) = 0, \quad N_{xy}(b', y) = 0, \quad 0 \leq y < \infty, \quad (13)$$

$$N_{xy}(x,0) = 0, \quad 0 \leq x < b', \quad (14)$$

$$N_{yy}(x,0) = \frac{1}{E} [-\sigma_{\infty}(x) + \sigma(x)], \quad c' < x < d', \quad (15a)$$

$$v(x,0) = 0, \quad 0 \leq x < c', \quad d' < x < b'; \quad (15b)$$

$$\beta_x(0,y) = 0, \quad M_{xy}(0,y) = 0, \quad V_x(0,y) = 0, \quad 0 \leq y < \infty, \quad (16)$$

$$M_{xx}(b',y) = 0, \quad M_{xy}(b',y) = 0, \quad V_x(b',y) = 0, \quad 0 \leq y < \infty, \quad (17)$$

$$M_{xy}(x,0) = 0, \quad V_y(x,0) = 0, \quad 0 \leq x < b', \quad (18)$$

$$M_{yy}(x,0) = \frac{1}{6E} [-m_{\infty}(x) + m(x)], \quad c' < x < d', \quad (19a)$$

$$\beta_y(x,0) = 0, \quad 0 \leq x < c', \quad d' < x < b'. \quad (19b)$$

The conditions stated above refer to the perturbation problem in which the crack surface tractions are the only nonzero external loads. Consequently, in addition to (12)-(19) it is required that

$$N_{yy}(x,\infty) = 0, \quad N_{xy}(x,\infty) = 0, \quad 0 \leq x < b', \quad (20)$$

$$M_{yy}(x,\infty) = 0, \quad M_{xy}(x,\infty) = 0, \quad V_y(x,\infty) = 0, \quad 0 \leq x < b'. \quad (21)$$

The input functions σ_{∞} and m_{∞} which appear in (15a) and (19a) are defined by

$$\sigma_{\infty}(x) = N_{22}^{\infty}(x_1,0)/h, \quad m_{\infty}(x) = 6M_{22}^{\infty}(x_1,0)/h^2 \quad (22)$$

where $N_{ij}^{\infty}(x_1, x_2)$ and $M_{ij}^{\infty}(x_1, x_2)$, ($i, j=1, 2$) are the membrane and moment resultants in the plate under the actual applied loads in the absence of any cracks. The functions $\sigma(x)$ and $m(x)$ are unknown and are defined by

$$\sigma(x) = \frac{N(x_1)}{h} = \frac{N(a^*x)}{h}, \quad m(x) = \frac{6M(x_1)}{h^2} = \frac{6M(a^*x)}{h^2} \quad (23)$$

where the membrane load $N(x_1)$ and the bending moment $M(x_1)$ represent the stress component $\sigma_{22}(x_1, 0, x_3)$ in the net ligament $c < x_1 < d$, $-\frac{h}{2} < x_3 < \frac{h}{2} = L$.

In the bending problem the solution of the differential equations (2)-(4) satisfying the symmetry conditions (16) and the regularity conditions (21) may be expressed as follows [9]:

$$w(x,y) = \frac{2}{\pi} \int_0^{\infty} (A_1 + \gamma A_2) e^{-\alpha y} \cos \alpha x \, d\alpha + \frac{2}{\pi} \int_0^{\infty} (C_1 \cosh \beta x + C_2 x \sinh \beta x) \cos \beta y \, d\beta, \quad (24)$$

$$\Omega(x,y) = \frac{2}{\pi} \int_0^{\infty} B_1 e^{-r_1 y} \sin \alpha x \, d\alpha + \frac{2}{\pi} \int_0^{\infty} B_2 \sinh r_2 x \sin \beta y \, d\beta, \quad (25)$$

$$\psi(x,y) = \frac{2}{\pi} \int_0^{\infty} [-A_1 + (2\kappa\alpha - \gamma)A_2] e^{-\alpha y} \cos \alpha x \, d\alpha + \frac{2}{\pi} \int_0^{\infty} [-(C_1 + 2\kappa\beta C_2) \cosh \beta x - C_2 x \sinh \beta x] \cos \beta y \, d\beta, \quad (26)$$

where $A_i(\alpha)$, $B_i(\alpha)$ and $C_i(\beta)$, ($i=1,2$) are unknown functions and

$$r_1 = \left[\alpha^2 + \frac{2}{\kappa(1-\nu)} \right]^{\frac{1}{2}}, \quad r_2 = \left[\beta^2 + \frac{2}{\kappa(1-\nu)} \right]^{\frac{1}{2}}. \quad (27)$$

By substituting from (24)-(26) into (7), (9)-(11) and by using five homogeneous conditions (17) and (18) five of the six unknown functions may be eliminated. The mixed boundary condition (19) would then determine the sixth.

Similarly from the plane stress solution of the plate satisfying the conditions (12), (14) and (20) the stresses and the y -component of the displacement may be expressed as [8]

$$N_{xx}(x,y) = -\frac{2}{\pi} \int_0^{\infty} h_1(\alpha) (1-\alpha y) e^{-\alpha y} \cos \alpha x \, d\alpha - \frac{2}{\pi} \int_0^{\infty} [h_2(\beta) \cosh \beta x + \beta x h_3(\beta) \sinh \beta x] \cos \beta y \, d\beta, \quad (28)$$

$$N_{yy}(x,y) = -\frac{2}{\pi} \int_0^{\infty} h_1(\alpha)(1+\alpha y)e^{-\alpha y} \cos \alpha x \, d\alpha \\ + \frac{2}{\pi} \int_0^{\infty} [(h_2+2h_3) \cosh \beta x + \beta x h_3 \sinh \beta x] \cos \beta y \, d\beta, \quad (29)$$

$$N_{xy}(x,y) = -\frac{2}{\pi} \int_0^{\infty} \alpha y h_1(\alpha) e^{-\alpha y} \sin \alpha x \, d\alpha \\ + \frac{2}{\pi} \int_0^{\infty} [(h_2+h_3) \sinh \beta x + \beta x h_3 \cosh \beta x] \sin \beta y \, d\beta, \quad (30)$$

$$\frac{E}{1+\nu} v(x,y) = \frac{2}{\pi} \int_0^{\infty} \frac{h_1}{\alpha} \left(\frac{1+\kappa}{2} + \alpha y \right) e^{-\alpha y} \cos \alpha x \, d\alpha \\ + \frac{2}{\pi} \int_0^{\infty} \left[\left(\frac{h_2}{\beta} + \frac{1+\kappa}{2} h_3 \right) \cosh \beta x + x h_3 \sinh \beta x \right] \sin \beta y \, d\beta. \quad (31)$$

In this case the unknown functions h_1 , h_2 and h_3 are determined from the remaining boundary conditions (13) and (15).

3. The Integral Equations

If we now replace the mixed boundary conditions (15) and (19) respectively by

$$\frac{\partial}{\partial x} v(x,0) = g_1(x), \quad 0 \leq x < b, \quad (32)$$

$$\frac{\partial}{\partial x} \beta_y(x,0) = g_2(x), \quad 0 \leq x < b, \quad (33)$$

it is seen that by using (17), (18), (13), (32) and (33) all nine unknown functions A_i , B_i , C_i , ($i=1,2$) and h_j , ($j=1,2,3$) which appear in the formulation of the problem given in the previous section may be expressed in terms of the new unknown functions g_1 and g_2 . From the definitions (32) and (33) it also follows that conditions (15b) and (19b) are equivalent to

$$g_i(x) = 0, \quad 0 \leq x < c', \quad d' < x < b', \quad (i=1,2), \quad (34)$$

$$\int_{c'}^{d'} g_i(x) dx = 0, \quad (i=1,2). \quad (35)$$

The functions g_1 and g_2 may now be determined from the two remaining conditions (15a) and (19a). Referring to [8] and [9] for details, the following integral equations may be obtained from these two conditions:

$$\frac{\sigma(x)}{E} - \frac{1}{2\pi} \int_{c'}^{d'} \left[\frac{1}{t-x} + \frac{1}{t+x} + k_1(x,t) - k_1(x,-t) \right] g_1(t) dt = \frac{\sigma_\infty(x)}{E}, \quad (36)$$

$$\begin{aligned} \frac{m(x)}{6E} - \frac{a^*(1-\nu^2)}{2\pi h \lambda^4} \int_{c'}^{d'} \left\{ \left[\frac{3+\nu}{1+\nu} \left(\frac{1}{t-x} + \frac{1}{t+x} \right) - \frac{4\kappa(1-\nu)}{1+\nu} \left[\frac{1}{(t-x)^3} + \frac{1}{(t+x)^3} \right] \right. \right. \\ \left. \left. + \frac{4}{1+\nu} \left[\frac{1}{t-x} K_2(\gamma|t-x|) + \frac{1}{t+x} K_2(\gamma|t+x|) \right] + k_2(x,t) \right. \right. \\ \left. \left. - k_2(x,-t) \right\} g_2(t) dt = \frac{m_\infty(x)}{6E}, \quad c' < x < d', \quad (37) \end{aligned}$$

where K_2 is the modified Bessel function of the second kind, the Fredholm kernels $k_1(x,t)$ and $k_2(x,t)$ are given in Appendix b and the constant γ is given by

$$\gamma^2 = \frac{2}{(1-\nu)\kappa} \quad (38)$$

The functions $\sigma(x)$ and $m(x)$ which appear in (36) and (37) are defined by (23) and represent the membrane and moment resultants of the tensile stress σ_{22} in the net ligament $c' < x < d'$. By using the plane strain solution for an edge crack occupying $(h/2) - L < x_3 \leq h/2$ in a strip of thickness h (Fig. 1) under membrane load $N(x_1)$ and bending moment $M(x_1)$ (applied in x_2x_3 plane) and by expressing the rate of change of the potential energy in terms of crack closure energy and the change of compliance, $\sigma(x)$ and $m(x)$ may be expressed in terms of the crack opening

displacement $2v(x,0,0)$ and the crack opening angle $2\beta_y(x,0)$ as follows (see [1] and [4] for details):

$$\sigma(x) = E[\gamma_{tt}(x)v(x) + \gamma_{tb}(x)\beta_y(x)] \quad (39)$$

$$m(x) = 6E[\gamma_{bt}(x)v(x) + \gamma_{bb}(x)\beta_y(x)] \quad (40)$$

where the functions γ_{ij} , ($i,j=t,b$) depend on the local crack depth $L(x)$ and hence are implicit functions of x . The algebraic expressions of these functions are given in [4]. From (32), (33) and (34) by observing that

$$v(x,+0) = \int_{c'}^x g_1(t)dt, \quad \beta_y(x,+0) = \int_{c'}^x g_2(t)dt, \quad (41)$$

and by using (39) and (40), the integral equations (36) and (37) may then be expressed as

$$\begin{aligned} \gamma_{tt}(x) \int_{c'}^x g_1(t)dt - \frac{1}{2\pi} \int_{c'}^{d'} \left[\frac{1}{t-x} + \frac{1}{t+x} + k_1(x,t) - k_1(x,-t) \right] g_1(t)dt \\ + \gamma_{tb}(x) \int_{c'}^x g_2(t)dt = \frac{1}{E} \sigma_\infty(x), \quad c' < x < d', \end{aligned} \quad (42)$$

$$\begin{aligned} \gamma_{bt}(x) \int_{c'}^x g_1(t)dt + \gamma_{bb}(x) \int_{c'}^x g_2(t)dt - \frac{a^*(1-\nu^2)}{2\pi h \lambda^4} \int_{c'}^{d'} \left\{ \frac{3+\nu}{1+\nu} \left(\frac{1}{t-x} \right. \right. \\ \left. \left. + \frac{1}{t+x} \right) - \frac{4\kappa(1-\nu)}{1+\nu} \left[\frac{1}{(t-x)^3} + \frac{1}{(t+x)^3} \right] + \frac{4}{1+\nu} \left[\frac{1}{t-x} K_2(\gamma|t-x|) \right. \right. \\ \left. \left. + \frac{1}{t+x} K_2(\gamma|t+x|) \right] + k_2(x,t) - k_2(x,-t) \right\} g_2(t)dt \\ = \frac{1}{6E} m_\infty(x), \quad c' < x < d'. \end{aligned} \quad (43)$$

From the following asymptotic behavior of the Bessel function $K_2(z)$ for small values of z

$$K_2(z) = \frac{2}{z^2} - \frac{1}{2} + O(z^2 \log z) \quad (44)$$

it can be shown that, as in (42), the integral equation (43) has a simple Cauchy type singular kernel. We also note that the system of singular integral equations (42) and (43) must be solved under the additional conditions (35).

After solving the integral equations (42) and (43) for g_1 and g_2 the Mode I stress intensity factor K at the leading edge of the crack may be obtained by substituting from (39)-(41) into the following expression giving K in a strip containing an edge crack of depth L and subjected to the membrane load σ and bending moment m [4]:

$$K(x) = \sqrt{h} [\sigma(x)g_t + m(x)g_b] \quad (45)$$

where g_t and g_b are functions of L/h and are obtained from the corresponding plane strain solution. From the results given in [12] the expressions for g_t and g_b valid in $0 < L/h < 0.8$ may be obtained as follows:

$$g_t(s) = \sqrt{\pi s} (1.1216 + 6.5200s^2 - 12.3877s^4 + 89.0554s^6 - 188.6080s^8 + 207.3870s^{10} - 32.0524s^{12}), \quad (46a)$$

$$g_b(s) = \sqrt{\pi s} (1.1202 - 1.8872s + 18.0143s^2 - 87.3851s^3 + 241.9124s^4 - 319.9402s^5 + 168.0105s^6), \quad (46b)$$

where $s = L(x)/h$.

We now note that for $0 < c' < d' < b$ the solution of the system of singular integral equations is of the form

$$g_i(x) = \frac{G_i(x)}{(x-c')^{\frac{1}{2}}(d'-x)^{\frac{1}{2}}}, \quad c' < x < d', \quad (i=1,2), \quad (47)$$

where the bounded unknown functions G_1 and G_2 may easily be obtained by using the technique described, for example, in [13].

The general crack geometry shown in Fig. 1 has two special cases. The first is the case of a symmetrically located single crack along $-d' < x < d'$, (i.e., $c'=0$, $d' < b'$). In this problem by using the symmetry considerations and by observing that $g_i(t) = -g_i(-t)$, ($i=1,2$), the integral equations (42) and (43) may be somewhat simplified as follows:

$$\begin{aligned} \gamma_{tt}(x) \int_{-d'}^x g_1(t) dt - \frac{1}{2\pi} \int_{-d'}^{d'} \left[\frac{1}{t-x} + k_1(x,t) \right] g_1(t) dt \\ + \gamma_{tb}(x) \int_{-d'}^x g_2(t) dt = \frac{1}{E} \sigma_\infty(x), \quad -d' < x < d', \end{aligned} \quad (48)$$

$$\begin{aligned} \gamma_{bt}(x) \int_{-d'}^x g_1(t) dt + \gamma_{bb}(x) \int_{-d'}^x g_2(t) dt - \frac{d(1-\nu^2)}{2\pi h \lambda^4} \int_{-d'}^{d'} \left[\frac{3+\nu}{1+\nu} \frac{1}{t-x} \right. \\ \left. - \frac{4\kappa(1-\nu)}{1+\nu} \frac{1}{(t-x)^3} + \frac{4}{1+\nu} \frac{1}{t-x} K_2(\gamma|t-x|) + k_2(x,t) \right] g_2(t) dt \\ = \frac{1}{6E} m_\infty(x), \quad -d' < x < d'. \end{aligned} \quad (49)$$

By using (44) it may again be shown that (49) has a simple Cauchy kernel and the solution of the integral equations is of the following form:

$$g_i(x) = \frac{F_i(x)}{(d'^2 - x^2)^{\frac{1}{2}}}, \quad -d' < x < d', \quad (i=1,2). \quad (50)$$

The second special case is that of corner cracks for which $0 < c' < d' = b'$. In this case it may be shown that as x and t approach the end point b' simultaneously, the kernels k_1 and k_2 in (42) and (43) become unbounded. As shown in [8] and [9] the singular part of these kernels may be separated and may be shown to be

$$k_{1s}(x,t) = k_{2s}(x,t) = \frac{1}{2b'-x-t} - \frac{6(b'-x)}{(2b'-x-t)^2} + \frac{4(b'-x)^2}{(2b'-x-t)^3}, \quad (51)$$

where

$$k_i(x,t) = k_{is}(x,t) + k_{if}(x,t) , \quad (i=1,2) \quad (52)$$

and k_{1f} and k_{2f} are bounded. Together with the Cauchy kernel $1/(t-x)$ in (42) and (43), (51) constitutes a generalized Cauchy kernel. It may be observed that the generalized Cauchy kernel $k_g(x,t) = 1/(t-x) + k_{is}(x,t)$ has the property that $k_g(x,b') = 0$, $k_g(b',t) = 0$ and consequently $g_1(t)$ and $g_2(t)$ are nonsingular at $t=b'$ [8]. Also, in this case the single-valuedness conditions (35) are not valid and, as pointed out in [8], are not needed for a unique solution of the integral equations.

4. The Results

First, some sample problems are solved in order to compare the results obtained from the line spring model in this paper with that obtained from the finite element solutions given in [5] and [6]. In [5] the single symmetric semi-elliptic surface crack problem is considered for a finite plate under uniform tension or cylindrical bending (i.e., $c=0$, $d < b$, Fig. 1). It is assumed that the half length of the plate is $\ell=5d$. Figures 2 and 3 show the comparison of the normalized stress intensity factors calculated along the crack front by the two methods. The normalizing stress intensity factor K_N shown in these figures is defined by

$$K_N = \sigma_\infty \sqrt{\pi L_0} / E(k) , \quad k = \sqrt{1 - L_0^2/d^2} \quad (53)$$

and is the stress intensity factor at the location $x_1 = 0$, $x_2 = 0$, $x_3 = L_0$, (i.e., the end points of the minor axis) of a flat elliptic crack (with semi axes d and L_0) in an infinite solid subjected to uniform tension $\sigma_{22} = \sigma_\infty$ in x_2 direction ($c=0$, Fig. 1). Note that, considering the simplicity of the line spring model, the agreement is not bad. One may also note that at the intersection point of the crack and the plate surface $x = x_1/d = 1$ the results based on the line spring model would not be expected to be very good. Furthermore, at the singular point on the free surface the power of the stress singularity seems to be less

than 1/2 [14] . Hence, theoretically the stress intensity factor defined on the basis of conventional 1/2 power should tend to zero as the point on the crack front approaches the free surface at an angle of $\pi/2$. Thus, strictly speaking, the bounded nonzero stress intensity factor given by the finite element solution at the surface do not seem to be correct either.

Figures 4 and 5 show the comparison of the stress intensity factors for a corner crack having the profile of a quarter ellipse and obtained from the line spring model and the finite element solution given in [6] . It should be noted that the finite element results are obtained for a finite plate in which the half length is equal to the total width of the plate and the crack is only on one corner (see the insert in Fig. 4). However, since the crack length-to plate width ratio in both cases is relatively small ($2a/2b = 1/10$ in line spring and $2a/b = 1/5$ in finite element solution), the stress intensity factors for the two geometries should be approximately equal. The figures again show that the agreement is quite good.

The calculated stress intensity factors are given in Tables 1-11. All stress intensity factors were calculated as a function of $x = x_1/a^*$, ($a^*=d$ for a single crack, $a^*=a$ for two cracks, Fig. 1) defining the location along the crack front and of the relative dimensions of the crack and the plate. The following notation and normalizing stress intensity factors are used in presenting the results:

$$\sigma_{b22}(r,0,x_1) \approx \frac{K_b(x)}{\sqrt{2\pi r}} \quad , \quad x = x_1/a^* \quad , \quad (54)$$

$$\sigma_{t22}(r,0,x_1) \approx \frac{K_t(x)}{\sqrt{2\pi r}} \quad , \quad x = x_1/a^* \quad (55)$$

where subscripts b and t correspond to plates under bending and tension, respectively, σ_{22} is the cleavage stress around the crack front, r and θ are the usual polar coordinates at the crack front in x_2x_3 plane (Fig. 1) and K_b and K_t are the corresponding Mode I stress intensity factors. The results are given for uniform membrane load $N_{22} = N_\infty$ and cylindrical

bending moment $M_{22} = M_{\infty}$ away from the crack region. The normalized stress intensity factors shown in the tables are defined by

$$k_b(x) = \frac{K_b(x)}{K_{bo}}, \quad k_t(x) = \frac{K_t(x)}{K_{to}}, \quad (56)$$

$$K_{to} = \left(\frac{N_{\infty}}{h}\right) \sqrt{h} g_t(s_o), \quad s_o = L_o/h, \quad (57)$$

$$K_{bo} = \left(\frac{6M_{\infty}}{h^2}\right) \sqrt{h} g_b(s_o), \quad s_o = L_o/h \quad (58)$$

where L_o is the maximum crack depth and the functions g_t and g_b are given by (45) and (46). One may note that $g_t(s_o)$ and $g_b(s_o)$ are the shape factors obtained from the corresponding plane strain solution of a plate with an edge crack of depth L_o and, for the values of L_o/h shown in the tables, are given by [12].

$s_o = L_o/h$	0.2	0.4	0.6	0.8
$g_t(s_o)/\sqrt{\pi s_o}$	1.3674	2.1119	4.035	11.988
$g_b(s_o)/\sqrt{\pi s_o}$	1.0554	1.2610	1.915	4.591

Table 1 shows the normalized stress intensity factors at the deepest penetration point of a centrally located single semielliptic surface crack (i.e., $c=0$, $d<b$, Fig. 1) in a plate under uniform tension N_{∞} or bending M_{∞} . Here the crack profile is given by

$$\frac{L_o^2}{L_o^2} + \frac{x_1^2}{d^2} = 1 \quad (59)$$

or

$$L(x) = L_o \sqrt{1-x^2}, \quad (x = x_1/a^*, \quad a^* = d) \quad (60)$$

and hence $x=0$ is the deepest point on the crack front. This is also the point where k_t assumes its maximum value. For $b/h = 10$ relatively complete and for other plate dimensions some sample results showing the variation of the stress intensity factors along the crack front are shown in Tables 2 and 3. Similar results are shown in Tables 4 and 5 for a single surface crack with a rectangular profile (i.e., for $L(x) = L_0$, $-1 < x < 1$). One may observe that, as expected, generally the stress intensity factors for the rectangular crack are higher than that for the semi-elliptic crack.

The results for two collinear semi-elliptic surface cracks (Fig. 1) are shown in tables 6 and 7. Here the crack profile is defined by (Fig. 1)

$$L(\bar{x}) = L_0 \sqrt{1-\bar{x}^2}, \quad \bar{x} = \frac{x_1-(c+a)}{a}, \quad -1 < \bar{x} < 1. \quad (61)$$

Table 6 shows the value $k_i(x^*)$, ($i=b,t$) and the location $\bar{x} = x^*$ of the maximum stress intensity factor for various crack geometries in a plate for which $b = 10h$ and $a = h$. The factor $D = a/(a+c)$ determines the crack location. Table 7 shows some sample results giving the distribution of the stress intensity factors along the crack front for two extreme crack locations considered. The skewness in this distribution does not seem to be very significant.

The results for a plate containing two corner cracks having a profile of a quarter ellipse are shown in Tables 8 and 9 (Fig. 1). In this case the crack profile (or the crack depth) L is defined by

$$L(\bar{x}) = L_0 \sqrt{1-\left(\frac{1-\bar{x}}{2}\right)^2}, \quad \bar{x} = \frac{x_1-(c+a)}{a}, \quad -1 < \bar{x} < 1. \quad (62)$$

Table 8 shows the normalized Mode I stress intensity factors at the maximum penetration point of the crack which is on the plate boundary $x = b'$ (i.e., for $x_1 = b$ or $\bar{x} = 1$ or $L = L_0$). Some results showing the distribution of the stress intensity factors are given in Table 9. The results were similar for all crack geometries in that for plates under

tension and for those having shallow cracks under bending the maximum stress intensity factor was on the boundary $x = b'$, whereas for deep cracks in plates under bending K was maximum at the surface $x_1 = c$ or $x = c'$ (Fig. 1). For corner cracks with a rectangular profile results similar to those shown in Tables 8 and 9 are given in Tables 10 and 11. For this crack geometry too one may note that generally the stress intensity factors for rectangular cracks are higher than those for the elliptic cracks.

From the formulation of the problem it may be seen that all results in the surface crack problem are dependent on the Poisson's ratio ν of the plate. The stress intensity factors given in this paper are calculated for $\nu = 0.3$. However, as shown [9], since the stress intensity factors are not very sensitive to the Poisson's ratio, the results given in Tables 1-11 should be valid for nearly all structural materials.

References

1. The Surface Crack: Physical Problems and Computational Solutions, J.L. Swedlow, ed. ASME, New York, 1972.
2. I.S. Raju and J.C. Newman, "Stress Intensity Factors for a Wide Range of Semi-Elliptical Surface Cracks in Finite Thickness Plates", *Journal of Engineering Fracture Mechanics*, Vol. 11, pp. 817-829, 1979.
3. J.R. Rice and N. Levy, "The Part-Through Surface Crack in an Elastic Plate", *J. Applied Mechanics*, Vol. 39, pp. 185-194, Trans. ASME, 1972.
4. F. Delale and F. Erdogan, "Line Spring Model for Surface Cracks in a Reissner Plate", *Int. J. Engng. Science*, Vol. 19, pp. 1331-1340, 1981.
5. J.C. Newman, Jr. and I.S. Raju, "Analysis of Surface Cracks in Finite Plates Under Tension or Bending Loads", NASA Technical Paper 1578, 1979.

6. J.C. Newman, Jr. and I.S. Raju, "Stress Intensity Factor Equations for Cracks in Three-Dimensional Finite Bodies", ASTM, STP791, 1983.
7. J.C. Newman, Jr. and I.S. Raju, "An Empirical Stress Intensity Factor Equation for the Surface Crack", Journal of Engineering Fracture Mechanics, Vol. 15, pp. 185-192, 1981.
8. G.D. Gupta and F. Erdogan, "The Problem of Edge Cracks in an Infinite Strip", J. Appl. Mech., Vol. 41, pp. 1001-1006, Trans. ASME, 1974.
9. H. Boduroglu and F. Erdogan, "Internal and Edge Cracks in a Plate of Finite Width Under Bending", J. Appl. Mech., Vol. 50, Trans. ASME, pp. 621-629, 1983.
10. E. Reissner, "On Bending of Elastic Plates", Quarterly of Applied Mathematics, Vol. 5, pp. 55-68, 1947-48.
11. F. Delale and F. Erdogan, "Transverse Shear Effect in a Circumferentially Cracked Cylindrical Shell", Quarterly of Applied Mathematics, Vol. 37, pp. 239-258, 1979.
12. A.C. Kaya and F. Erdogan, "Stress Intensity Factors and COD in an Orthotropic Strip", Int. Journal of Fracture, Vol. 16, pp. 171-190, 1980.
13. F. Erdogan, "Mixed Boundary Value Problems in Mechanics", Mechanics-Today, S. Nemat-Nasser, ed. Vol. 4, pp. 1-86, Pergamon Press, Oxford, 1978.
14. J.P. Benthem, "The Quarter Infinite Crack in a Half Space: Alternative and Additional Solutions", Int. J. Solids Structures, Vol. 16, pp. 119-130, 1980.

Appendix a

The definition of normalized quantities

$$x = x_1/a^* , y = x_2/a^* , z = x_3/a^* , \quad (\text{A.1})$$

$$u = u_1/a^* , v = u_2/a^* , w = u_3/a^* , \quad (\text{A.2})$$

$$\phi = \frac{F}{a^{*2}hE} , \beta_x = \beta_1 , \beta_y = \beta_2 , \quad (\text{A.3})$$

$$\sigma_{xx} = \sigma_{11}/E , \sigma_{yy} = \sigma_{22}/E , \sigma_{xy} = \sigma_{12}/E , \quad (\text{A.4})$$

$$N_{\alpha\beta} = \frac{N_{ij}}{hE} , M_{\alpha\beta} = \frac{M_{ij}}{h^2E} , (\alpha,\beta) = (x,y) , (i,j) = (1,2) , \quad (\text{A.5})$$

$$V_x = V_1/hB , V_y = V_2/hB , \quad (\text{A.6})$$

$$B = \frac{5}{6} \frac{E}{2(1+\nu)} , \kappa = \frac{E}{B\lambda^4} , \lambda^4 = 12(1-\nu^2)a^{*2}/h^2 . \quad (\text{A.7})$$

$$b' = b/a^* , c' = c/a^* , d' = d/a^*$$

In the problem described by Fig. 1, $a^* = a = (d-c)/2$ for $0 < c < d \leq b$ and $a^* = d$ for $c = 0, d < b$.

Appendix b

The Fredholm kernels k_1 and k_2 which appear in the integral equations (36) and (37)

$$k_1(x,t) = \int_0^{\infty} \frac{e^{-(2b'-t)\beta}}{1+4\beta b' e^{-2\beta b'} - e^{-4\beta b'}} \{-[1+(3+2\beta b')e^{-2\beta b'}] \cosh\beta x - 2\beta x e^{-2\beta b'} \sinh\beta x - [2\beta x \sinh\beta x + (3-2\beta b' + e^{-2\beta b'}) \cosh\beta x][1-2\beta(b'-t)]\} d\beta, \quad (B.1)$$

$$k_2(x,t) = \int_0^{\infty} \left\{ \left[-\frac{3+v}{1+v} - \frac{1-v}{1+v} \beta(b'-t) \right] \frac{1+e^{-2\beta x}}{1-e^{-2\beta b'}} e^{-(2b'-t-x)\beta} - \frac{2\kappa(1-v)}{1+v} \frac{1+e^{-2r_2 x}}{1-e^{-2r_2 b'}} (\beta^2 e^{-(b'-t)r_2} - \beta r_2 e^{-(b'-t)\beta}) e^{-(b'-x)r_2} + \left[\left(\frac{2\beta}{1-v} - \frac{2b'\beta^2}{1+v} \frac{1+e^{-2b'\beta}}{1-e^{-2b'\beta}} \right) (1+e^{-2\beta x}) + \frac{4}{1+v} \{ \kappa\beta^3 (1+e^{-2\beta x}) + \frac{\beta^2}{2} x(1-e^{-2\beta x}) - \frac{v}{1-v} \beta(1+e^{-2\beta x}) \} \right] \frac{1}{D} D_1 e^{-(2b'-t-x)\beta} + D_2 e^{-(b'-x)\beta} e^{-(b'-t)r_2} \right] - \frac{4\kappa}{1+v} \beta^2 r_2 (1+e^{-2r_2 x}) \frac{1}{D} [D_1 e^{-(b'-t)\beta} + D_2 e^{-(b'-t)r_2}] \frac{1-e^{-2b'\beta}}{1-e^{-2b'r_2}} e^{-(b'-x)r_2} \} d\beta, \quad (B.2)$$

$$D_1 = \frac{2\beta}{\gamma^2} r_2 (1-e^{-2b'\beta}) \frac{1+e^{-2b'r_2}}{1-e^{-2b'r_2}} - 2(1+e^{-2b'\beta}) + \frac{1+e^{-2b'\beta}}{\kappa\gamma^2} \left[1-(b'-t)\beta \right] - (1-v) \left[\frac{\beta}{2} (b'-t) - \kappa\beta^2 \right] (1-e^{-2b'\beta}), \quad (B.3)$$

$$D_2 = -\frac{2\beta^2}{\gamma^2} \frac{1+e^{-2b'r_2}}{1-e^{-2b'r_2}} (1-e^{-2b'\beta}) - \kappa\beta^2(1-\nu)(1-e^{-2b'\beta}) \quad , \quad (B.4)$$

$$D = 4b'\beta^2 e^{-2b'\beta} - \left(\frac{3+\nu}{1-\nu} \beta + 2\kappa\beta^3\right) (1-e^{-4b'\beta}) \\ + 2\beta^2 \kappa r_2 \frac{1+e^{-2b'r_2}}{1-e^{-2b'r_2}} (1-e^{-2b'\beta})^2 \quad . \quad (B.5)$$

Table 1. The normalized stress intensity factors at the maximum penetration point ($x=0$) of a symmetrically located single semi-elliptic surface crack in a plate under uni-form tension or bending ($\nu=0.3$).

$\frac{b}{h}$	$\frac{d}{h}$	$L_o = 0.2h$		$L_o = 0.4h$		$L_o = 0.6h$		$L_o = 0.8h$	
		$k_b(0)$	$k_t(0)$	$k_b(0)$	$k_t(0)$	$k_b(0)$	$k_t(0)$	$k_b(0)$	$k_t(0)$
10	0.5	.709	.729	.308	.390	.0518	.175	-.0290	0.0503
	0.6	.737	.755	.342	.421	.0705	.192	-.0257	.0555
	0.8	.777	.792	.398	.470	.104	.221	-.0188	.0648
	1	.805	.818	.443	.508	.132	.246	-.0121	.0730
	4/3	.837	.848	.501	.559	.174	.282	-.0014	.0848
	2	.876	.884	.584	.630				
	4	.930	.934	.723	.752	.390	.464	.0726	.155
	6	.953	.956	.800	.819	.499	.556	.127	.203
	8	.967	.969	.853	.865	.592	.634	.190	.256
	9.5	.975	.976	.885	.893	.659	.689	.249	.305
9.61	.976	.977	.887	.894	.664	.693	.254	.310	
9.8	.977	.978	.891	.898	.672	.700	.264	.318	
8	0.5	.709	.729	.308	.390	.0519	.175	-.0290	.0503
	0.6	.738	.755	.342	.421	.0706	.192	-.0256	.0556
	0.8	.778	.792	.399	.470	.104	.221	-.0188	.0649
	1	.805	.818	.444	.509	.133	.247	-.0120	.0731
	2	.877	.885	.586	.632	.246	.341	.0189	.105
	4	.932	.936	.730	.758	.400	.472	.0774	.159
	6	.957	.959	.814	.830	.525	.576	.144	.216
	7.69	.971	.972	.867	.876	.626	.660	.223	.282
	7.84	.972	.973	.872	.880	.635	.667	.233	.290
6	0.5	.710	.729	.307	.391	.0521	.176	-.0289	.0503
	0.6	.738	.756	.343	.422	.0710	.192	-.0256	.0556
	0.9	.794	.807	.424	.492	.122	.235	-.0152	.0693
	1.2	.827	.839	.483	.543	.160	.270	-.0051	.0807
	1.5	.851	.861	.530	.583	.196	.301	.0046	.0910
	3	.915	.920	.681	.715	.341	.423	.0531	.137
	4	.930	.934	.723	.752	.390	.464	.0726	.155
	5	.953	.955	.802	.818	.507	.560	.136	.208
	5.77	.963	.964	.839	.850	.576	.616	.187	.250
	5.88	.964	.965	.844	.855	.587	.625	.197	.258

Table 1 (cont)

$\frac{b}{h}$	$\frac{d}{h}$	$L_o = 0.2h$		$L_o = 0.4h$		$L_o = 0.6h$		$L_o = .8h$	
		$k_b(0)$	$k_t(0)$	$k_b(0)$	$k_t(0)$	$k_b(0)$	$k_t(0)$	$k_b(0)$	$k_t(0)$
4	0.5	.711	.730	.309	.392	.0528	.176	-.0289	.0504
	0.666	.755	.771	.366	.441	.0839	.204	-.0231	.0591
	0.8	.780	.795	.403	.474	.106	.223	-.0184	.0653
	1	.809	.821	.450	.514	.137	.250	-.0112	.0738
	1.33	.843	.853	.512	.568	.183	.289	.0006	.0866
	1.5	.856	.865	.540	.591	.204	.307	.0068	.0929
	2	.886	.893	.608	.650	.265	.358	.0257	.111
	3.92	.951	.953	.800	.815	.519	.565	.152	.218
2	0.5	.716	.735	.316	.398	.0557	.179	-.0287	.0508
	0.6	.747	.763	.355	.431	.0768	.197	-.0249	.0564
	0.8	.791	.804	.421	.488	.117	.232	-.0166	.0671
	0.9	.808	.820	.450	.513	.136	.248	-.0121	.0722
	1.0	.823	.843	.477	.537	.156	.265	-.0072	.0774
	4/3	.864	.872	.561	.608	.224	.321	.0118	.0961
	1.9	.916	.919	.701	.726	.385	.450	.0754	.150
	1.96	.920	.924	.718	.740	.411	.471	.0903	.162

Table 2. Distribution of the stress intensity factors along the crack front in a plate containing a single symmetric semi-elliptic surface crack ($b/h = 10$, $\nu = 0.3$, $x = x_1/d$).

	k_b	k_t	k_b	k_t	k_b	k_t	k_b	k_t
L_o/h	0.2		0.4		0.6		0.8	
x	$b/h = 10$, $d/h = 0.5$, $\nu = 0.3$							
0.929	0.628	.547	.428	.340	.191	.152	.0486	.444
0.828	.672	.609	.392	.349	.154	.156	.0314	.472
0.688	.694	.656	.361	.364	.123	.162	.0113	.510
0.516	.704	.691	.336	.376	.0924	.169	-.0061	.512
0.319	.708	.715	.318	.385	.0672	.173	-.0187	.502
0.108	.709	.727	.308	.390	.0535	.175	-.0276	.503
0	.709	.729	.307	.390	.0518	.175	-.0290	.503
$b/h = 10$, $d/h = 1$, $\nu = 0.3$								
0.929	.631	.545	.505	.391	.272	.205	.0809	.0649
0.828	.709	.639	.496	.426	.239	.215	.0621	.0677
0.688	.756	.710	.480	.457	.209	.226	.0396	.0718
0.516	.783	.762	.464	.482	.177	.236	.0183	.0729
0.319	.798	.798	.451	.499	.149	.243	.0163	.0724
0.108	.804	.816	.444	.507	.134	.246	-.0103	.0728
0	.805	.818	.443	.508	.132	.246	-.0121	.0730
$b/h = 10$, $d/h = 4$, $\nu = 0.3$								
0.929	.623	.535	.561	.420	.402	.285	.168	.121
0.828	.739	.661	.626	.517	.420	.339	.163	.137
0.688	.819	.763	.666	.601	.426	.387	.144	.150
0.516	.875	.844	.695	.671	.418	.425	.120	.156
0.319	.910	.901	.713	.722	.402	.451	.0953	.156
0.108	.927	.930	.722	.748	.391	.463	.0756	.155
0	.930	.934	.723	.752	.390	.464	.0726	.155
$b/h = 10$, $d/h = 8$, $\nu = 0.3$								
0.929	.622	.533	.571	.423	.453	.316	.238	.170
0.828	.747	.667	.665	.542	.513	.403	.260	.209
0.688	.837	.778	.735	.653	.560	.487	.261	.240
0.516	.901	.868	.791	.749	.586	.558	.245	.256
0.319	.944	.931	.830	.821	.593	.607	.219	.259
0.108	.965	.965	.850	.860	.592	.631	.194	.256
0	.967	.969	.853	.865	.592	.634	.190	.256

Table 2 (cont.)

	k_b	k_t	k_b	k_t	k_b	k_t	k_b	k_t
L_o/h	0.2		0.4		0.6		0.8	
x	b/h = 10 , d/h = 9.8 , $\nu = 0.3$							
0.929	.629	.538	.597	.442	.508	.355	.312	.225
0.828	.753	.673	.692	.562	.572	.446	.341	.270
0.688	.844	.784	.763	.675	.626	.536	.345	.305
0.516	.909	.875	.822	.775	.658	.614	.328	.323
0.319	.952	.939	.865	.851	.670	.669	.298	.324
0.108	.974	.973	.888	.892	.672	.697	.268	.319
0	.977	.978	.891	.898	.672	.700	.264	.318

Table 3. Distribution of the stress intensity factors along the crack front in a plate containing a single symmetric semi-elliptic surface crack ($b/h = 2, 4, 6$; $\nu=0.3$).

	k_b	k_t	k_b	k_t	k_b	k_t	k_b	k_t
L_o/h	0.2		0.4		0.6		0.8	
x	$b/h = 2, d/h = 1, \nu = 0.3$							
0.929	.646	.559	.542	.421	.306	.232	.0941	0.0752
0.828	.726	.654	.533	.456	.271	.240	.0736	.0768
0.688	.774	.726	.517	.487	.238	.249	.0492	.0796
0.516	.801	.779	.500	.511	.204	.257	.0261	.0793
0.319	.816	.814	.486	.527	.174	.262	.0077	.0777
0.108	.823	.832	.478	.536	.158	.264	-.0053	.0774
0	.823	.834	.477	.537	.156	.265	-.0072	.0774
	$b/h = 4, d/h = 1, \nu = 0.3$							
0.929	.634	.548	.512	.397	.278	.210	.0833	.0668
0.828	.713	.642	.504	.432	.245	.220	.0642	.0694
0.688	.760	.713	.488	.463	.214	.230	.0414	.0733
0.516	.787	.766	.471	.488	.182	.240	.0198	.0741
0.319	.802	.801	.458	.505	.154	.246	.0028	.0734
0.108	.808	.819	.451	.513	.139	.249	-.0094	.0737
0	.809	.821	.450	.514	.137	.250	-.0112	.0738
	$b/h = 6, d/h = 1.2, \nu = 0.3$							
0.929	.632	.545	.522	.402	.296	.221	.0921	.0723
0.828	.717	.645	.523	.446	.266	.234	.0732	.0754
0.688	.770	.722	.513	.483	.237	.247	.0501	.0796
0.516	.801	.778	.501	.512	.206	.258	.0277	.0808
0.319	.819	.817	.490	.532	.178	.266	.0096	.0802
0.108	.827	.836	.474	.541	.162	.270	-.0032	.0806
0	.827	.839	.483	.543	.160	.270	-.0051	.0807

Table 4. The normalized stress intensity factors at the center ($x=0$) of a single symmetric rectangular surface crack in a plate under tension or bending ($\nu=0.3$).

$\frac{b}{h}$	$\frac{d}{h}$	$L_o = 0.2h$		$L_o = 0.4h$		$L_o = 0.6h$		$L_o = 0.8h$	
		$k_b(0)$	$k_t(0)$	$k_b(0)$	$k_t(0)$	$k_b(0)$	$k_t(0)$	$k_b(0)$	$k_t(0)$
10	0.5	.765	.784	.340	.429	.0607	.194	-.0316	.0599
	2	.915	.922	.652	.699	.284	.388	.0261	.122
	5	.970	.973	.847	.868	.544	.611	.134	.222
	9.8	.999	.999	.987	.989	.914	.927	.557	.603
8	0.5	.766	.785	.340	.429	.0608	.194	-.0316	.0599
	1	.853	.865	.496	.563	.154	.276	-.0105	.0851
	4	.963	.966	.814	.840	.487	.562	.104	.195
	7.84	.998	.998	.982	.985	.892	.907	.503	.554
6	0.5	.766	.785	.341	.429	0.0610	.194	-.0316	.0600
	1	.855	.867	.498	.566	.155	.277	-.0103	.0854
	3	.951	.955	.767	.797	.414	.500	.0721	.165
	5.88	.997	.998	.975	.978	.857	.878	.434	.491
4	0.5	.768	.787	.343	.431	0.0619	.195	-.0315	.0602
	1	.859	.870	.505	.571	.159	.281	-.0095	.0863
	2	.930	.936	.690	.732	.320	.419	.0370	.133
	3.92	.996	.996	.959	.965	.797	.826	.341	.408
2	0.5	.776	.794	.352	.439	.0655	.198	-.0312	.0609
	1	.880	.890	.545	.606	.186	.304	-.0041	.0923
	1.5	.941	.945	.710	.749	.334	.432	.0395	.135
	1.96	.990	.991	.916	.927	.666	.715	.205	.285

Table 5. Distribution of the stress intensity factors along the crack front in a plate containing a single symmetric rectangular surface crack, $x = x_1/d$.

	k_b	k_t	k_b	k_t	k_b	k_t	k_b	k_t
L_o/h	0.2		0.4		0.6		0.8	
x	b/h = 2, d/h = 1, $\nu = 0.3$							
0.929	.585	.618	.233	.334	.0289	.159	-.0295	0.0458
0.828	.737	.759	.354	.440	.0798	.209	-.0261	.0619
0.688	.814	.829	.439	.514	.122	.248	-.0190	.0741
0.516	.852	.864	.495	.562	.154	.276	-.0120	.0831
0.319	.871	.881	.528	.591	.174	.294	-.0070	.0890
0.108	.879	.889	.543	.605	.184	.302	-.0044	.0920
0	.880	.890	.545	.606	.186	.304	-.0041	.0923
	b/h = 6, d/h = 1, $\nu = 0.3$							
0.929	.566	.601	.210	.314	.0181	.149	-.0302	.0439
0.828	.715	.738	.321	.411	.0623	.194	-.0283	.0586
0.688	.789	.806	.399	.480	.0996	.228	-.0227	.0694
0.516	.827	.841	.451	.524	.127	.253	-.0169	.0773
0.319	.846	.858	.482	.551	.145	.269	-.0127	.0825
0.108	.854	.866	.496	.564	.154	.276	-.0105	.0851
0	.855	.867	.498	.566	.155	.277	-.0103	.0854
	b/h = 10, d/h = 1, $\nu = 0.3$							
0.929	.423	.470	.112	.228	-.0172	.108	-.0293	.0309
0.828	.574	.609	.191	.298	.0038	.138	-.0343	.0417
0.688	.667	.694	.252	.352	.0250	.160	-.0350	.0492
0.516	.721	.744	.297	.390	.0421	.177	-.0339	.0545
0.319	.751	.771	.325	.415	.0539	.188	-.0325	.0580
0.108	.764	.783	.339	.427	.0599	.193	-.0317	.0597
0	.765	.784	.340	.429	.0607	.194	-.0316	.0599

Table 6. The location $x=x^*$ and magnitude $k_b(x^*)$ and $k_t(x^*)$ of the normalized stress intensity factors in a plate containing two collinear semi-elliptic surface cracks, $D=a/(a+c)$.

D		$L_o = 0.2h$		$L_o = 0.4h$		$L_o = 0.6h$		$L_o = 0.8h$	
		$k_b(x^*)$	$k_t(x^*)$	$k_b(x^*)$	$k_t(x^*)$	$k_b(x^*)$	$k_t(x^*)$	$k_b(x^*)$	$k_t(x^*)$
0.112	x^*	0.2	0.05	.929	.319	.929	.929	.929	.929
	$k(x^*)$.831	.839	.649	.554	.409	.308	.138	.107
0.125	x^*	0	0	.929	.040	.929	.108	.929	.516
	$k(x^*)$.812	.824	.522	.518	.287	.523	.867	.756
.250	x^*	0	0	.929	0	.929	0	.929	.516
	$k(x^*)$.807	.820	.509	.512	.275	.248	.0822	.735
0.5	x^*	0	0	-.929	0	-.929	0	-.828	.516
	$k(x^*)$.811	.823	.521	.517	.285	.251	.0858	.0744
0.75	x^*	-0.50	0	-.929	-.050	-.929	-.108	-.929	-.688
	$k(x^*)$.818	.829	.550	.528	.310	.259	.0951	.786

Table 7. Distribution of the normalized stress intensity factors along the crack front in a plate containing two collinear semi-elliptic surface cracks, $\bar{x} = [x_1 - (c+a)]/a$ (Fig. 1).

	k_b	k_t	k_b	k_t	k_b	k_t	k_b	k_t
L_o/h	0.2		0.4		0.6		0.8	
\bar{x}	b/h = 10, d/h = 1, D = a/(c+a) = 0.112, v = 0.3							
0.929	.688	.596	.649	.505	.409	.308	.138	.107
0.828	.766	.689	.623	.527	.351	.300	.106	.102
0.688	.805	.754	.584	.541	.297	.294	.0720	.0975
0.516	.824	.798	.548	.550	.246	.289	.0411	.0915
0.319	.831	.827	.519	.554	.204	.285	.0175	.0858
0.108	.831	.839	.500	.553	.178	.280	.0013	.0829
0	.829	.839	.494	.550	.173	.278	-.0016	.0821
-0.108	.826	.835	.491	.546	.172	.275	-.0004	.0814
-0.319	.816	.814	.492	.532	.184	.269	.0117	.0809
-0.516	.799	.776	.500	.512	.209	.261	.0293	.0818
-0.688	.769	.721	.513	.484	.240	.250	.0516	.0814
-0.828	.720	.649	.526	.450	.270	.239	.0751	.0780
-0.929	.640	.553	.533	.413	.303	.229	.0949	.0758
	b/h = 10, d/h = 1, D = a/(c+a) = 0.75, v = 0.3							
0.929	.637	.551	.521	.404	.288	.217	.0872	.0698
0.828	.716	.645	.514	.440	.254	.227	.0678	.0721
0.688	.764	.717	.499	.472	.224	.237	.0446	.0757
0.516	.793	.771	.484	.498	.192	.247	.0225	.0763
0.319	.809	.807	.472	.516	.164	.254	.0050	.0753
0.108	.816	.826	.467	.526	.149	.258	-.0075	.0754
0	.818	.829	.467	.528	.148	.258	-.0093	.0755
-0.108	.818	.828	.469	.528	.151	.259	-.0073	.0755
-0.319	.814	.812	.480	.522	.169	.258	.0057	.0760
-0.516	.801	.778	.497	.509	.200	.253	.0243	.0778
-0.688	.776	.727	.517	.488	.236	.247	.0481	.0786
-0.828	.730	.657	.538	.460	.272	.240	.0735	.0766
-0.929	.651	.563	.550	.427	.310	.235	.0951	.0757

Table 8. The normalized intensity factors on the edges ($x=\pm b'$) of a plate containing two symmetric corner cracks having a profile of a quarter ellipse (Fig. 1).

$\frac{b}{h}$	$\frac{a}{h}$	$L_o = 0.2h$		$L_o = 0.4h$		$L_o = 0.6h$		$L_o = 0.8h$	
		$k_b(b')$	$k_t(b')$	$k_b(b')$	$k_t(b')$	$k_b(b')$	$k_t(b')$	$k_b(b')$	$k_t(b')$
2	0.25	.775	.790	.380	.485	.0975	.219	-.0172	.0678
	0.3	.797	.810	.415	.485	.120	.239	-.0117	.0743
	0.4	.828	.840	.473	.535	.159	.271	-.0014	.0857
	0.5	.852	.862	.522	.477	.197	.303	.0089	.0963
	0.6	.872	.880	.568	.616	.234	.334	.0199	.107
	0.7	.889	.896	.610	.652	.273	.366	.0321	.118
	0.8	.905	.910	.653	.688	.317	.401	.0470	.131
4	0.26	.777	.792	.384	.459	.102	.223	-.0152	.0700
	0.4	.821	.833	.463	.527	.156	.269	.0003	.0873
	0.6	.858	.867	.539	.593	.215	.319	.0179	.106
	0.8	.883	.890	.597	.642	.264	.361	.0336	.121
	1	.901	.907	.644	.683	.310	.399	.0492	.136
	1.2	.916	.921	.685	.718	.354	.435	.0657	.150
	1.4	.929	.933	.722	.750	.398	.471	.0838	.166
1.6	.939	.942	.756	.779	.443	.508	.105	.184	
6	0.27	.781	.796	.391	.464	.106	.226	-.0140	.0714
	0.3	.792	.806	.410	.481	.119	.237	-.0105	.0755
	0.6	.856	.866	.536	.591	.214	.319	.0187	.107
	0.9	.889	.896	.613	.657	.281	.376	.0409	.128
	1.2	.910	.916	.669	.705	.337	.422	.0609	.147
	1.5	.926	.930	.713	.744	.387	.464	.0809	.165
	1.8	.938	.941	.750	.776	.434	.503	.102	.183
	2.1	.948	.950	.782	.803	.479	.540	.124	.202
2.4	.956	.958	.811	.828	.523	.576	.149	.223	
8	.28	.785	.799	.397	.470	.110	.230	-.0129	.0727
	0.4	.821	.833	.462	.526	.156	.269	.0004	.0875
	0.8	.879	.887	.589	.636	.260	.358	.0343	.122
	1.2	.908	.914	.665	.702	.334	.420	.0607	.147
	1.6	.927	.932	.718	.748	.394	.470	.0846	.168
	2	.941	.944	.760	.784	.447	.514	.108	.189
	2.4	.951	.953	.793	.813	.494	.554	.133	.210
	2.8	.959	.961	.821	.837	.538	.591	.158	.232
3.2	.965	.967	.845	.858	.580	.626	.186	.255	

Table 8 - cont.

$\frac{b}{h}$	$\frac{a}{h}$	$L_o = 0.2h$		$L_o = 0.4h$		$L_o = 0.6h$		$L_o = 0.8h$	
		$k_b(b')$	$k_t(b')$	$k_b(b')$	$k_t(b')$	$k_b(b')$	$k_t(b')$	$k_b(b')$	$k_t(b')$
10	0.25	.772	.787	.376	.452	.0967	.218	-.0165	.0684
	0.75	.873	.882	.576	.625	.249	.349	.0307	.118
	1	.895	.902	.630	.672	.299	.391	.0483	.135
	1.5	.922	.927	.704	.736	.378	.457	.0786	.163
	2	.939	.943	.755	.780	.440	.510	.106	.188
	2.5	.951	.953	.793	.813	.494	.555	.133	.211
	3.0	.959	.961	.823	.840	.541	.594	.160	.234
	3.5	.966	.968	.848	.861	.584	.630	.188	.258
	4.0	.972	.973	.869	.880	.624	.664	.218	.283
4.5	.976	.977	.888	.896	.664	.696	.252	.312	
20	1	.895	.901	.629	.671	.298	.390	.0483	.135

Table 9. Distribution of the normalized stress intensity factors along the crack front in a plate containing two (elliptic) corner cracks, $\bar{x} = [x_1 - (c+a)]/a$ (Fig. 1).

	k_b	k_t	k_b	k_t	k_b	k_t	k_b	k_t
L_o/h	0.2		0.4		0.6		0.8	
\bar{x}	b/h = 2, a/h = 0.5, $\nu = 0.3$							
0.999	.852	.862	.522	.577	.197	.303	.0089	.0963
0.936	.846	.856	.515	.571	.191	.297	.0073	.0936
0.784	.834	.843	.503	.557	.182	.286	.0050	.0883
0.558	.824	.828	.493	.543	.177	.274	.0064	.0834
0.279	.813	.808	.492	.528	.184	.266	.0138	.0805
-0.026	.799	.777	.498	.510	.204	.257	.0263	.0798
-0.329	.776	.732	.511	.488	.231	.248	.0450	.0794
-0.600	.736	.669	.526	.460	.261	.240	.0679	.0768
-0.815	.668	.583	.537	.427	.294	.231	.0882	.0748
-0.953	.549	.460	.532	.390	.336	.232	.112	.0772
	b/h = 8, a/h = 0.8, $\nu = 0.3$							
0.999	.879	.887	.589	.636	.260	.358	.0343	.122
0.936	.874	.882	.582	.630	.253	.351	.0317	.118
0.784	.866	.872	.570	.617	.242	.339	.0277	.112
0.558	.857	.859	.561	.602	.237	.326	.0281	.105
0.279	.844	.836	.557	.583	.243	.314	.0357	.101
-0.026	.825	.800	.557	.559	.259	.302	.0489	.0990
-0.329	.793	.746	.558	.525	.282	.286	.0677	.0966
-0.600	.741	.671	.558	.481	.304	.269	.0896	.0917
-0.815	.658	.573	.547	.428	.326	.249	.108	.0869
-0.953	.521	.434	.502	.361	.345	.231	.127	.0850

Table 10. The normalized stress intensity factors at the edges $x = \pm b'$ of a plate containing two symmetric rectangular corner cracks.

$\frac{b}{h}$	$\frac{a}{h}$	$L_o = 0.2h$		$L_o = 0.4h$		$L_o = 0.6h$		$L_o = 0.8h$	
		$k_b(b')$	$k_t(b')$	$k_b(b')$	$k_t(b')$	$k_b(b')$	$k_t(b')$	$k_b(b')$	$k_t(b')$
2	0.25	.821	.835	.415	.494	.108	.238	-.0185	.0773
	0.5	.895	.903	.581	.638	.223	.337	-.0119	.109
	0.8	.954	.958	.754	.787	.388	.477	.0620	.156
4	0.26	.820	.835	.419	.497	.112	.242	-.0163	.0797
	0.4	.860	.871	.507	.574	.174	.295	.0014	.0985
	1	.937	.942	.716	.755	.359	.453	.0595	.154
	1.6	.976	.978	.856	.876	.550	.617	.139	.227
6	0.27	.823	.838	.426	.504	.117	.246	-.0149	0.0812
	0.6	.891	.900	.589	.645	.240	.353	.0227	.120
	1.6	.956	.960	.788	.817	.453	.534	.0983	.190
	2.4	.984	.985	.902	.915	.648	.700	.202	.283
8	0.28	.827	.841	.433	.510	.122	.250	-.0136	.0826
	0.8	.912	.919	.648	.696	.294	.399	.0409	.138
	2	.967	.970	.833	.856	.525	.595	.133	.222
	3.2	.988	.989	.927	.937	.714	.756	.255	.331
10	0.27	.823	.837	.425	.503	.117	.246	-.0150	.0811
	1	.927	.933	.692	.734	.341	.439	.0573	.153
	2.5	.974	.976	.864	.882	.581	.643	.165	.251
	4	.991	.992	.943	.951	.761	.796	.302	.374

Table 11. Distribution of the normalized stress intensity factors in a plate with rectangular corner cracks, $\bar{x} = [x_1 - (c+a)]/a$.

	k_b	k_t	k_b	k_t	k_b	k_t	k_b	k_t
L_o/h	0.2		0.4		0.6		0.8	
\bar{x}	b/h = 2, a/h = 0.5, v = 0.3							
0.999	.895	.903	.581	.638	.223	.337	.0119	.109
0.936	.892	.901	.576	.634	.218	.332	.0102	.107
0.784	.887	.896	.564	.623	.207	.323	.0059	.103
0.558	.879	.889	.548	.609	.193	.310	.0003	.0967
0.279	.868	.879	.525	.589	.175	.295	-.0057	.0902
-0.026	.851	.863	.493	.561	.153	.275	-.0122	.0828
-0.329	.818	.833	.444	.518	.124	.249	-.0195	.0739
-0.600	.756	.776	.370	.454	.0852	.214	-.0268	.0626
-0.815	.630	.660	.262	.359	.0373	.168	-.0314	.0481
-0.953	.385	.434	.115	.229	-.0098	.107	-.0260	.0284
	b/h = 8, a/h = 0.8, v = 0.3							
0.999	.912	.919	.648	.696	.294	.399	.0409	.138
0.936	.911	.918	.643	.692	.289	.394	.0383	.135
0.784	.907	.915	.633	.683	.277	.384	.0322	.129
0.558	.902	.910	.619	.671	.261	.370	.0249	.121
0.279	.894	.902	.598	.652	.242	.353	.0172	.114
-0.026	.880	.890	.567	.625	.217	.331	.0086	.105
-0.329	.856	.868	.520	.584	.183	.301	-.0015	.0934
-0.600	.809	.824	.446	.520	.137	.260	-.0133	.0792
-0.815	.705	.729	.331	.420	.0759	.205	-.0245	.0610
-0.953	.462	.505	.160	.270	.0073	.131	-.0263	.0367

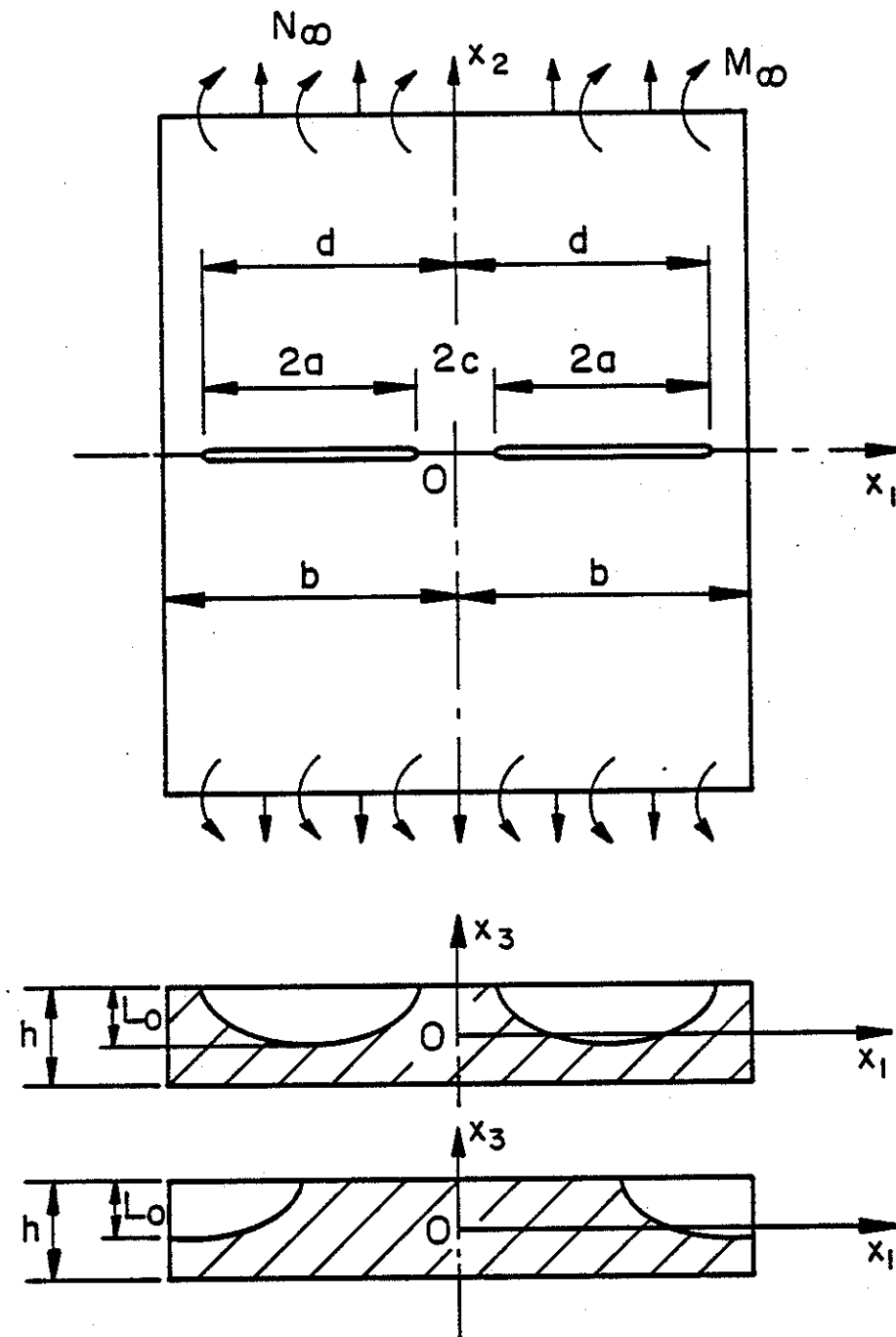


Fig. 1 The geometry of the plate with surface cracks

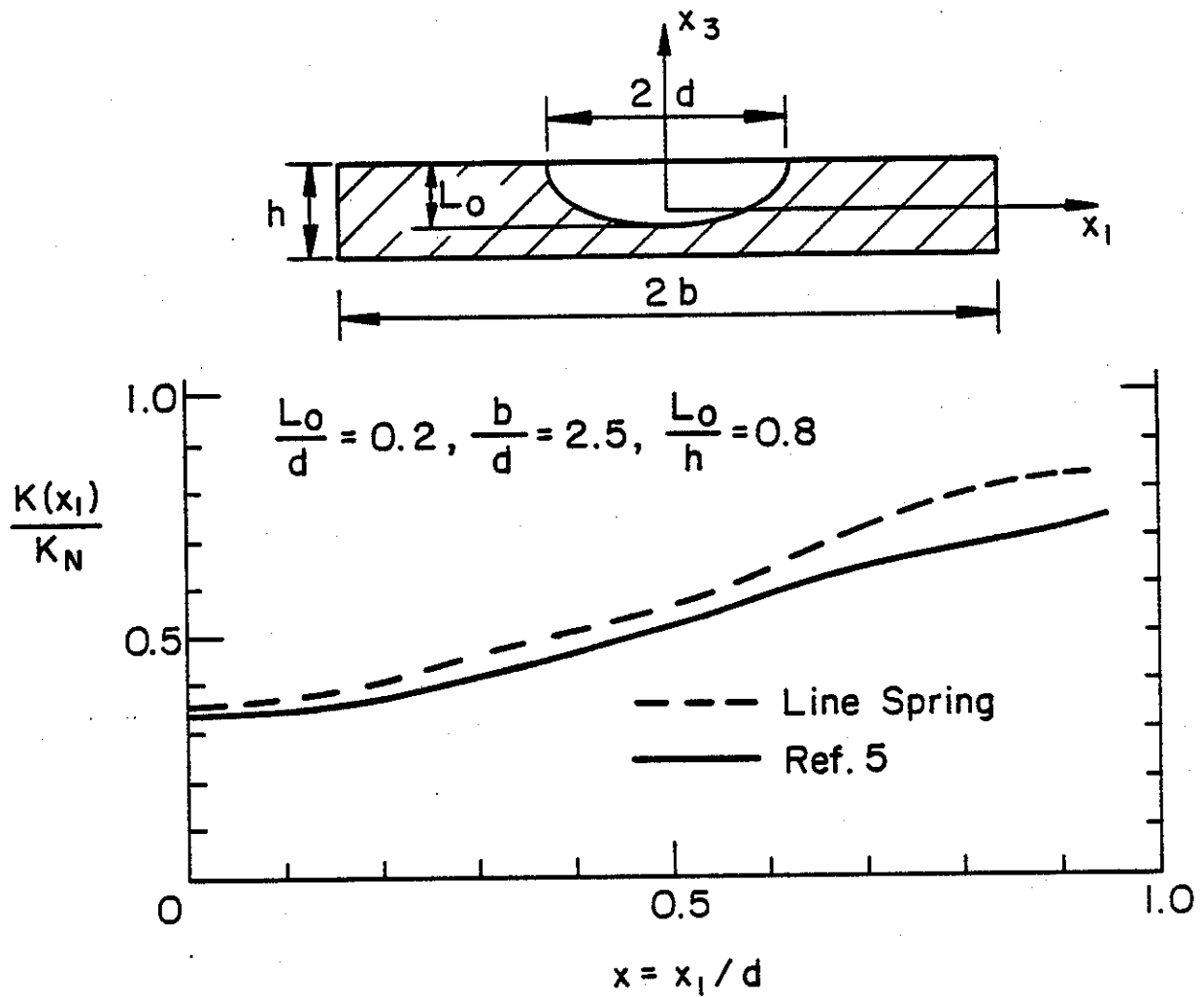


Fig. 2 Comparison of stress intensity factors calculated by the finite element and line spring methods in a plate containing a symmetrically located semi-elliptic surface crack and subjected to uniform bending.

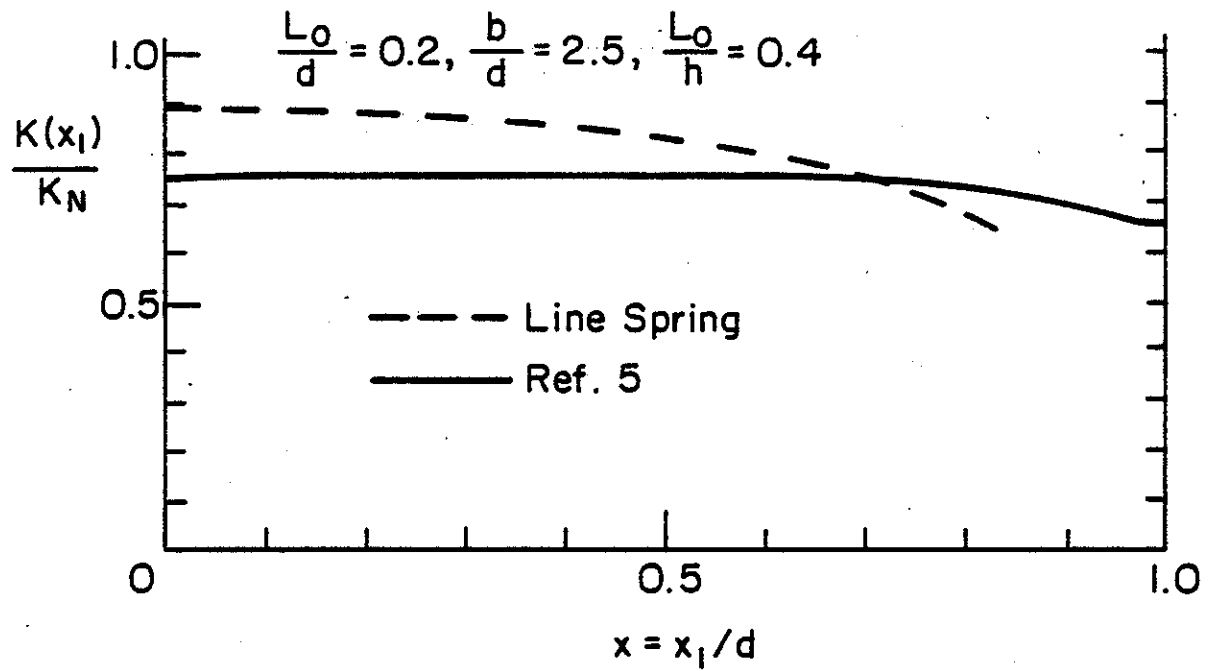
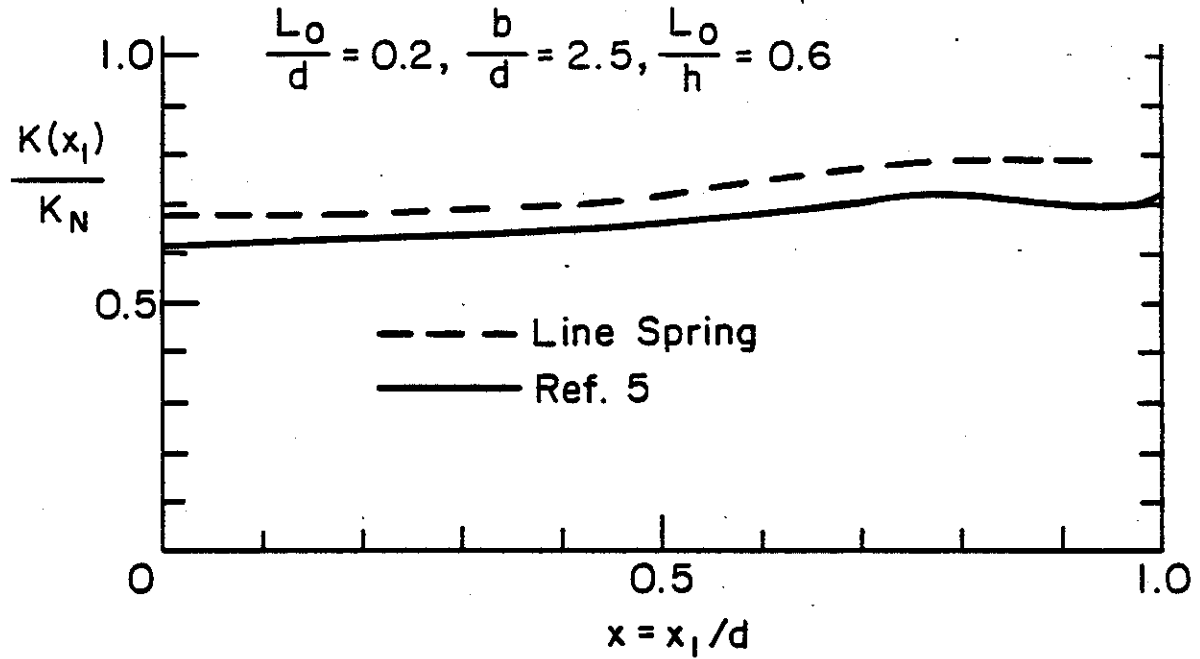


Fig. 3 Comparison of the stress intensity factors calculated by the finite element and line spring methods in a plate containing a single symmetric semi-elliptic surface crack and subjected to uniform bending.

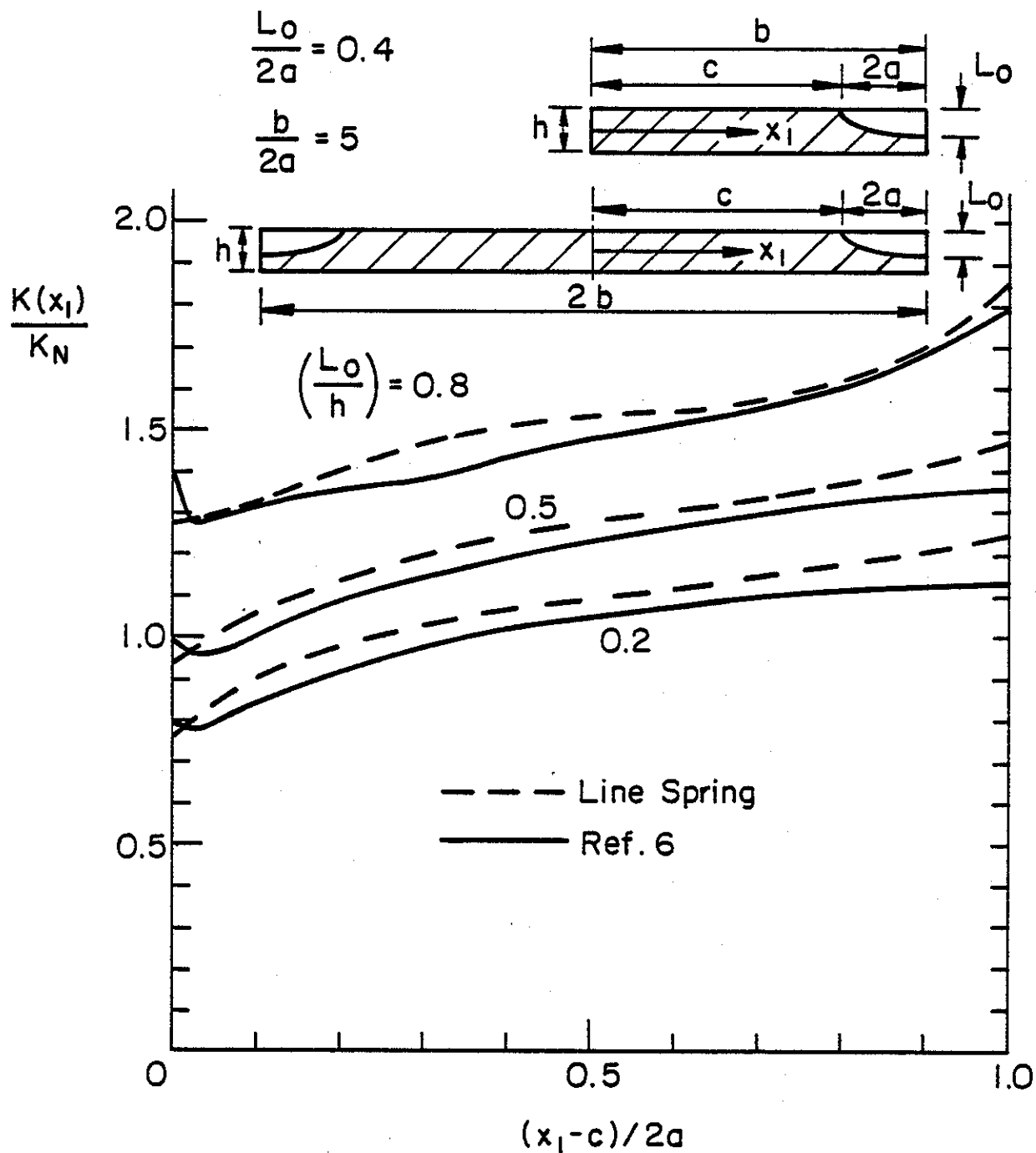


Fig. 4 Comparison of the stress intensity factors calculated by the finite element and line spring methods in a plate containing elliptic corner cracks and subjected to uniform tension, $L_0/2a = 0.4$, $b/2a = 5$.

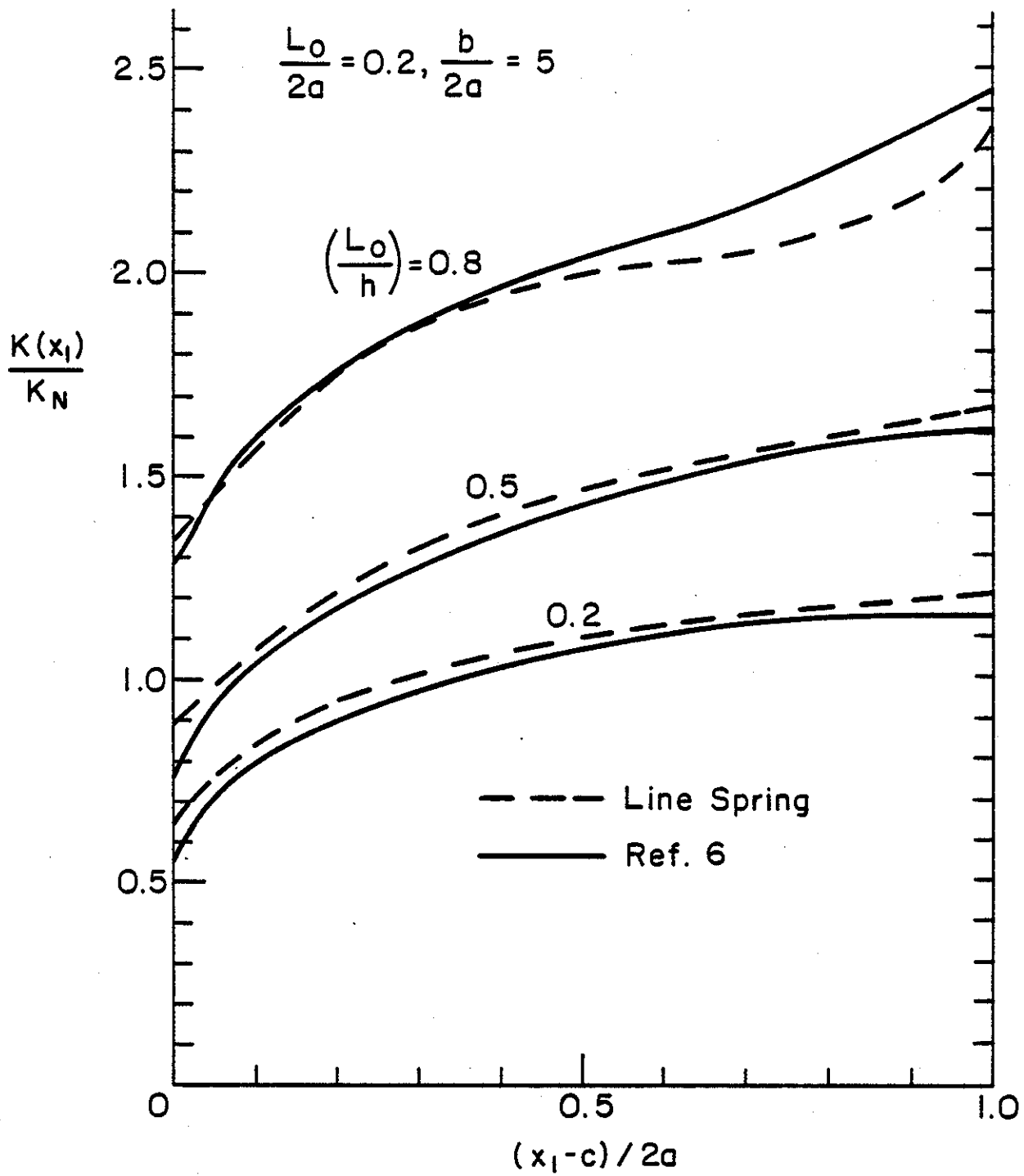


Fig. 5 Comparison of the stress intensity factors calculated by the finite element and line spring methods in a plate containing elliptic corner cracks and subjected to uniform tension, $L_0/2a = 0.2$, $b/2a = 5$.

APPENDIX B

FURTHER RESULTS ON CRACK-INCLUSION INTERACTION PROBLEM

Liu Xue-Hui and F. Erdogan

1. Introduction

The general formulation of the crack-inclusion interaction problem was given in Appendix A of the previous report (Ref. 1 of Part I of this report). The general problem considered in [1] is described in Fig. B1. The inclusion-crack intersection problems studied in [1] included the cases of the common end points (i.e., $a=0$, $c=0$, Fig. B1) and the crack terminating at the inclusion. The intersection problem in which the inclusion end terminates at the crack was not studied. The special case of 90 degree angle of intersection is shown in Fig. B2 and is studied in this report.

2. The Formulation

The formulation of the problem is identical to that given in [1], except that in this case we have to consider two separate cracks along ($-a < x < 0$, $y=0$) and ($0 < x < b$, $y=0$). The reason for this is that at ($x=0$, $y=+0$) the stress state is expected to be singular with a power different than $1/2$ and ($-a, 0$), ($0, b$) and ($0, d$) must be treated as three separate lines of displacement or stress discontinuity. To formulate the problem we define the following unknown functions:

$$\frac{\partial}{\partial x} [u_y(x, +0) - u_y(x, -0)] = g_1(x), \quad 0 < x < b,$$

$$\frac{\partial}{\partial x} [u_x(x, +0) - u_x(x, -0)] = h_1(x), \quad 0 < x < b,$$

$$\frac{\partial}{\partial x} [u_y(x, +0) - u_y(x, -0)] = g_2(x), \quad -a < x < 0,$$

$$\frac{\partial}{\partial x} [u_x(x, +0) - u_x(x, -0)] = h_2(x), \quad -a < x < 0$$

$p(y)$: distributed body force simulating the inclusion, $0 < y < d$.

The Green's functions for the dislocations g and h and the concentrated body force p were given in [1]. The integral equations for the unknown functions defined in (1) are obtained from the boundary conditions on the crack surfaces and the displacement compatibility condition along the stiffener. These conditions may be expressed as (Fig. B2)

$$\begin{aligned}
 \sigma_{1dyy}(x,0) + \sigma_{2dyy}(x,0) + \sigma_{pyy}(x,0) + \sigma_{ayy}(x,0) &= 0, \quad 0 < x < b, \\
 \sigma_{1dxy}(x,0) + \sigma_{2dxy}(x,0) + \sigma_{pxy}(x,0) + \sigma_{axy}(x,0) &= 0, \quad 0 < x < b, \\
 \sigma_{1dyy}(x,0) + \sigma_{2dyy}(x,0) + \sigma_{pyy}(x,0) + \sigma_{ayy}(x,0) &= 0, \quad -a < x < 0, \quad (2a-e) \\
 \sigma_{1dxy}(x,0) + \sigma_{2dxy}(x,0) + \sigma_{pxy}(x,0) + \sigma_{axy}(x,0) &= 0, \quad -a < x < 0, \\
 \varepsilon_{1dyy}(0,y) + \varepsilon_{2dyy}(0,y) + \varepsilon_{pyy}(0,y) + \varepsilon_{ayy}(0,y) &= \varepsilon_s(y), \quad 0 < y < d,
 \end{aligned}$$

where σ_{idyy} , σ_{idxy} and ε_{idyy} are the relevant stress and strain components due to the dislocation pairs g_i and h_i ($i=1,2$), σ_{pyy} , σ_{pxy} and ε_{pyy} are due to the concentrated body force p , σ_{ayy} , σ_{axy} and ε_{ayy} are the applied stress and strain components and $\varepsilon_s(y)$ is the strain in the inclusion. If the stress state away from the crack-inclusion region is given by σ_{ij}^∞ , ($i,j=x,y$), then the applied stress and strain components are

$$\begin{aligned}
 \sigma_{ayy}(x,0) &= \sigma_{yy}^\infty, \quad \sigma_{axy}(x,0) = \sigma_{xy}^\infty, \\
 \varepsilon_{ayy}(0,y) &= \frac{1+\kappa}{8\mu} \left[-\frac{3-\kappa}{1+\kappa} \sigma_{xx}^\infty + \sigma_{yy}^\infty \right], \quad (3a-c)
 \end{aligned}$$

where μ is the shear modulus and $\kappa=3-4\nu$ for plane strain and $\kappa=(3-\nu)/(1+\nu)$ for plane stress. By observing that the inclusion is under a longitudinal distributed force $-p(y)$, the strain in the inclusion may be expressed as

$$\varepsilon_s(y) = -\frac{1+\kappa_s}{8\mu_s A_s} \int_y^d p(r) dr \quad (4)$$

where κ_s and μ_s are the elastic constants and A_s is the cross-sectional area of the inclusion per unit thickness in z direction. The expressions for all the remaining terms are given in [1]. Thus, by using the kernels developed in [1], the system of equations (2) may be expressed as follows:

$$\begin{aligned} \frac{2\mu}{\pi(\kappa+1)} \left(\int_0^b \frac{g_1(t)dt}{t-x} + \int_{-a}^0 \frac{g_2(t)dt}{t-x} \right) - \frac{1}{2\pi(1+\kappa)} \int_0^d \left[\frac{(2+\kappa)t}{t^2+x^2} - \frac{t(3x^2-t^2)}{(t^2+x^2)^2} \right] p(t)dt \\ = -\sigma_{yy}^{\infty}, \quad 0 < x < b, \end{aligned} \quad (5)$$

$$\begin{aligned} \frac{2\mu}{\pi(\kappa+1)} \left(\int_0^b \frac{h_1(t)dt}{t-x} + \int_{-a}^0 \frac{h_2(t)dt}{t-x} \right) - \frac{1}{2\pi(1+\kappa)} \int_0^d \left[\frac{\kappa x}{t^2+x^2} + \frac{x(3t^2-x^2)}{(t^2+x^2)^2} \right] p(t)dt \\ = -\sigma_{xy}^{\infty}, \quad 0 < x < b, \end{aligned} \quad (6)$$

$$\begin{aligned} \frac{2\mu}{\pi(\kappa+1)} \left(\int_0^b \frac{g_1(t)dt}{t-x} + \int_{-a}^0 \frac{g_2(t)dt}{t-x} \right) - \frac{1}{2\pi(1+\kappa)} \int_0^d \left[\frac{(2+\kappa)t}{t^2+x^2} - \frac{t(3x^2-t^2)}{(t^2+x^2)^2} \right] p(t)dt \\ = -\sigma_{yy}^{\infty}, \quad -a < x < 0, \end{aligned} \quad (7)$$

$$\begin{aligned} \frac{2\mu}{\pi(\kappa+1)} \left(\int_0^b \frac{h_1(t)dt}{t-x} + \int_{-a}^0 \frac{h_2(t)dt}{t-x} \right) - \frac{1}{2\pi(1+\kappa)} \int_0^d \left[\frac{\kappa x}{t^2+x^2} + \frac{x(3t^2-x^2)}{(t^2+x^2)^2} \right] p(t)dt \\ = -\sigma_{xy}^{\infty}, \quad -a < x < 0, \end{aligned} \quad (8)$$

$$\begin{aligned} \frac{1}{\pi} \int_0^b \frac{t(t^2+3y^2) - \frac{3-\kappa}{1+\kappa} t(t^2-y^2)}{(t^2+y^2)^2} g_1(t)dt + \frac{1}{\pi} \int_0^b \frac{y(y^2-t^2) - \frac{3-\kappa}{1+\kappa} y(3t^2+y^2)}{(t^2+y^2)^2} h_1(t)dt \\ + \frac{1}{\pi} \int_{-a}^0 \frac{t(t^2+3y^2) - \frac{3-\kappa}{1+\kappa} t(t^2-y^2)}{(t^2+y^2)^2} g_2(t)dt + \frac{1}{\pi} \int_{-a}^0 \frac{y(y^2-t^2) - \frac{3-\kappa}{1+\kappa} y(3t^2+y^2)}{(t^2+y^2)^2} h_2(t)dt \\ + \frac{\kappa+3 + \frac{3-\kappa}{1+\kappa}(\kappa-1)}{4\mu} \frac{1}{\pi} \int_0^d \frac{p(t)dt}{t-y} = -\frac{(1+\kappa)E}{2\mu A_s E_s} \int_0^y p(t)dt + \frac{1+\kappa}{2\mu} \left(\frac{3-\kappa}{1+\kappa} \sigma_{xx}^{\infty} - \sigma_{yy}^{\infty} \right), \\ 0 < y < d, \end{aligned} \quad (9)$$

The integral equations (5)-(9) must be solved under the following single-valuedness and equilibrium conditions:

$$\int_{-a}^0 g_2(t)dt + \int_0^b g_1(t)dt = 0 , \quad (10)$$

$$\int_{-a}^0 h_2(t)dt + \int_0^b h_1(t)dt = 0 , \quad (11)$$

$$\int_0^d p(t)dt = 0 . \quad (12)$$

From Fig. B2 it is clear that the end points $x=b$, $x=-a$ and $y=d$ are points of stress singularity with standard $1/2$ power [1]. However, the nature of the singularity at $x=y=0$ is not known and does not appear to have been studied before. To study this and to solve the problem described by equations (5)-(12) we express the unknown functions as follows:

$$g_1(t) = \frac{F_1(t)}{t^\alpha(b-t)^{\beta_1}} , \quad h_1(t) = \frac{F_2(t)}{t^\alpha(b-t)^{\beta_2}} , \quad (0 < t < b) ,$$

$$g_2(t) = \frac{F_3(t)}{(-t)^\alpha(t+a)^{\beta_3}} , \quad h_2(t) = \frac{F_4(t)}{(-t)^\alpha(t+a)^{\beta_4}} , \quad (-a < t < 0) ,$$

$$p(t) = \frac{\mu F_5(t)}{t^\alpha(d-t)^{\beta_5}} , \quad (0 < t < d) . \quad (13a-e)$$

where F_1, \dots, F_5 are unknown bounded functions and

$$0 < \text{Re}(\alpha, \beta_k) < 1 , \quad (k = 1, \dots, 5) . \quad (14)$$

By substituting now from (13) into (5)-(9) and by using the function theoretic method (see, for example, [28]) to perform the asymptotic analysis near the crack and inclusion tips ($x=b$, $y=0$), ($x=-a$, $y=0$) and ($y=d$, $x=0$) we first obtain the following standard characteristic equations:

$$\cot \pi \beta_k = 0 \quad , \quad (k = 1, 2, 3, 4, 5) \quad (15)$$

giving $\beta_k = 1/2$, ($k=1, \dots, 5$). Similarly, the asymptotic analysis around the singular point ($x=0, y=0$) yields

$$\frac{F_1(0)}{b^{\beta_1}} \frac{\cot \pi \alpha}{x^\alpha} - \frac{F_3(0)}{a^{\beta_3}} \frac{1}{x^\alpha \sin \pi \alpha} + \frac{F_5(0)}{d^{\beta_5}} \frac{c_1^{-\alpha/2}}{2x^\alpha \sin \frac{\pi \alpha}{2}} = R_1(x) \quad ,$$

$$\frac{F_2(0)}{b^{\beta_2}} \frac{\cot \pi \alpha}{x^\alpha} - \frac{F_4(0)}{a^{\beta_4}} \frac{1}{x^\alpha \sin \pi \alpha} + \frac{F_5(0)}{d^{\beta_5}} \frac{c_2^{-(1-\alpha)/2}}{2x^\alpha \cos \frac{\pi \alpha}{2}} = R_2(x) \quad ,$$

$$\frac{F_1(0)}{b^{\beta_1}} \frac{1}{x^\alpha \sin \pi \alpha} - \frac{F_3(0)}{a^{\beta_3}} \frac{\cot \pi \alpha}{x^\alpha} + \frac{F_5(0)}{d^{\beta_5}} \frac{c_1^{-\alpha/2}}{2x^\alpha \sin \frac{\pi \alpha}{2}} = R_3(x) \quad ,$$

$$\frac{F_2(0)}{b^{\beta_2}} \frac{1}{x^\alpha \sin \pi \alpha} - \frac{F_4(0)}{a^{\beta_4}} \frac{\cot \pi \alpha}{x^\alpha} - \frac{F_5(0)}{d^{\beta_5}} \frac{c_2^{-(1-\alpha)/2}}{2x^\alpha \cos \frac{\pi \alpha}{2}} = R_4(x) \quad ,$$

$$\begin{aligned} \frac{F_1(0)}{b^{\beta_1}} \frac{c_3 + c_4^\alpha/2}{2y^\alpha \sin \frac{\pi \alpha}{2}} + \frac{F_2(0)}{b^{\beta_2}} \frac{c_3 - c_4(1-\alpha)/2}{2y^\alpha \cos \frac{\pi \alpha}{2}} - \frac{F_3(0)}{a^{\beta_3}} \frac{c_3 + c_4^\alpha/2}{2y^\alpha \sin \frac{\pi \alpha}{2}} \\ + \frac{F_4(0)}{a^{\beta_4}} \frac{c_3 - c_4(1-\alpha)/2}{2y^\alpha \cos \frac{\pi \alpha}{2}} + \frac{F_5(0)}{d^{\beta_5}} \frac{c_5 \cot \pi \alpha}{y^\alpha} = R_5(x) \quad , \end{aligned} \quad (16a-e)$$

where the functions R_1, \dots, R_5 represent all the bounded terms near and at ($x=0, y=0$) and the constants c_i are given by

$$c_1 = (\kappa+3)/4 \quad , \quad c_2 = (\kappa-1)/4 \quad , \quad c_3 = 2(\kappa-1)/(\kappa+1) \quad ,$$

$$c_4 = 8/(\kappa+1) \quad , \quad c_5 = 2\kappa/(\kappa+1) \quad . \quad (17)$$

If we now multiply both sides of (16a-d) by x^α and (16e) by y^α and let $x=0, y=0$ we obtain a system of five linear homogeneous algebraic equations in $F_1(0), \dots, F_5(0)$. Since $F_1(0), \dots, F_5(0)$ are nonzero, the determinant of the

coefficients of this algebraic system must be zero, giving the following characteristic equation to determine the power of singularity α

$$\{c_5(2\cos^2 \frac{\pi\alpha}{2} - 1) + [c_2 - (1-\alpha)/2][c_3 - c_4(1-\alpha)/2] - (c_1 - \alpha/2)(c_3 + c_4\alpha/2)\}(1 - \cos^2 \frac{\pi\alpha}{2})\cos^2 \frac{\pi\alpha}{2} = 0 \quad (18)$$

From (18) and (17) it may be observed that α is a function of κ and hence, for a given value of the Poisson's ratio ν , would have slightly different values for plane strain and plane stress cases. The values of α obtained from (18) are given in Table B1. Around the point $(x=0, y=+0)$ the stress state has the behavior

$$\sigma_{ij} \cong \frac{1}{r^\alpha}, \quad (r^2 = x^2 + y^2) \quad (19)$$

Table B1. The power α of stress singularity at $(x=0, y=+0)$.

ν	α	
	Plane Strain	Plane Stress
0	0	0
0.1	0.1329561	0.1237571
0.2	0.2189266	0.1926872
0.3	0.2888271	0.2416508
0.4	0.3500900	0.2794708
0.5	0.4053884	0.3100165

From Table B1 it may be seen that the stress singularity for the plane strain case is somewhat stronger than that for the plane stress case.

3. The Stress Intensity Factors

The system of singular integral equations (5)-(9) is solved by normalizing the intervals $(0,b)$, $(-a,0)$ and $(0,d)$ and by using Gauss-Jacobi integration formulas [28]. The normalization is accomplished by defining

$$t = \frac{b}{2} (r+1) , x = \frac{b}{2} (s+1) , (0 < (x,t) < b, -1 < (r,s) < 1) ;$$

$$t = \frac{a}{2} (r-1) , x = \frac{a}{2} (s-1) , (-a < (x,t) < 0, -1 < (r,s) < 1) ;$$

$$t = \frac{d}{2} (r+1) , y = \frac{d}{2} (s+1) , (0 < (y,t) < d, -1 < (r,s) < 1) ;$$

$$g_1(t) = G_1(r)w_1(r) , h_1(t) = G_2(r)w_1(r) , w_1(r) = (1+r)^{-\alpha}(1-r)^{-1/2} ,$$

$$g_2(t) = G_3(r)w_2(r) , h_2(t) = G_4(r)w_2(r) , w_2(r) = (1-r)^{-\alpha}(1+r)^{-1/2} ,$$

$$p(t) = G_5(r)w_3(r) , w_3(r) = (1+r)^{-\alpha}(1-r)^{-1/2} , (-1 < r < 1) . \quad (20)$$

With (20) the stress intensity factors at the singular points may be defined and evaluated as follows:

$$k_1(b) = \lim_{x \rightarrow b} \sqrt{2(x-b)} \sigma_{yy}(x,0) = - \frac{2\mu}{1+\kappa} \frac{\sqrt{b}}{2^\alpha} G_1(1) , \quad (21)$$

$$k_2(b) = \lim_{x \rightarrow a} \sqrt{2(x-b)} \sigma_{xy}(x,0) = - \frac{2\mu}{1+\kappa} \frac{\sqrt{b}}{2^\alpha} G_2(1) , \quad (22)$$

$$k_1(-a) = \lim_{x \rightarrow -b} \sqrt{-2(x+a)} \sigma_{yy}(x,0) = \frac{2\mu}{1+\kappa} \frac{\sqrt{a}}{2^\alpha} G_3(-1) , \quad (23)$$

$$k_2(-a) = \lim_{x \rightarrow -b} \sqrt{-2(x+a)} \sigma_{xy}(x,0) = \frac{2\mu}{1+\kappa} \frac{\sqrt{a}}{2^\alpha} G_4(-1) , \quad (24)$$

$$\begin{aligned}
k_1(d) &= \lim_{y \rightarrow d+0} \sqrt{2(y-d)} \sigma_{xx}(0,y) = -\lim_{y \rightarrow d-0} \frac{1}{2} \frac{\kappa-1}{\kappa+1} \sqrt{2(d-y)} p(y) \\
&= -\frac{\kappa-1}{2(\kappa+1)} \frac{\sqrt{d}}{2^\alpha} G_5(1) . (*) \tag{25}
\end{aligned}$$

At the singular point ($x=0, y=+0$) we define the stress intensity factors in terms of the tensile and shear cleavage stresses as follows:

$$k_{xx}(0) = \lim_{y \rightarrow 0} \sqrt{2} y^\alpha \sigma_{xx}(0,y) , \tag{26}$$

$$k_{xy}(0) = \lim_{y \rightarrow 0} \sqrt{2} y^\alpha \sigma_{xy}(+0,y) . \tag{27}$$

From (26) and the solution of the problem k_1 may be found as follows:

$$\begin{aligned}
k_{xx}(0) &= \frac{2\mu}{\kappa+1} \frac{1}{2^\alpha} \left[\frac{(1-\alpha)a^\alpha G_1(-1)}{2 \sin \frac{\pi\alpha}{2}} + \frac{(2-\alpha)a^\alpha G_2(-1)}{2 \cos \frac{\pi\alpha}{2}} - \frac{(1-\alpha)b^\alpha G_3(1)}{2 \sin \frac{\pi\alpha}{2}} \right. \\
&\quad \left. + \frac{(2-\alpha)b^\alpha G_4(1)}{2 \cos \frac{\pi\alpha}{2}} \right] - \frac{\kappa-1}{2(\kappa+1)} \frac{1}{2^\alpha} \frac{d^\alpha G_5(-1)}{\sin \pi\alpha} . \tag{28}
\end{aligned}$$

Also, from the general local equilibrium condition

$$\sigma_{xy}(+0,y) - \sigma_{xy}(-0,y) + p(y) = 0 \tag{29}$$

and from $|\sigma_{xy}^+| = |\sigma_{xy}^-|$ we obtain

$$k_{xy}(0) = -\lim_{y \rightarrow 0} \frac{\sqrt{2}}{2} y^\alpha p(y) = -\left(\frac{d}{2}\right)^\alpha \frac{G_5(-1)}{2} . \tag{30}$$

(*) See [1] Appendix A

4. The Results

The only solution which was not discussed in [1] is the crack-inclusion intersection problem shown in Fig. B2. Particularly important in this case is the stress state around the point of intersection ($x=0, y=+0$) as it relates to the initiation of a branching crack at this point. In calculating the results it is assumed that away from the crack inclusion region the medium is subjected to a uniform stress state given by $\sigma_{xx}^{\infty}, \sigma_{yy}^{\infty}, \sigma_{xy}^{\infty}$. Since the superposition is valid, the problem is solved by taking one of these three stress components nonzero at a time. The results are shown in Figures B3-B12. At the crack tips the figures show the normalized Mode I and Mode II stress intensity factors defined by

$$k_1^i(a) = \frac{k_1(a)}{\sigma_{ij}^{\infty} \sqrt{a/2}}, \quad k_2^i(a) = \frac{k_2(a)}{\sigma_{ij}^{\infty} \sqrt{a/2}}, \quad k_1^i(b) = \frac{k_1(b)}{\sigma_{ij}^{\infty} \sqrt{b/2}},$$

$$k_2^i(b) = \frac{k_2(b)}{\sigma_{ij}^{\infty} \sqrt{b/2}}, \quad (i,j=x,y). \quad (31a-d)$$

At the inclusion tip ($x=0, y=d$) we define [1]

$$k_1^i(d) = k_1(d)/k_0, \quad k_0 = \frac{1-\kappa}{2(1+\kappa)} \sigma_{ij}^{\infty} \sqrt{d/2}^{\alpha}, \quad (i,j=x,y). \quad (32a-b)$$

The tensile and shear stress intensity factors at ($x=0, y=+0$) are normalized as follows:

$$k_{xx}^i(0) = k_{xx}(0)/(\sigma_{ij}^{\infty} \sqrt{d/2}), \quad k_{xy}^i(0) = 2k_{xy}(0)/(\sigma_{ij}^{\infty} \sqrt{d/2}), \quad (i,j=x,y). \quad (*)$$

(33a,b)

Figure B3 shows the normalized Mode I stress intensity factors at the crack tips for a uniform stress σ_{yy}^{∞} away from the crack-inclusion region. Note

(*) Note the factor of 2 in (33b); k_{xy}^i is the "stress intensity factor" corresponding to $p(y)$ at $y=0$ (see Eqs. 29 and 30).

that as the crack tip approaches the crack-inclusion intersection point ($x=0$, $y=0$) the corresponding stress intensity factor becomes unbounded (see, also, the results given in [1]). For this loading condition the Mode II stress intensity factors are very small and, hence, are not presented. Figure B4 shows the Mode II stress intensity factors at the crack tip for the pure shear loading σ_{xy}^{∞} which are nearly identical to those shown in Fig. B3. Similarly, for the shear loading the Mode I stress intensity factors are very small and, therefore, are not presented. The normalized stress intensity factor at the inclusion tip ($x=0$, $y=d$) is shown in Fig. B5 for the three uniform applied stresses σ_{xx}^{∞} , σ_{yy}^{∞} and σ_{xy}^{∞} . In the results shown in figures B3-B12 it is assumed that the medium is under plane strain condition, the Poisson's ratio of the plane is 0.3 and, unless stated otherwise, the stiffness parameter

$$\gamma = \frac{\mu(1+\kappa_s)}{A_s \mu_s (1+\kappa)} \quad (34)$$

has a value of 0.1. The effect of γ on $k_I(d)$ is shown in Fig. B6.

The effect of the relative location (a/b) of the inclusion on the stress intensity factors $k_{xx}(0)$ and $k_{xy}(0)$ at crack-inclusion intersection point ($x=0$, $y=+0$) is shown in Figures B7 and B8. Figures B9 and B10 show the effect of the stiffness parameter γ on $k_{xx}(0)$ and $k_{xy}(0)$. The effect of the inclusion length d on the stress intensity factors is shown in Figures B11 and B12.

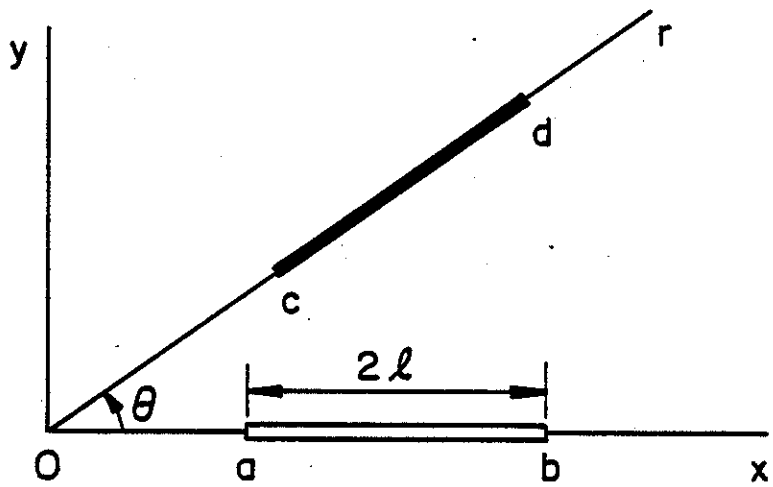
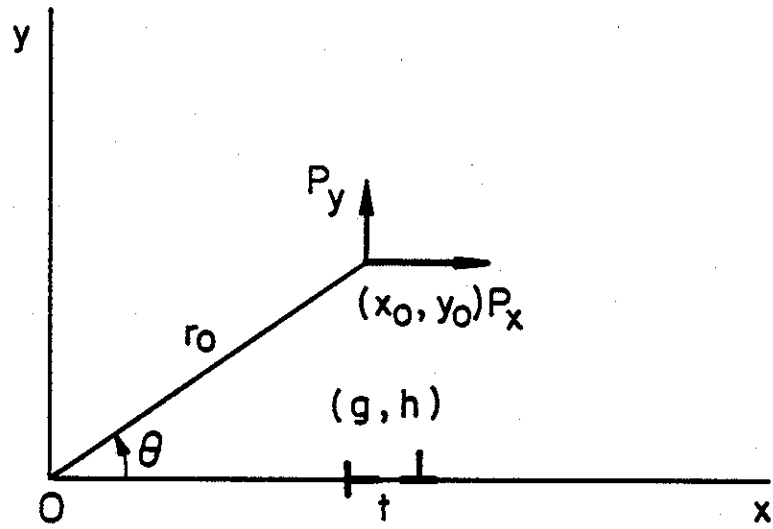


Figure B1. The geometry and notation for the crack-inclusion problem.

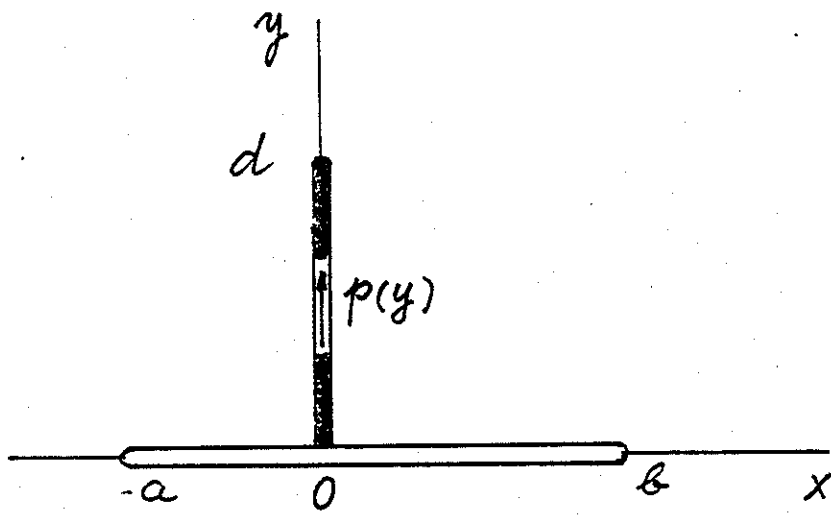


Figure B2. The crack-inclusion geometry.

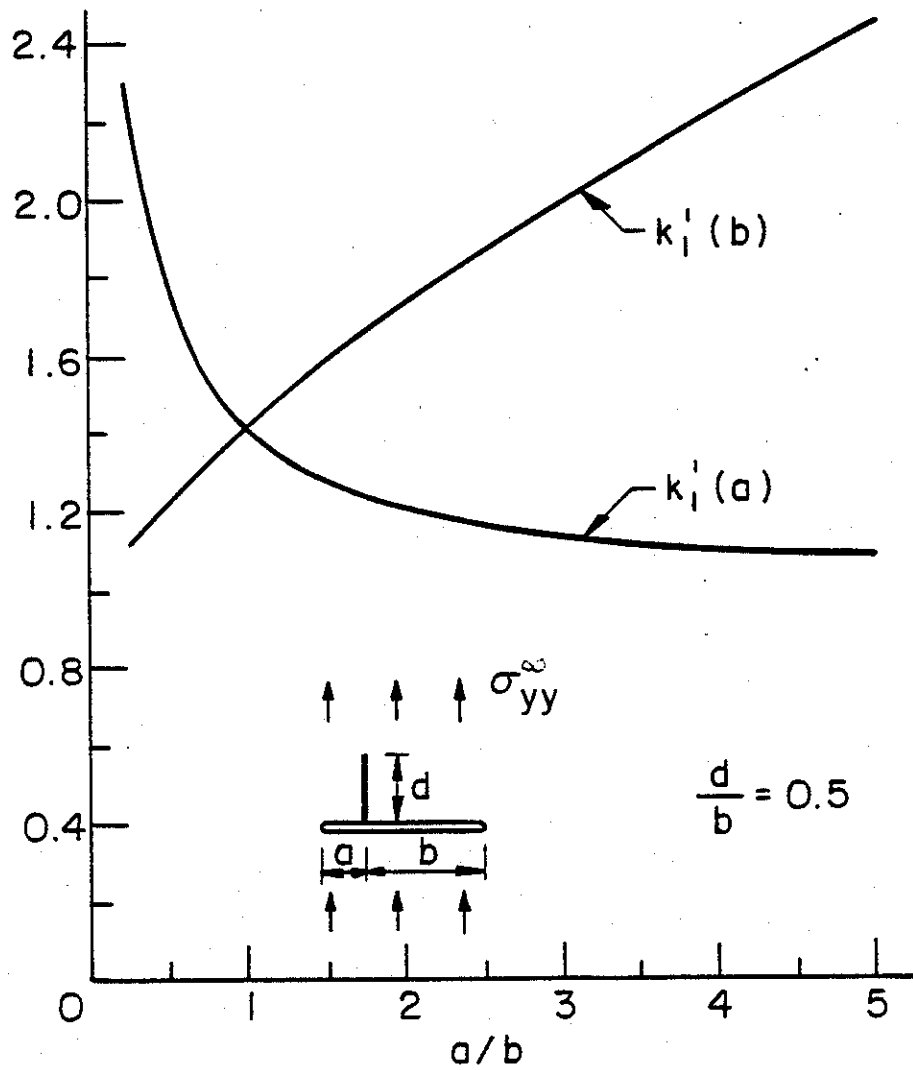


Figure B3. Normalized Mode I stress intensity factors at the crack tip, $\nu=0.3$, $\gamma=0.1$.

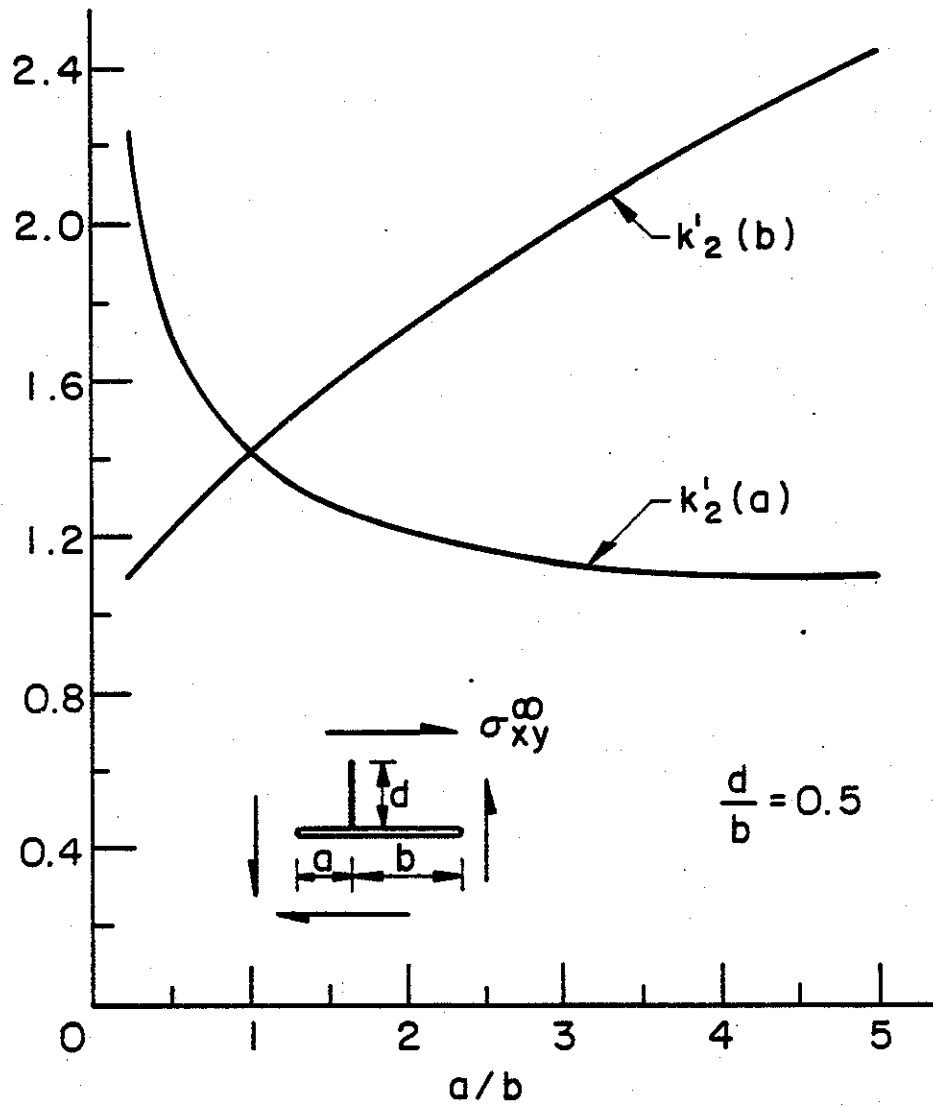


Figure B4. Normalized Mode II stress intensity factors at the crack tips, $\nu=0.3$, $\gamma=0.1$.

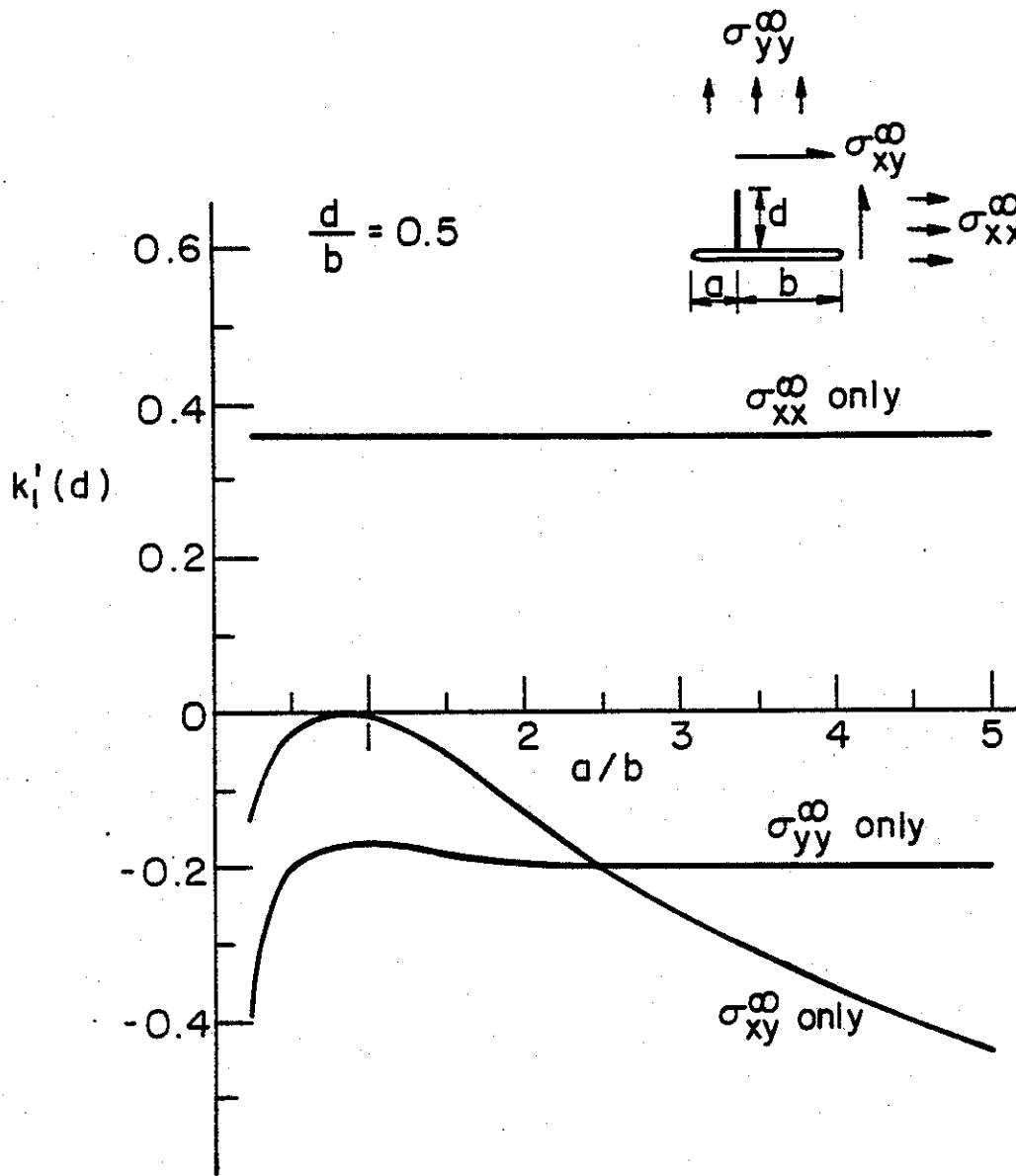


Figure B5. Normalized stress intensity factor at the inclusion end, $\nu=0.3$, $\gamma=0.1$.

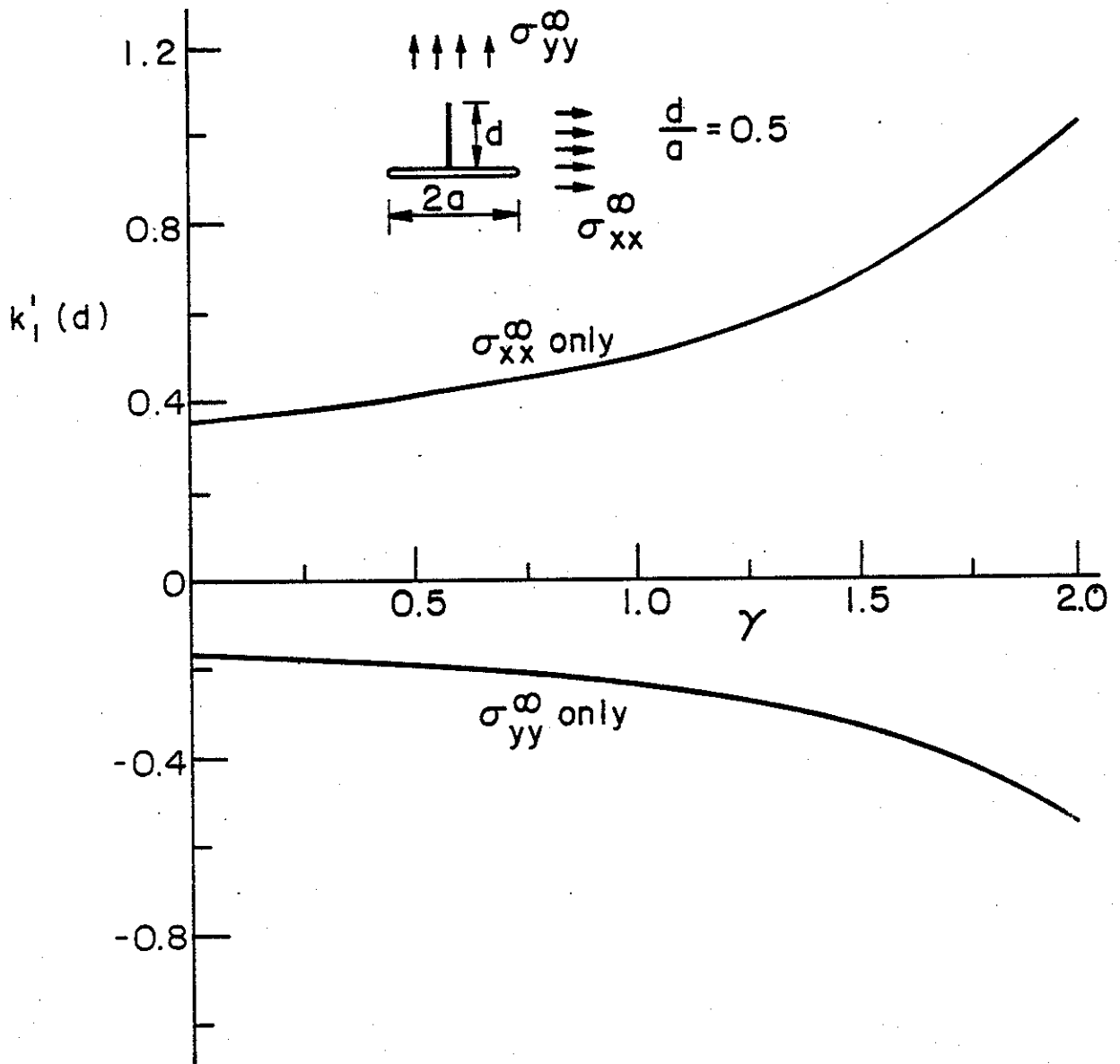


Figure B6. The effect of the stiffness parameter γ on the stress intensity factor at the inclusion end, $\nu=0$, $b=a$.

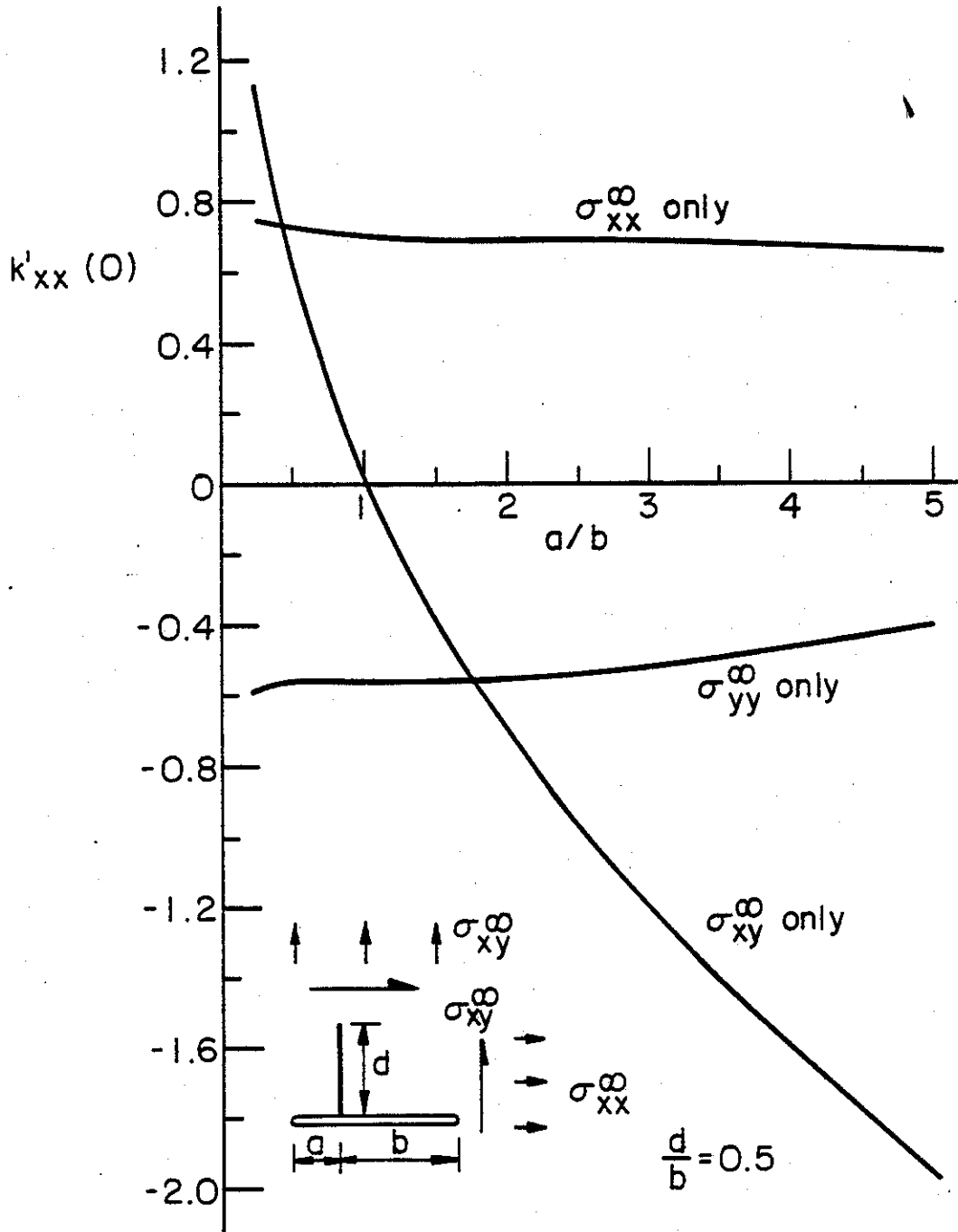


Figure B7. "Tensile" component $k_{xx}(0)$ of the stress intensity factor at the crack-inclusion intersection point, $\nu=0.3$, $\gamma=0.1$.

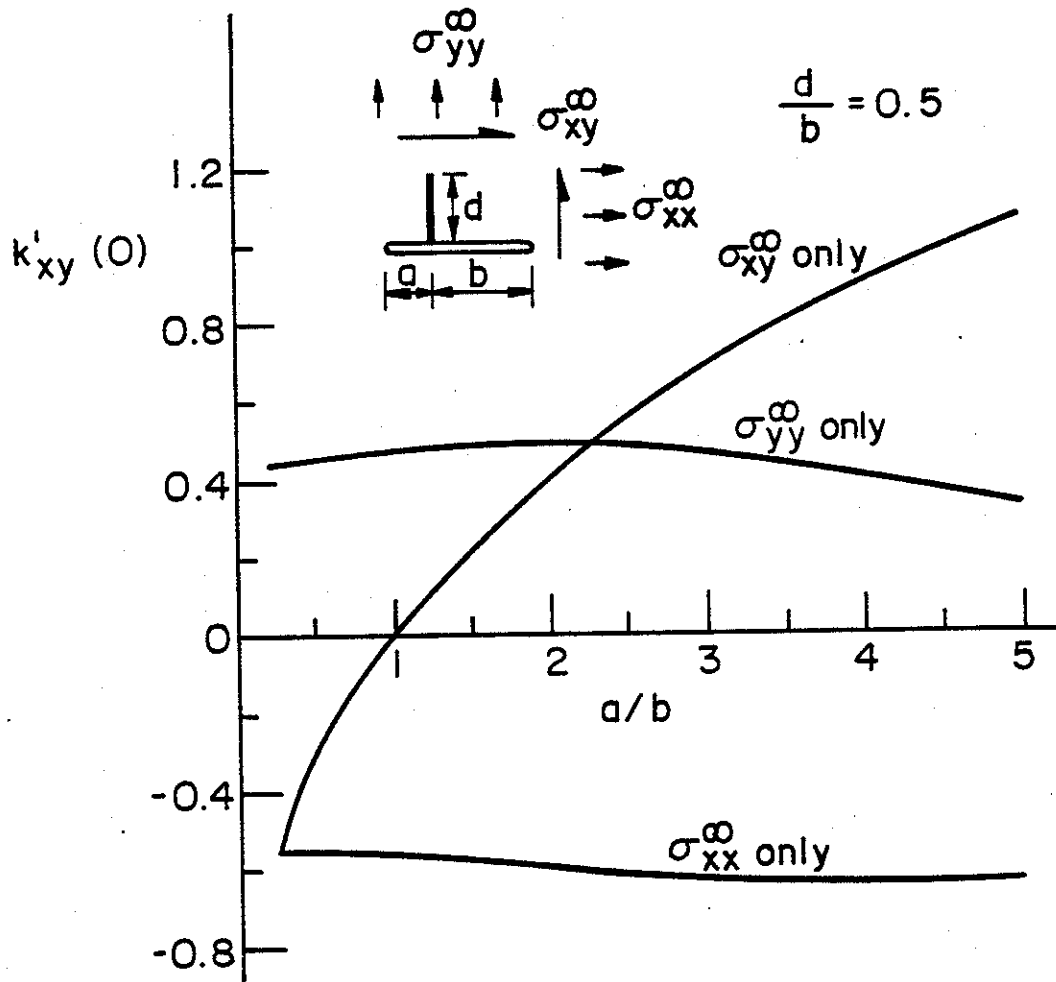


Figure B8. "Shear" component $k_{xy}(0)$ of the stress intensity factor at the crack-inclusion intersection point, $\nu=0.3$, $\gamma=0.1$.

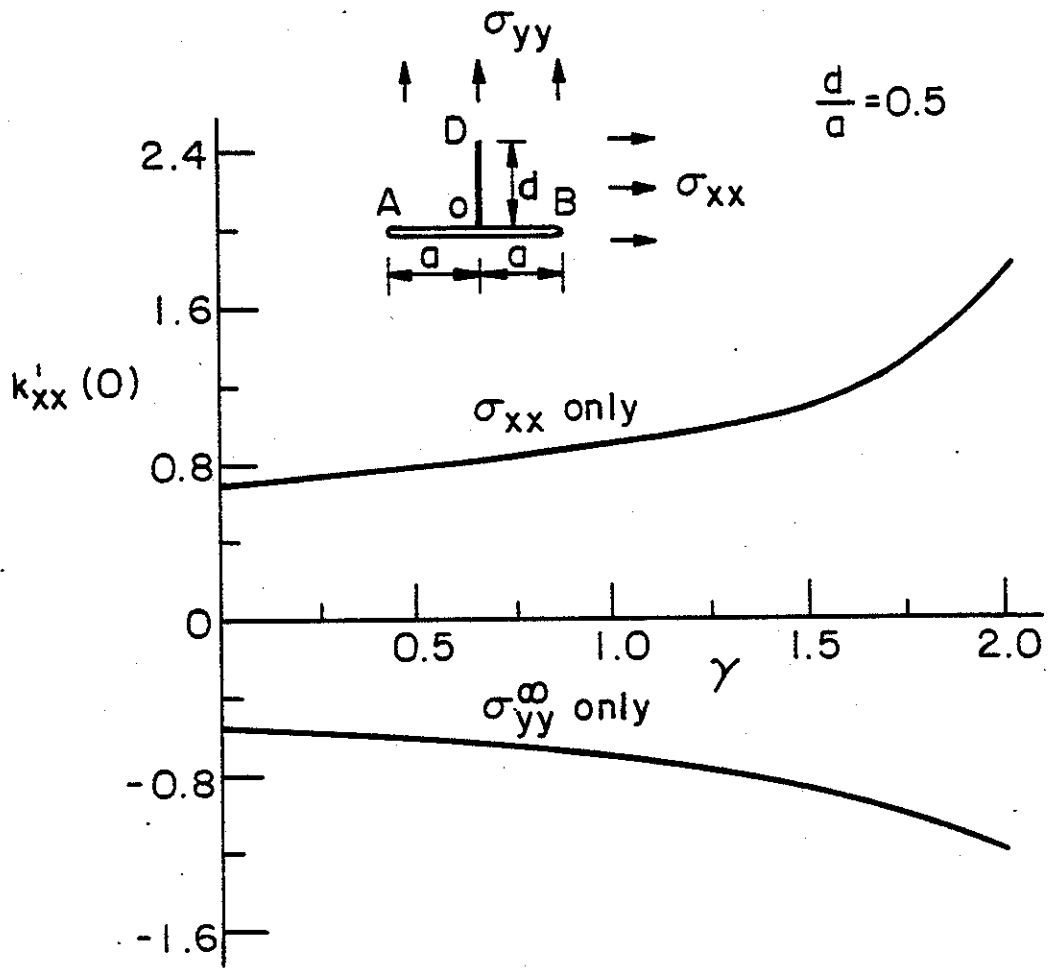


Figure B9. The effect of stiffness ratio γ on $k_{xx}(0)$, $\nu=0.3$, $a=b=2d$.

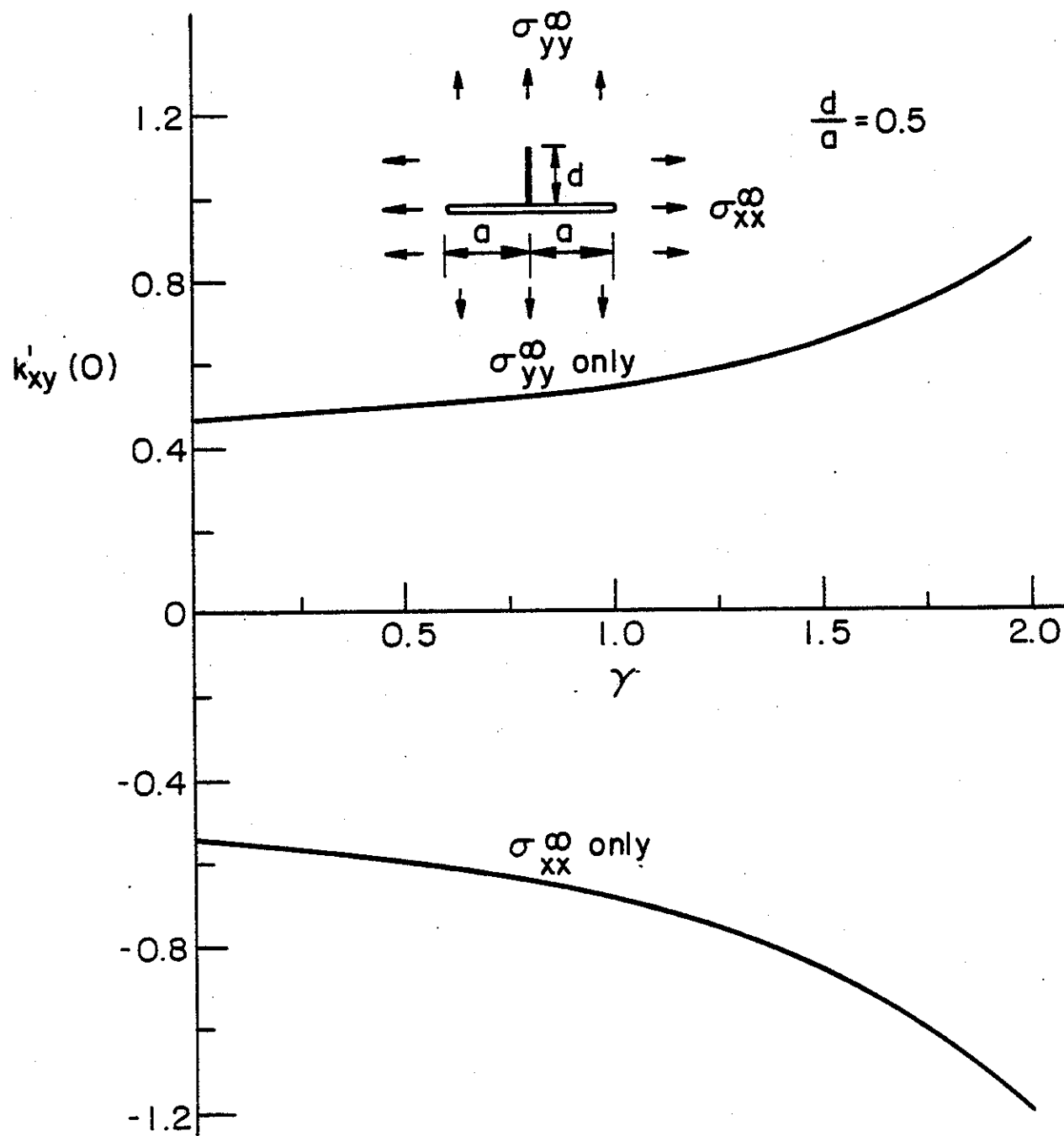


Figure B10. The effect of γ on $k_{xy}(0)$, $\nu=0.3$, $a=b=2d$.

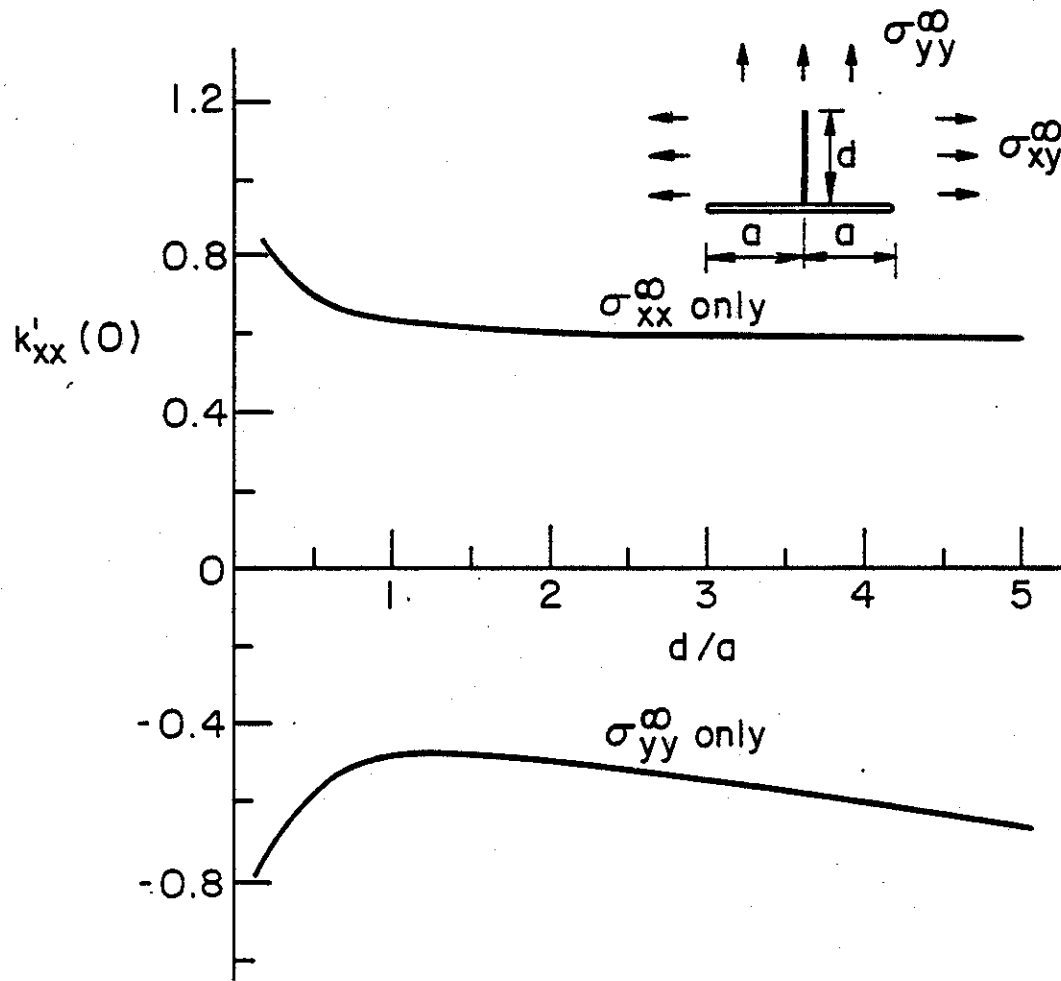


Figure B11. The effect of the inclusion length d on $k_{xx}(0)$, $\nu=0.3$, $\gamma=0.1$, $a=b$.

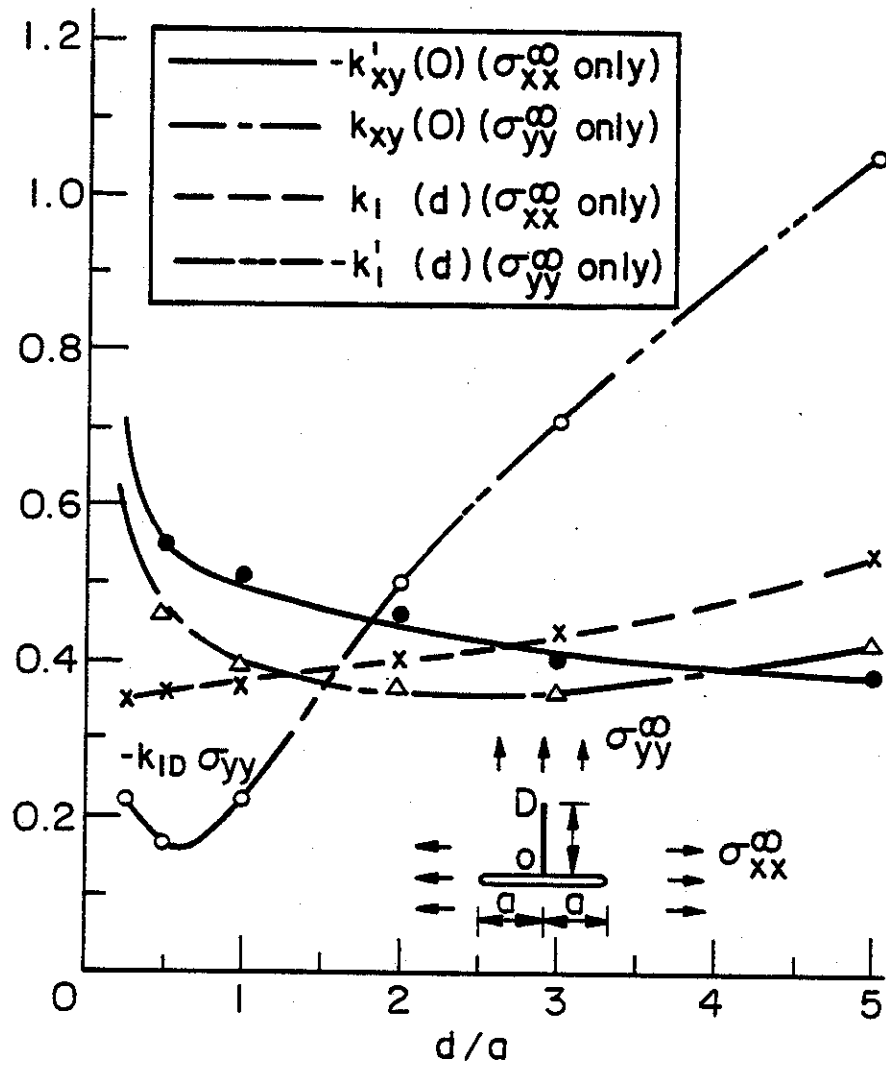


Figure B12. The effect of the inclusion length d on the stress intensity factors at the inclusion ends ($x=0, y=d$) and ($x=0, y=+0$), $\nu=0.3, \gamma=0.1$.